Engineered Residual Stress Implementation (ERSI) Stress Intensity Comparisons Round Robin

Report number ERSI-2021-01
Revision IR

Prepared by:
Robert Pilarczyk, Hill Engineering LLC
Jesse Guymon, Hill Engineering LLC

Participants:
Börje Andersson, BARE Research
Joe Cardinal, Southwest Research Institute
Jim Harter, LexTech Inc.
Adrian Loghin, Simmetrix Inc.
Sebastian Nervi, Engineering Software Research and Development (ESRD) Inc.
Jim Newman, Mississippi State University
Per Nordlund, Hexagon MI
Kevin Walker, QinetiQ Australia

6 June 2022

TABLE OF CONTENTS

LIST OF ABBREVIATIONS AND ACRONYMS

The following is a list of all acronyms and abbreviations likely used in this document:

a	Bore crack length
c	Surface crack length
Cx	Cold Expansion
D	Diameter
E	Young's Modulus
ERSI	Engineered Residual Stress Implementation
FCG	Fatigue Crack Growth
FEA	Finite Element Analysis
FEM	Finite Element Modeling
F_{sn}	Shah-Newman Correction Factor
F_w	Finite Width Correction Factor
Fwa	Finite Width Correction Factor along the bore ("a" direction)
Fwc	Finite Width Correction Factor along the surface ("c" direction)
FW_Err_a	Finite Width Error near the 'a' vertex
FW_Err_c	Finite Width Error near the 'c' vertex
FW_{Newman}	Finite Width Correction from [6]
ϕ	Parametric Angle
K_{FEM}	Mode I Stress Intensity Factor from Finite Element Model
K_I	Mode I Stress Intensity Factor
K_{Ia}	Mode I Stress Intensity Factor along the bore ("a" direction)
K_{IC}	Mode I Stress Intensity Factor along the surface ("c" direction)
K1	Stress Intensity Factor Evaluation Condition
K2	Reference Stress Intensity Factor from Andersson
K_t	Stress Concentration Factor, Tension Loading
L	Length
OEM	Original Equipment Manufacturer
SIF	Stress Intensity Factor
r	Hole Radius
t	Thickness
USAF	United States Air Force
USAFA	United States Air Force Academy
ν	Poisson's Ratio
W	Width

1. INTRODUCTION

1.1. Background

The Engineered Residual Stress Implementation (ERSI) working group is an organization initially established by individuals within and supporting the United States Air Force (USAF) to:

1) Develop a roadmap for the implementation of engineered deep residual stress for fatigue and fracture critical aerospace components
2) Highlight the gaps in the state-of-the-art
3) Define the most effective ways to document requirements and guidelines for a more holistic, physics-informed method for fleet-wide implementation

Since its inception in 2016, ERSI has grown to over 120 participants from different countries, Department of Defense organizations, national labs, universities, original equipment manufacturers (OEMs), industry partners, and USAF Aircraft Structural Integrity Program managers.

In 2017, an initial Fatigue Crack Growth (FCG) Analysis Methods round robin was completed to quantify the epistemic uncertainties in the prediction of crack growth life, given a fixed set of input data, for baseline and cold expanded (Cx) fastener holes [1,2]. Specific input data were developed to minimize the effect of random uncertainties; however, the analysts were free to use any means to incorporate the residual stresses into their FCG life prediction. The effort was an opportunity to exercise various analytical methods, comparing them to experimental results and uncovering strengths and weaknesses of the various approaches.

During the initial round robin, the prediction sensitivity to the analysis inputs was highlighted with one specific case identifying the possible influence of an error in the Mode I Stress Intensity Factor (K_I) for applied remote loading. For several cases, this error resulted in no crack growth for the given conditions ($\Delta K_I < \Delta K_{I,threshold}$). The no crack growth result appeared to be due to either an error in the K-solution and/or the ΔK-rate data in the threshold region used in the life analyses, however other factors could also be contributing. The extent of the error was unclear, so further work was needed to quantify any error or discrepancy in the K-solutions and the ΔK-rate data used on the 2024-T351 alloy. The investigation on the proper ΔK-rate data is beyond the scope of the current study.

As a result of these findings and subsequent discussions amongst the FCG community, a follow-on collaborative round robin was established to investigate differences in stress intensity factors readily available in commercially available software like AFGROW and NASGRO.

1.2. Objectives

The primary objective of the Stress Intensity Factor (SIF) round robin was to evaluate differences between available SIF solutions for a single corner crack at a fastener hole with remote uniform tension loading. The evaluations included not only the root SIF solution but any corrections to account for single vs multiple cracks, finite width, and hole offset. These solutions were compared to explicit Finite Element Analysis (FEA) results of each case. Any findings were intended to drive improvements to solutions available to the fracture mechanics community.

2. ROUND ROBIN OVERVIEW

This round robin considered seven different cases of corner cracks at a hole in a rectangular plate and requested SIF solutions along the crack front from the participants. A building block approach was utilized to understand the influence of not only the root SIF, but any additional corrections applied to the solution. The following sections provide a detailed description of each case considered and the requirements for reporting the results.

2.1. Overview of Cases

Table 1 provides an overview of the cases evaluated for the round robin, with each case adding an additional level of complexity. Case 1 represents the root SIF solution, without any corrections for single cracks, finite width, or hole offset, and uses a crack aspect ratio (a/c) of 1.0. With each additional case, corrections to the root solution are evaluated as well as variations in the crack aspect ratio.

Table 1: Summary of Round Robin Cases Evaluated

Case	Configuration
1	Infinite Plate, Double Crack
2	Infinite Plate, Single Crack
3	Finite Plate, Single Crack
4	Finite Plate, Single Crack, Offset Hole
5	Narrow Plate, Single Crack
6	Infinite Plate, Single Crack, a/c = 1.5
7	Infinite Plate, Single Crack, a/c = 0.5

2.2. Analysis Inputs

Figure 1 illustrates the overall geometry, crack configuration, and loading conditions utilized in the round robin. All seven cases considered a rectangular plate with width (W), length (L), and thickness (t), with a single hole of diameter (D). For all cases except for Case 4, a centered hole is used where the hole offset distance defines the location of the hole relative to the width of the coupon. All cases considered a single corner crack at the hole, as shown on the left-hand side of Figure 1, except for Case 1, which considered double symmetric corner cracks. The crack length along the surface is defined as (c), while the crack length along the bore is (a). For all cases considered, a minimum of thirty (30) SIF extraction points along the crack front were requested from the participants. All cases considered a uniform tension stress of 10 ksi applied at the ends of the coupon, as illustrated on the right-hand side of Figure 1. In addition, all cases used the same material properties of Young's modulus (E) of 10,400 ksi, and Poisson's ratio (ν) of 0.3. Participants reported the Mode I SIF versus the parametric angle (Φ), as defined in the illustration in Figure 2. For a semi-circular crack (i.e., $a = c$), the parametric angle is equivalent to the angle along the crack front.

Table 2 provides a summary of the matrix of cases considered in this round robin and includes all the details required to perform the analyses. For the finite plate configurations (Cases 3-5), the participants were instructed to use L = 3W. In terms of crack aspect ratio, all cases considered a/c = 1, except for Case 6 (used a/c = 1.5) and Case 7 (used a/c = 0.5).

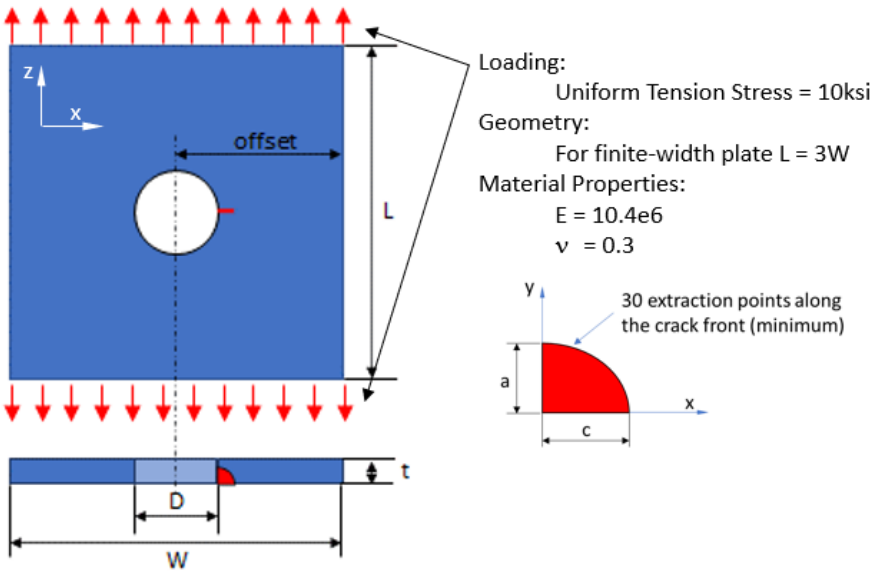

Figure 1: Typical round robin corner crack at a hole configuration

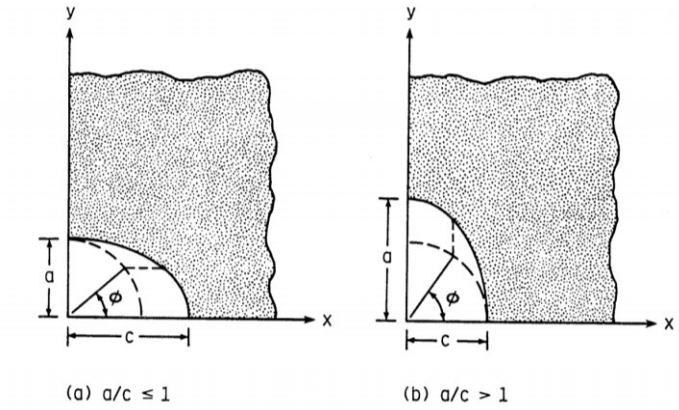

Figure 2: Parametric angle definition for SIF reporting [6]

Table 2: Round robin matrix of cases

Case	Surface Crack Length (c) (inch)	Bore Crack Length (a) (inch)	Corner Crack Configuration	Width (inch)	Thickness (inch)	Hole Diameter (inch)	Hole Offset (inch)
1	0.050	0.050	Double Symmetric	100.00	0.25	0.50	50.00
2	0.050	0.050	Single	100.00	0.25	0.50	50.00
3	0.050	0.050	Single	4.00	0.25	0.50	2.00
4	0.050	0.050	Single	4.00	0.25	0.50	0.60
5	0.050	0.050	Single	1.20	0.25	0.50	0.60
6	0.050	0.075	Single	100.00	0.25	0.50	50.00
7	0.100	0.050	Single	100.00	0.25	0.50	50.00

3. SUBMISSIONS

Nine submissions were received from eight participants which included solutions utilized by AFGROW and NASGRO, solutions from Newman/Raju and Fawaz/Andersson, and explicit FEA of each case. FEA approaches utilized various tools and methods which provides an additional opportunity to evaluate the different approaches and their impact on the accuracy of the SIF.

Seven reference solutions (correlating with the seven cases) with relative errors in K_I on the order of 0.03% or less were provided by Andersson (Submission 6) under USAF contract and were utilized as the reference solutions for all cases. A summary of each submission is included in the following sections.

3.1. Submission 1: Fawaz-Andersson Solutions, AFGROW

Submission 1 utilized SIF solutions from Fawaz-Andersson [3] for a single corner crack at a fastener hole, which are currently utilized in the Advanced Model solutions in AFGROW. To correct for a finite width, the Newman correction [6] is utilized where applicable (Cases 3-5). The Harter correction [4] is utilized to account for offset holes (Cases 4-5).

3.2. Submission 2: Newman-Raju Fit to Fawaz-Andersson

Submission 2 used updated SIF equations developed by Newman [5] which are based on modifying the Newman-Raju [6] equations to fit the Fawaz-Andersson [3] solutions for two symmetric corner cracks at a hole. Case 1 has a double crack, but all the others (Cases 2-7) have a single crack.

Since the SIF equations were for two-symmetric corner cracks at a hole, a correction factor was needed to account for the single corner crack (Cases 2-7), like the Shah [7] correction. However, the correction used was a recent improvement to the correction factor developed by Shah in 1976. The Shah-Newman correction factor was developed by using an equation for a single through crack at a hole and finding an equivalent through crack of equal area as the corner crack. The Shah-Newman correction factor is:

$$F_{sn} = 0.707 + 0.393\ z - 0.1\ z^4 \qquad \text{(EQ 2-1)}$$

and

$$z = 1 / [1 + \pi\ (a/t)\ (c/r) / 4] \qquad \text{(EQ 2-2)}$$

where "t" is plate thickness and "r" is hole radius. Note that the correction factor is independent of the parametric angle (Φ). Thus, F_{sn} is applied at the two-crack free surface ($\Phi = 0$ and $\pi/2$) locations.

Figure 3 shows the error in the two-symmetric to single corner crack correction factor equation developed by Shah [7] and the newly developed equation by Newman. The equation is referred to as the Shah-Newman (F_{sn}) correction factor. The very accurate reference solutions for a single and two-symmetric corner cracks at a circular hole were obtained from Andersson at the crack-free-surface ($\phi = 0$) location. Herein, only the results for $r/t = 1$ and $10 < a/c < 0.25$ are presented. As shown, the Shah equation underestimated the correction factor by about 5%, however, the new Shah-Newman equation was within +/- 2%.

The finite width (F_w) correction factor equation from Newman-Raju [6] was used where applicable (Cases 3, 4 and 5). Cases 1, 2, 6 and 7 are for an infinite width plate.

For all cases, the circular hole was in the center of the plate, except for Case 4 which has the offset hole. The single crack in the offset case was located on the short ligament side. That offset hole case (Case 4) was assessed in two separate ways as follows:

1. The offset distance from the hole center to the nearest edge is 0.6 inch. This first option was to assume the total width was 1.2 inch and the hole is in the center. This is a conservative option and is expected to overpredict SIFs.

2. The second option was to also assume a central hole in a finite width plate but modify the width such that the stress concentration at the edge of the hole at the location of interest (shortest ligament side) matches the correct stress concentration for the offset hole geometry. This was found to be a total width of 1.43 inches. The "true" total width is 4.0 inch, with the hole offset to one side such that the distance from the center of the 0.5 inch diameter hole to the closest edge is 0.6 inch. This is modelled as a 1.43 inch wide plate with a 0.5 inch diameter central hole, which will produce the same stress concentration at the location of interest. This option is expected to produce a more accurate solution than option 1 and is utilized for comparisons throughout the remainder of this summary report (referred to as the K_t match approach).

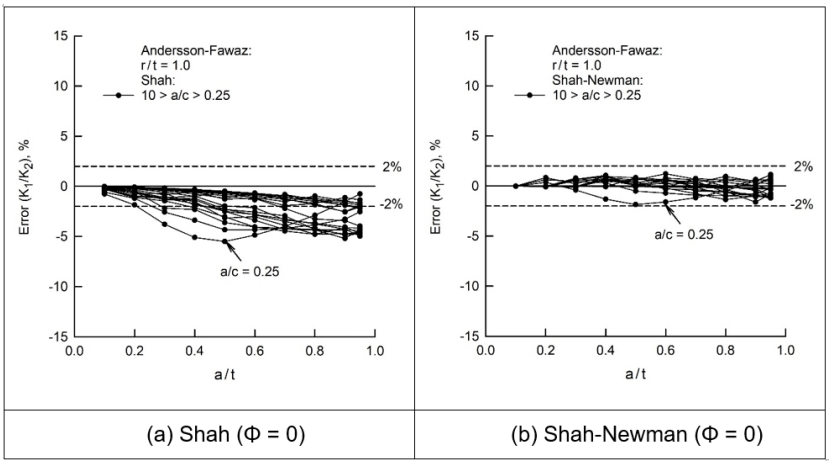

Figure 3: Errors in the two-symmetric to single corner crack correction factor equations; Shah (left), Shah-Newman (right).

3.3. Submission 3: Newman-Raju (1986)

Submission 3 utilized the 1986 Newman-Raju solution [6]. To correct for a single corner crack, the Shah correction [7] was utilized for Cases 2-7. To correct for a finite width, the Newman correction [6] is utilized where applicable (Cases 3-5). To account for offset holes (Case 4-5), two methods were investigated (see details from Submission 2). The K_t match approach was utilized for the results and comparisons presented in Section 4.

3.4. Submission 4: NASGRO (CC04 & CC02): Newman-Raju

Submission 4 utilized the NASGRO CC04 solution, which incorporates the 1986 Newman-Raju solution [6]. For Cases 2-7, the NASGRO CC02 model which corrects for a single corner crack using the Shah correction [7] was utilized. CC02 correction factors for finite width effects and offset holes used a solution for a through crack from an offset hole in a plate [8].

These legacy NASGRO solutions (CC02 and CC04) were included in the round robin exercise for comparison purposes but have been superseded by CC16 and are not recommended for use.

3.5. Submission 5: NASGRO (CC16): Fawaz-Andersson

Submission 5 utilized the NASGRO CC16 solution, which incorporates the Fawaz-Andersson solutions [3]. Fundamentally based on the original Fawaz-Andersson solutions, CC16 represents the a-tip and c-tip SIFs with single values based on the local maximum (peak value) observed near the surface, which is usually around 2 to 3 degrees, but varies from case to case. To correct for a finite width, a modified version of the Newman finite width correction factor [6] was used [9] where applicable (Cases 3-5). To account for offset holes (Case 4-5), the Harter offset correction from AFGROW [4] is utilized in CC16.

For the comparisons in this study, the CC16 results are compared to the local maximum results at the angles reported for the Andersson (2021) solutions.

3.6. Submission 6: Andersson: FEA (2021)

Submission 6 explicitly modeled each condition utilizing the STRIPE FE-software for the hp-version of the finite element method. STRIPE was developed at the Aeronautical Research Institute of Sweden, FFA, 1984. A detailed overview of the modeling approach is included in the Appendix. Convergence tests were completed for each case, and it's shown that the pointwise relative error in K at arbitrary points along the seven crack fronts can be estimated to be less than 0.03%, and for Case 2, of order 0.01%. As a result of the convergence studies, this submission was utilized as the reference solution for all submission comparisons completed in Section 4.

3.7. Submission 7: SimModeler Crack: FEA (2021)

Submission 7 utilized SimModeler Crack to create 3D FEMs and compute Mode I SIFs for the benchmark problems considered in this study. SimModeler Crack is a pre- and post-processor designed for component level finite element-based 3D fatigue crack growth simulations. In SimModeler Crack, SIFs are computed via displacement correlation technique based on a model solution performed in ANSYS, ABAQUS or CalculiX. The same modeling process was followed for each 3D model generated in this study. For all models, a similar overall mesh refinement and a uniform mesh size that provides about 300 element edges along the crack front were used for all benchmark cases. Additional modeling details are included in the Appendix. For Case 2, an average relative difference of 0.23% from Andersson semi-analytic solution was computed, with similar differences expected for the other cases.

3.8. Submission 8: StressCheck: FEA (2021)

Submission 8 utilized StressCheck to create 3D FEMs and compute Mode I SIFs for the cases provided. For the initial submission, the modeling approach utilized recommended modeling practices for cracked bodies, with automatically generated graded meshing towards the crack front. These results were intended to represent the approach an everyday practitioner would utilize to complete fracture mechanics analyses targeting an estimated error in the computation of SIF within 2%. Sensitivity studies have shown that a variation of 2% in the computation of SIFs have an influence of 20% or less on predicted fatigue life [10]. Errors in these solutions are compared to other submission in Section 4. Higher accuracy can always be achieved at the cost of increased computational effort or an alternative discretization approach as presented in Section 5.3.

The same round robin cases were analyzed utilizing a fully parametric model with guided meshing targeting an estimated error in the computation of SIF $\leq 0.5\%$. This is the recommended approach when solving handbook type models with very simple geometries as it generates high accuracy results while minimizing computational time. As a reference, using a typical Windows 10 engineering laptop (2.9GHz Intel Xeon with 32GB RAM), each case takes less than 1 minute to run a sequence of solutions with uniform p-extension (p-levels 6 to 8), perform global and local error estimations, and extract the SIF at 200 points along the crack front. Additional details are available in [12].

3.9. Submission 9: Marc: FEA (2021)

Submission 9 utilized Marc from Hexagon MI (former MSC Software) to create 3D FEMs and compute Mode I SIFs for the cases provided. Marc is a general-purpose non-linear solver with special capabilities for crack initiation and crack growth using automatic remeshing. The mesh for the crack evaluation was generated automatically, using the recommended minimum number of evaluation point of 30 as the number of nodes along the crack front. Additional modeling details are included in the Appendix.

3.10. Submission Summary

A tabulated summary of the details for each submission are included in Table 3.

Table 3: Summary of Submissions

Submission #	Title	SIF solution source	Single Corner Crack Correction (Cases 2, 3, 4, 5, 6, 7)	Finite Width Correction (Cases 3, 4, 5)	Offset Hole Correction (Cases 4, 5)
1	Fawaz-Andersson Solutions, AFGROW	Fawaz-Andersson [3] (as implemented in AFGROW Advanced Model)	n/a	Newman correction [6]	Harter correction [4]
2	Newman-Raju Fit to Fawaz-Andersson	Updated equations by Newman [5] based on fit to Fawaz-Andersson solutions [3]	Shah-Newman Correction (2020)	Newman correction [6]	• center hole (conservative option) • Kt match approach
3	Newman-Raju (1986)	1986 Newman-Raju solution [6]	Shah correction	Newman correction [6]	Kt match approach
4	NASGRO (CC04 & CC02): Newman-Raju	1986 Newman-Raju solution [6] (as implemented in NASGRO CC04)	Shah correction (as implemented in NASGRO CC02)	NASGRO CC02 [8]	NASGRO CC02 [8]
4	NASGRO (CC16): Fawaz-Andersson	Fawaz-Andersson solutions [3] (as implemented in NASGRO CC16)	n/a	Modified version [9] of the Newman correction [6]	Harter correction [4] (as implemented in NASGRO CC16)
6	Andersson: FEA (2021)	Explicitly modeled each condition utilizing the STRIPE FE-software for the hp-version of the finite element method			
7	SimModeler Crack: FEA (2021)	Utilized SimModeler Crack to create 3D FEMs and compute Mode I SIFs via displacement correlation technique			
8	StressCheck: FEA (2021)	Utilized StressCheck software based on the hp-version of the finite element method, to create 3D models and compute Mode I SIFs using the Contour Integral Method (CIM).			
9	Marc: FEA (2021)	Utilized Marc to create 3D FEMs and compute Mode I SIFs			

4. COMPARISON OF RESULTS

The following sections include a summary of the comparisons for the seven cases evaluated. For these comparisons, the Mode I SIF is plotted along the crack front as a function of normalized parametric angle, and the percent difference relative to Submission 6 from Andersson is also presented. A summary table of the inputs for each case is included.

4.1. Case 1: Two Symmetric Corner Cracks at a Hole, Infinite Plate

Case 1 represented the initial starting point to evaluate the root SIF solutions for corner cracks at a fastener hole. Several of the notable solutions available are evaluated with this comparison, which represents an infinite plate with two symmetric corner cracks at a centered hole. The corner cracks have an aspect ratio of 1.0, with equal crack lengths in the '*a*' and '*c*' directions (see Figure 1). For this case, single crack, finite width, and hole offset corrections are not utilized. A summary of the Case 1 inputs is detailed below in Table 4. Figure 4 and Figure 5 detail the SIF and percent difference for all the submissions, with results within ±2% of the Andersson submission, with the exception of near surface points that demonstrated lack of convergence.

Table 4: Case 1 Input Parameters

Case	1
Configuration	Infinite Plate, Double Crack
Crack Configuration	Double Symmetric Corner Cracks
Surface Crack Length (*c*) (inch)	0.050
Bore Crack Length (*a*) (inch)	0.050
Width (inch)	100.00
Thickness (inch)	0.25
Hole Diameter (inch)	0.50
Hole Offset (inch)	50.00
a/c	1.00
a/t	0.20
W/D	200.00
r/t	1.00
r/W	0.0025

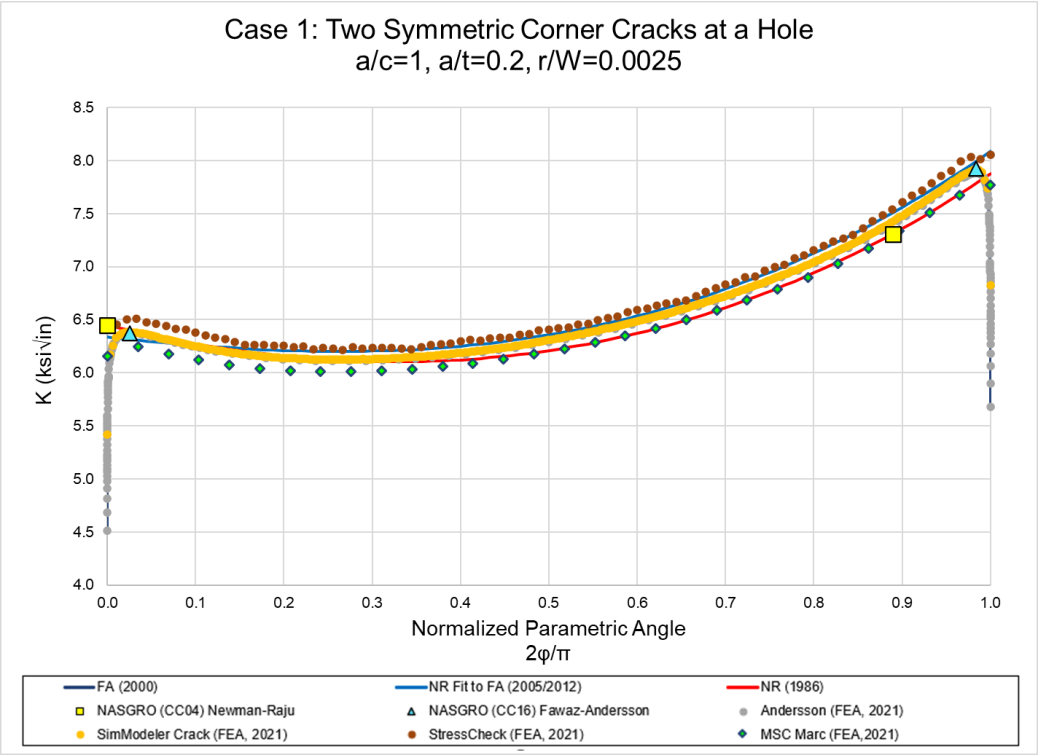

Figure 4: Stress Intensity vs. Normalized Parametric Angle (Case 1)

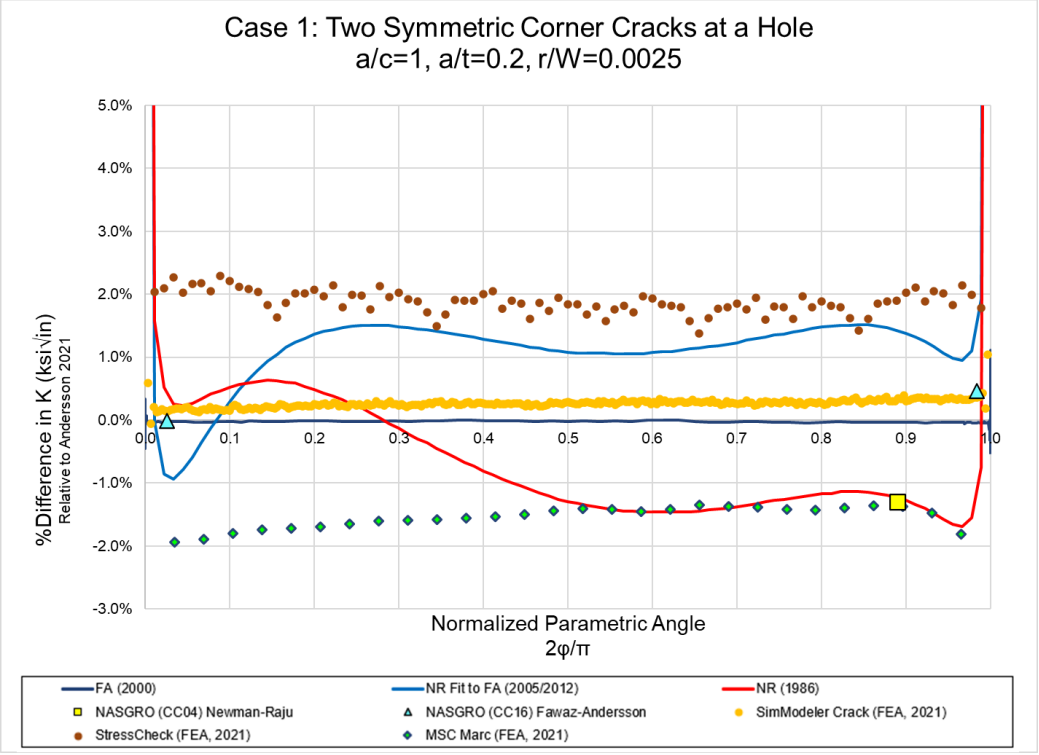

Figure 5: Percent Difference in Stress Intensity vs. Normalized Parametric Angle (Case 1)

4.2. Case 2: Single Corner Crack at a Hole, Infinite Plate

Case 2 was a continuation from the comparisons from Case 1, incorporating the effects of a single corner crack. Submissions 2-4 utilize the Shah or Shah/Newman corrections to adjust a double corner crack solution to a single crack solution. Submissions 1 and 5 utilized single crack modeling during the development of their root SIF solutions. A summary of the Case 2 inputs is detailed below in Table 5. Figure 6 and Figure 7 detail the SIF and percent difference for all the submissions, with results generally within ±2% of the Andersson submission, with the exception of near surface points that demonstrated greater divergence. Submission 4 (NASGRO CC02) resulted in differences that exceeded 4% for the point representative of the hole bore.

Table 5: Case 2 Input Parameters

Case	2
Configuration	Infinite Plate, Single Crack
Crack Configuration	Single Corner Crack
Surface Crack Length (*c*) (inch)	0.050
Bore Crack Length (*a*) (inch)	0.050
Width (inch)	100.00
Thickness (inch)	0.25
Hole Diameter (inch)	0.50
Hole Offset (inch)	50.00
a/c	1.00
a/t	0.20
W/D	200.00
r/t	1.00
r/W	0.0025

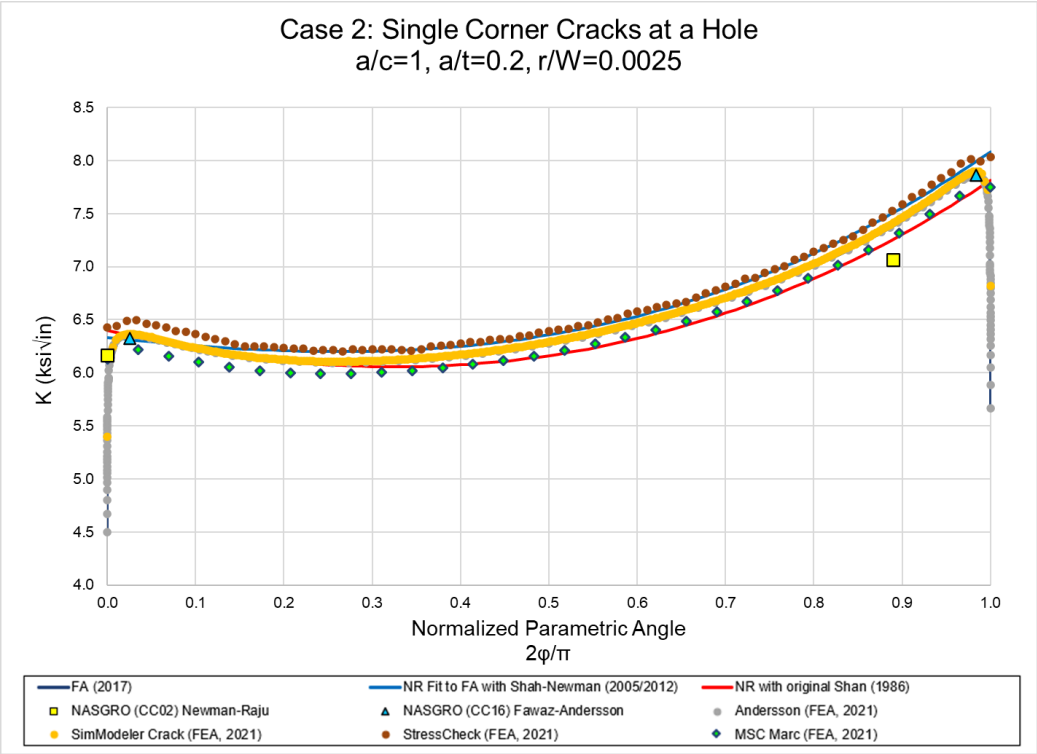

Figure 6: Stress Intensity vs. Normalized Parametric Angle (Case 2)

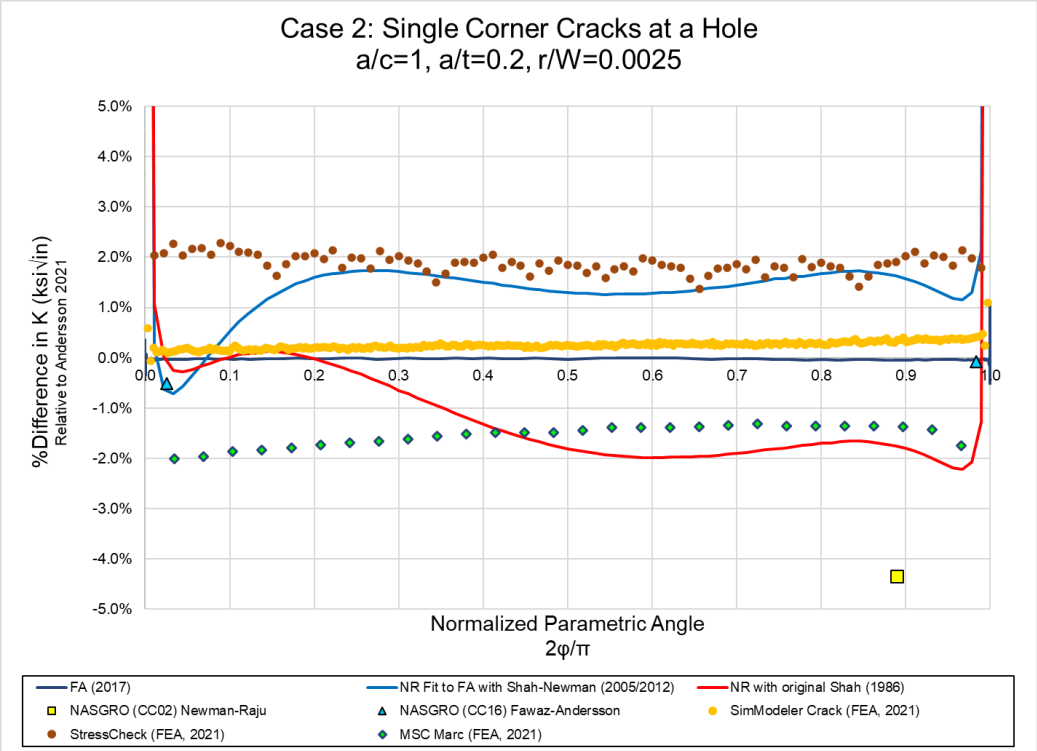

Figure 7: Percent Difference in Stress Intensity vs. Normalized Parametric Angle (Case 2)

4.3. Case 3: Single Corner Crack at a Hole, Finite Plate

Case 3 was a continuation from the comparisons from Case 1 and 2, incorporating finite width effects. Submissions 1-3 utilized the Newman finite width correction [6]. Submission 4 used the correction from [8] and Submission 5 used the correction from [4]. A summary of the Case 3 inputs is detailed below in Table 6. Figure 8 and Figure 9 detail the SIF and percent difference for all the submissions, with results generally within ±2% of the Andersson submission, with the exception of near surface points that demonstrated greater divergence. Submission 3 (Newman-Raju 1986) resulted in differences that exceeded 2% over a range of 0.4-1.0 normalized parametric angle, representative of the crack front near the hole bore.

Table 6: Case 3 Input Parameters

Case	3
Configuration	Finite Plate, Single Crack
Crack Configuration	Single Corner Crack
Surface Crack Length (*c*) (inch)	0.050
Bore Crack Length (*a*) (inch)	0.050
Width (inch)	4.00
Thickness (inch)	0.25
Hole Diameter (inch)	0.50
Hole Offset (inch)	2.00
a/c	1.00
a/t	0.20
W/D	8.00
r/t	1.00
r/W	0.0625

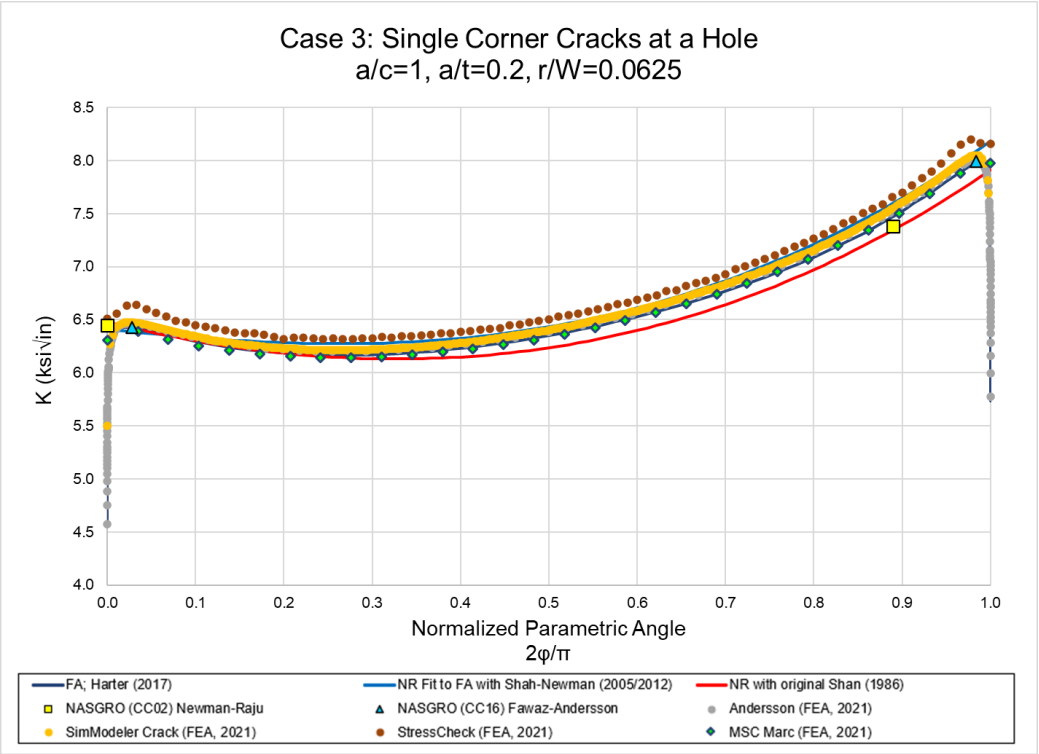

Figure 8: Stress Intensity vs. Normalized Parametric Angle (Case 3)

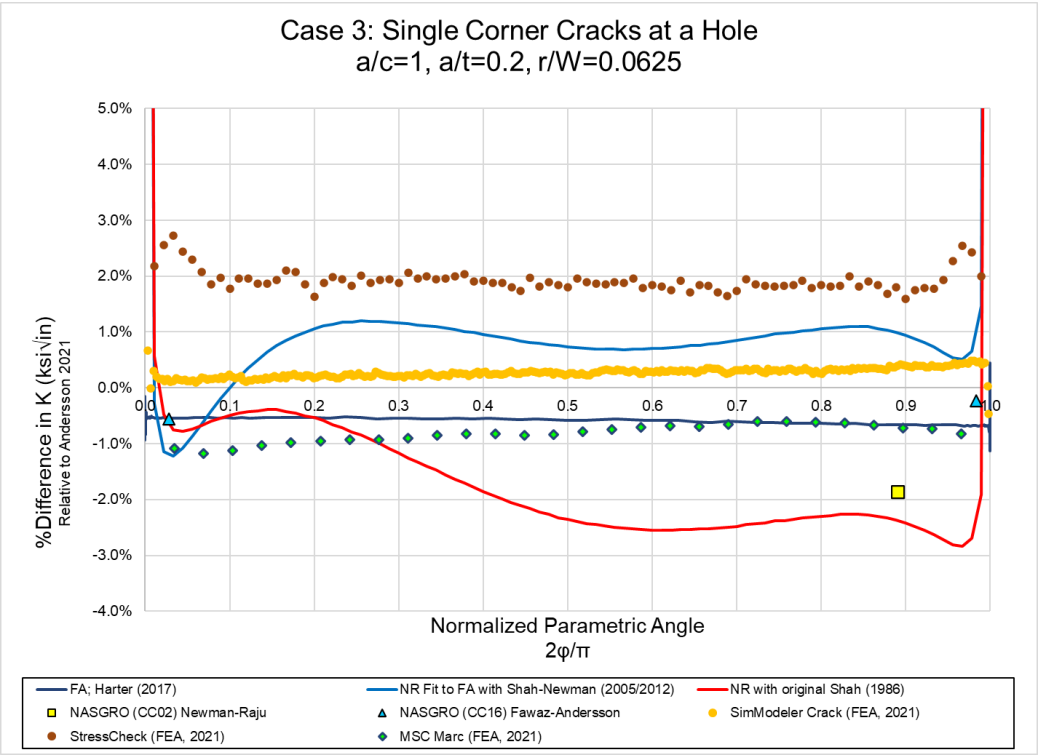

Figure 9: Percent Difference in Stress Intensity vs. Normalized Parametric Angle (Case 3)

4.4. Case 4: Single Corner Cracks at a Hole, Finite Plate, Offset Hole

Case 4 was a continuation from the comparisons from Cases 1-3, incorporating hole offset effects. Submission 1 utilized the Harter offset correction. Submission 2-3 investigated two approaches to characterize the short offset, however, the K_t match approach was utilized for comparison. Submission 4 used the correction from [8] and Submission 5 used the correction from [9]. A summary of the Case 4 inputs is detailed below in Table 7. Figure 10 and Figure 11 detail the SIF and percent difference for all the submissions. Significant differences were observed for Submissions 1-4 with differences relative to the Andersson submission of nearly 10%.

Table 7: Case 4 Input Parameters

Case	4
Configuration	Finite Plate, Single Crack
Crack Configuration	Single Corner Crack
Surface Crack Length (*c*) (inch)	0.050
Bore Crack Length (*a*) (inch)	0.050
Width (inch)	4.00
Thickness (inch)	0.25
Hole Diameter (inch)	0.50
Hole Offset (inch)	0.60
a/c	1.00
a/t	0.20
W/D	8.00
r/t	1.00
r/W	0.0625

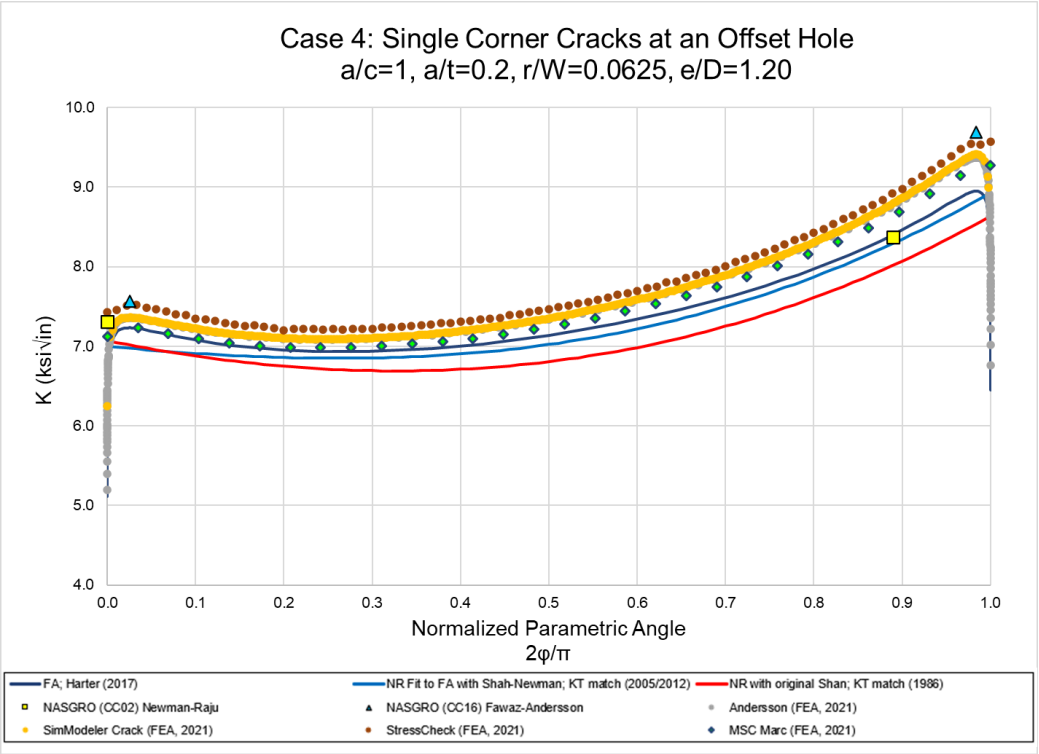

Figure 10: Stress Intensity vs. Normalized Parametric Angle (Case 4)

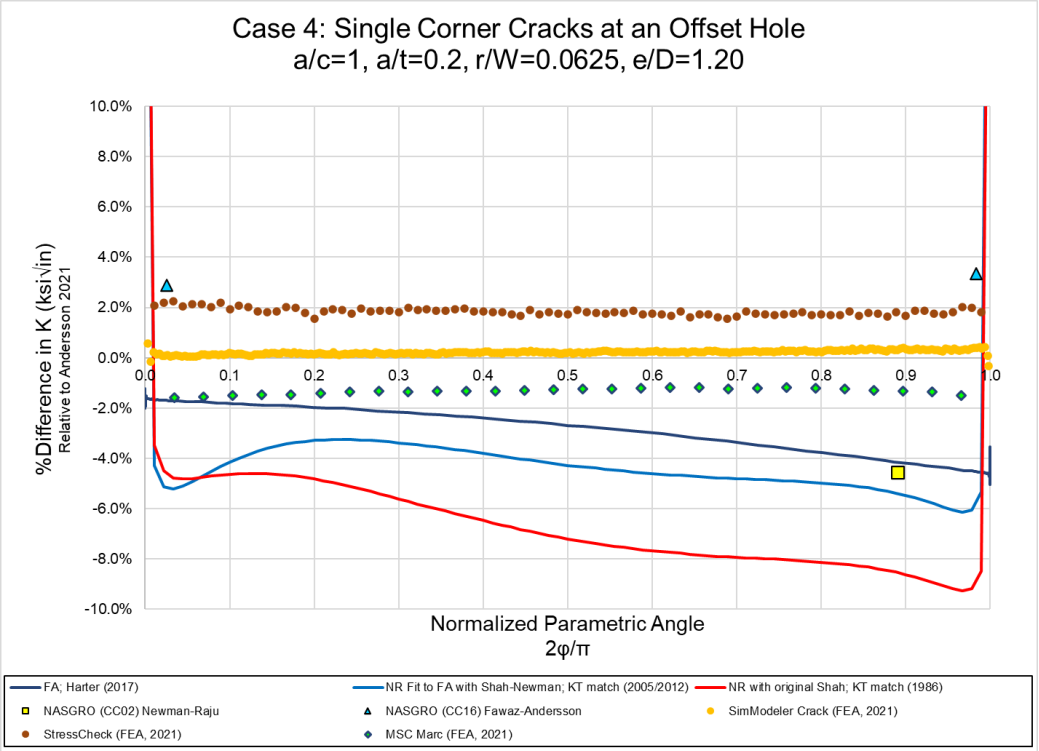

Figure 11: Percent Difference in Stress Intensity vs. Normalized Parametric Angle (Case 4)

4.5. Case 5: Single Corner Crack at a Hole, Narrow Plate

Case 5 was a continuation from the comparisons from the previous cases, however, investigated a relatively "narrow" width. Submissions 1-3 utilized the Newman finite width correction. Submission 4 used the correction from [8] and Submission 5 used the correction from [9]. A summary of the Case 5 inputs is detailed below in Table 8. Figure 12 and Figure 13 detail the SIF and percent difference for all the submissions. Significant differences were observed for Submissions 1-3 which utilized the Newman finite width correction with differences relative to the Andersson submission ranging from 5-12%.

Table 8: Case 5 Input Parameters

Case	5
Configuration	Narrow Plate, Single Crack
Crack Configuration	Single Corner Crack
Surface Crack Length (*c*) (inch)	0.050
Bore Crack Length (*a*) (inch)	0.050
Width (inch)	1.20
Thickness (inch)	0.25
Hole Diameter (inch)	0.50
Hole Offset (inch)	0.60
a/c	1.00
a/t	0.20
W/D	2.40
r/t	1.00
r/W	0.2083

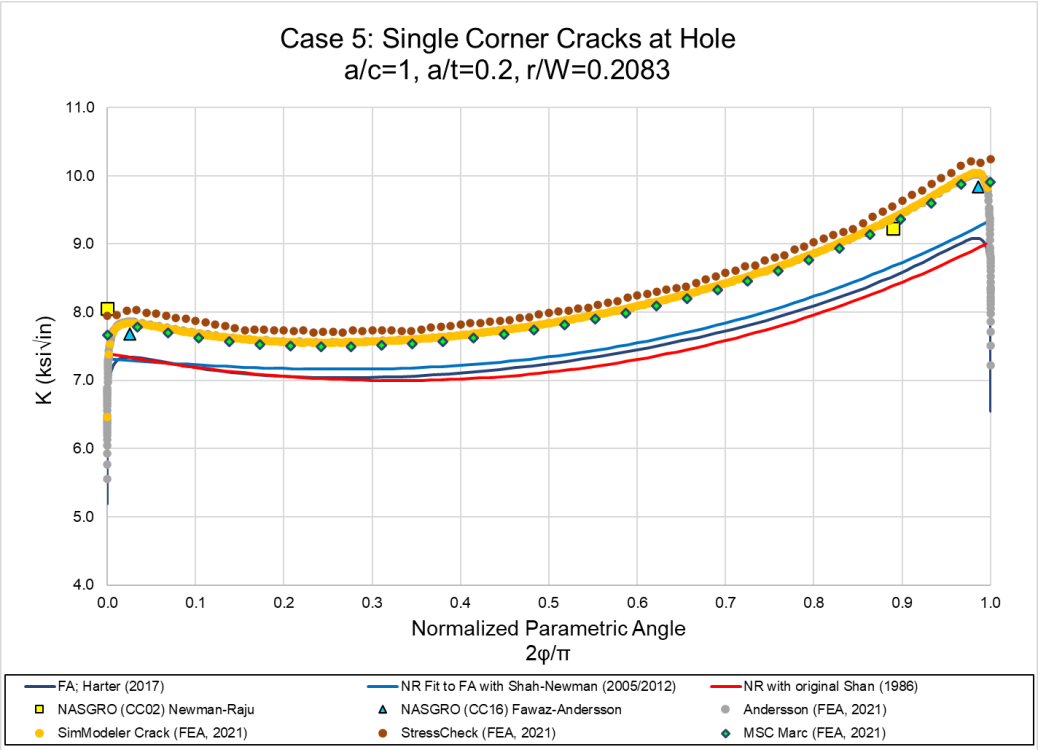

Figure 12: Stress Intensity vs. Normalized Parametric Angle (Case 5)

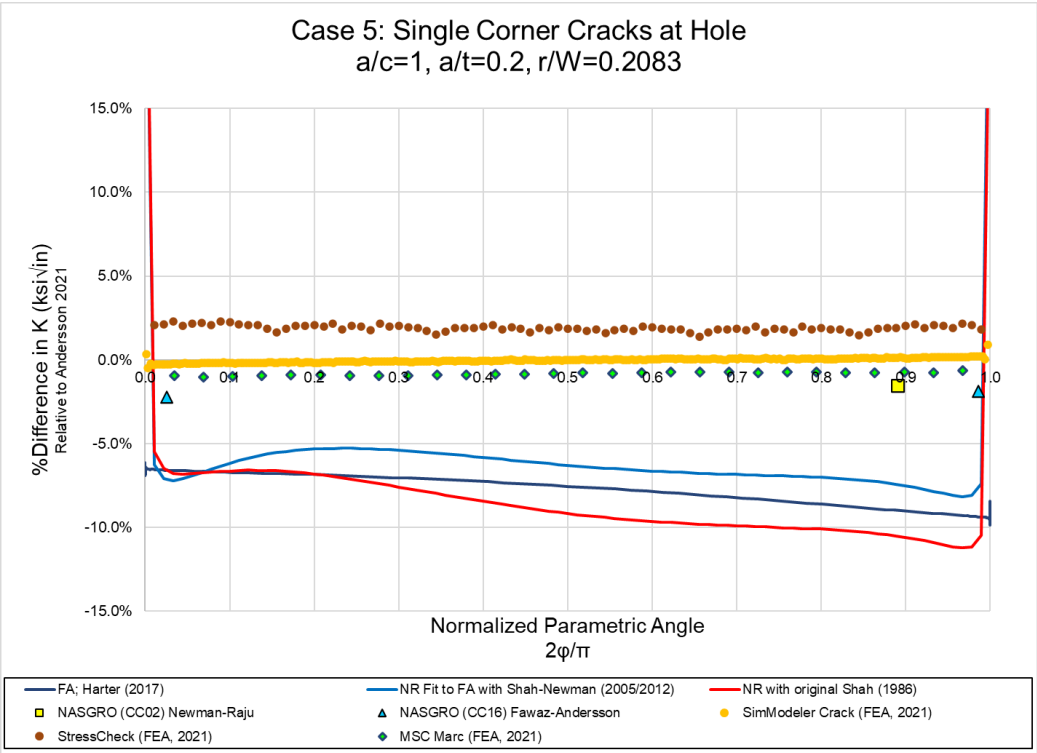

Figure 13: Percent Difference in Stress Intensity vs. Normalized Parametric Angle (Case 5)

4.6. Case 6: Single Corner Crack at a Hole, Infinite Plate, a/c=1.5

Case 6 replicated the configuration for Case 2, an infinite plate with a single corner crack, however, variations in crack aspect ratio were investigated. For this particular case, a crack aspect ratio of *a/c*=1.5 was utilized. A summary of the Case 6 inputs is detailed below in Table 9. Figure 14 and Figure 15 detail the SIF and percent difference for all the submissions, with results generally within ±2% of the Andersson submission, with the exception of near surface points that demonstrated greater divergence. Submission 3 (Newman-Raju 1986) demonstrated a greater range of difference across the crack front, ranging between ±4%. Submission 4 (NASGRO CC02) resulted in differences over 4% for the point representative of the hole bore.

Table 9: Case 6 Input Parameters

Case	6
Configuration	Infinite Plate, Single Crack, a/c=1.5
Crack Configuration	Single Corner Crack
Surface Crack Length (*c*) (inch)	0.050
Bore Crack Length (*a*) (inch)	0.750
Width (inch)	100.00
Thickness (inch)	0.25
Hole Diameter (inch)	0.50
Hole Offset (inch)	50.00
a/c	1.50
a/t	0.30
W/D	200.00
r/t	1.00
r/W	0.0025

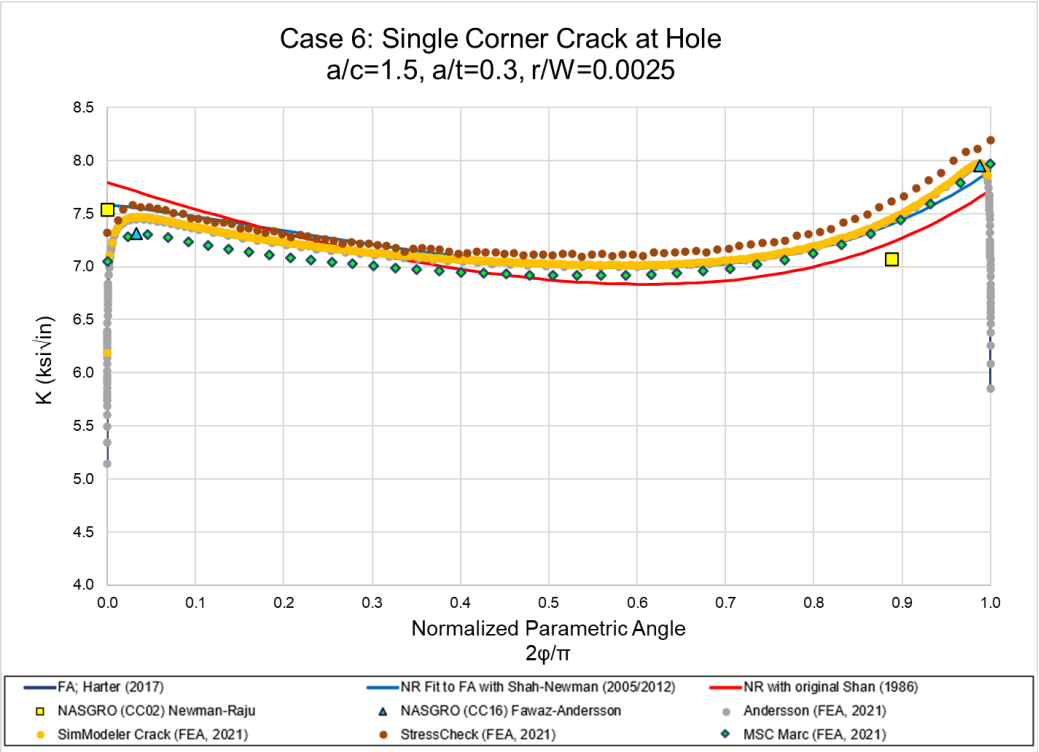

Figure 14: Stress Intensity vs. Normalized Parametric Angle (Case 6)

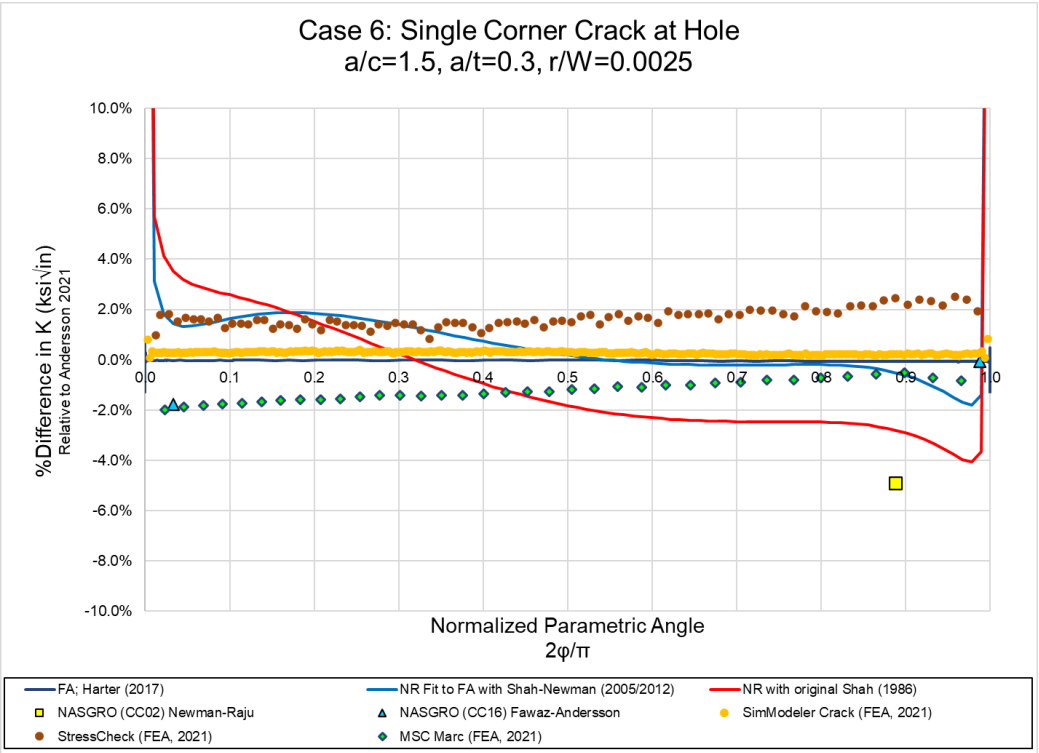

Figure 15: Percent Difference in Stress Intensity vs. Normalized Parametric Angle (Case 6)

4.7. Case 7: Single Corner Crack at a Hole, Infinite Plate, a/c=0.5

Similar to Case 6, Case 7 replicated the configuration for Case 2 but included variations in crack aspect ratio. For this particular case, a crack aspect ratio of *a/c*=0.5 was utilized. A summary of the Case 7 inputs is detailed below in Table 10. Figure 16 and Figure 17 detail the SIF and percent difference for all the submissions, with results generally within ±2% of the Andersson submission, with the exception of near surface points that demonstrated greater divergence. Submission 3 (Newman-Raju 1986) demonstrated a greater range of difference across the crack front, averaging roughly 8% difference. Submission 4 (NASGRO CC02) resulted in differences of 10% for the point representative of the hole bore.

Table 10: Case 7 Input Parameters

Case	7
Configuration	Infinite Plate, Single Crack, a/c=0.5
Crack Configuration	Single Corner Crack
Surface Crack Length (*c*) (inch)	0.100
Bore Crack Length (*a*) (inch)	0.050
Width (inch)	100.00
Thickness (inch)	0.25
Hole Diameter (inch)	0.50
Hole Offset (inch)	50.00
a/c	0.50
a/t	0.20
W/D	200.00
r/t	1.00
r/W	0.0025

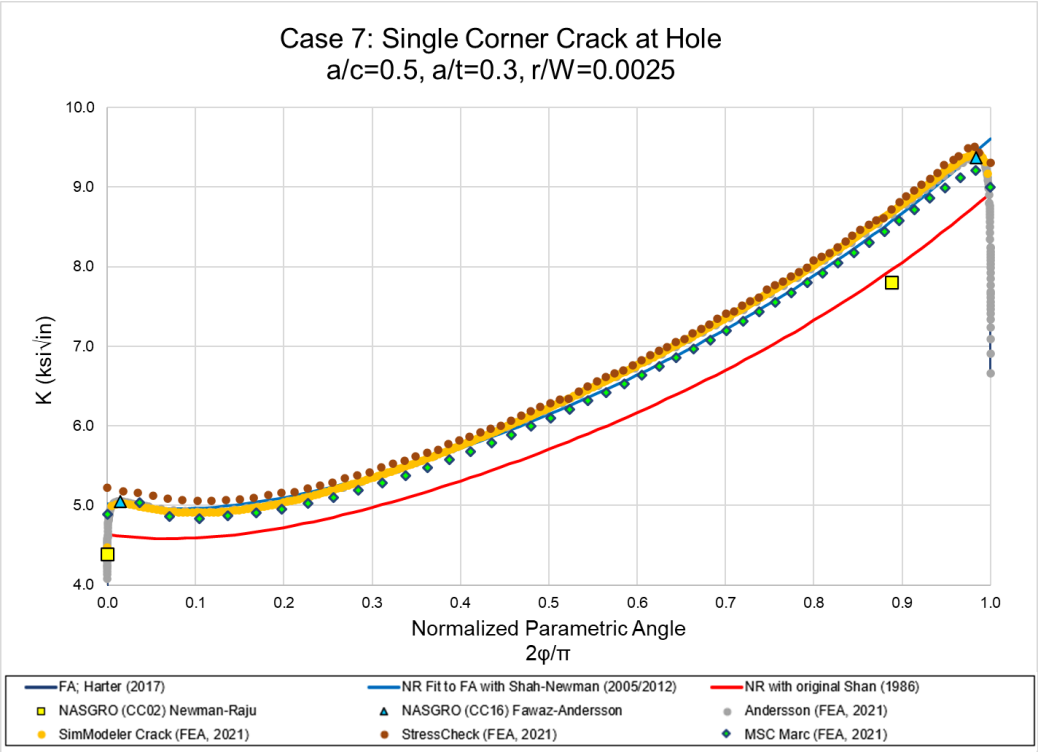

Figure 16: Stress Intensity vs. Normalized Parametric Angle (Case 7)

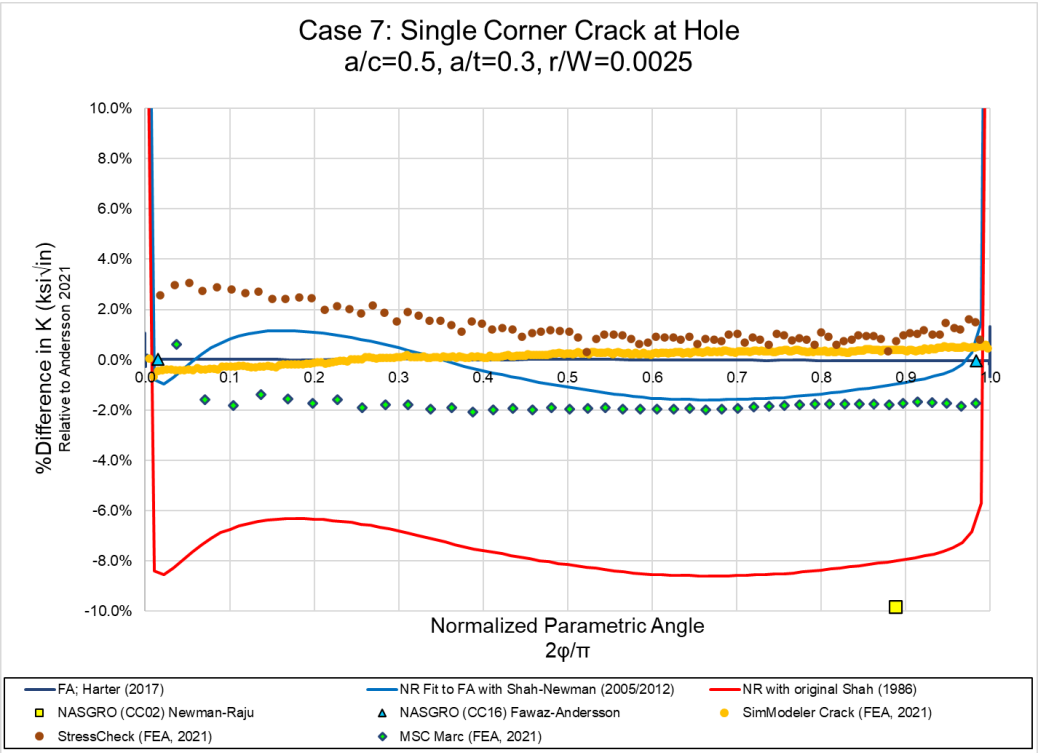

Figure 17: Percent Difference in Stress Intensity vs. Normalized Parametric Angle (Case 7)

5. FOLLOW-ON INVESTIGATIONS

Below is a summary of follow-on investigations resulting from the initial submission of results and subsequent collaboration amongst the participants.

5.1. Case 2 Convergence Study

Two convergence studies were carried in parallel:

- Andersson (Submission 6)
    - Made use of an hp-formulation. The convergence study showed that the original solution (Andersson FEA 2021) delivered March 2021, had a relative K ≤ 0.03% at arbitrary points along the crack front. A solution was then derived with a relative error of order 0.01% along the entire crack front including the vertex regions. This was possible by utilizing the known mathematical behavior of the solution near a vertex. By using a least-square approximation to the calculated p=8 solution (obtained with a fine mesh) two analytical expressions for K near and at the two vertices were obtained which are ~0.01% in error. By using these two analytic expressions and the p=8 solution away from vertices, a very accurate semi-analytical expression for K is achieved which was used for comparison with solutions from Loghin.
- Loghin (Submission 7)
    - Making use of a built-in element formulation in ANSYS and seven uniform meshes (100, 200, 300, 1000, 2000, 3070, 8200 element edges) along the crack front via SimModeler, a follow-on convergence study was completed. SIF values were computed in SimModeler using the displacement correlation technique. The semi-analytical solution derived by Andersson was used as a reference in the convergence study to calculate relative differences for each solution provided in this report. It is demonstrated that, with increased mesh refinement, SimModeler solution is within 0.2% relative difference from Andersson semi-analytical formulation.

5.2. Finite Width Correction

The commonly used Newman finite width correction [6] appears to be incorrect for Case 5. Finite width corrections for several example cases for W/D < 6 were determined from the ratio of these results to wide plate (W/D = 50) FE solutions for the same crack and hole geometries. A wide range of crack aspect ratio (a/c) and hole radius to plate thickness (r/t) values were evaluated in this study. The results for these sample cases indicate that the Newman closed-form finite width correction tends to underestimate the finite width correction for cracks when a/t ~< 0.6-0.8. In addition, this correction is assumed to apply equally to both crack growth directions. FE results for 2 < W/D <= 4 indicate that the difference in the width correction for each growth direction is > 5%. For W/D <= 2, the difference becomes exceptionally large (10 – 25+%). The required finite width corrections are shown with the Newman correction for these cases in Figure 18.

It also appears that the width correction for narrow plates is a function of several parameters (i.e., a/c, a/t, and r/t). This issue should be investigated thoroughly since major modifications are required for the closed-form finite width correction. A modified closed-form solution has been developed to address these issues and will be available for use with AFGROW in the near future.

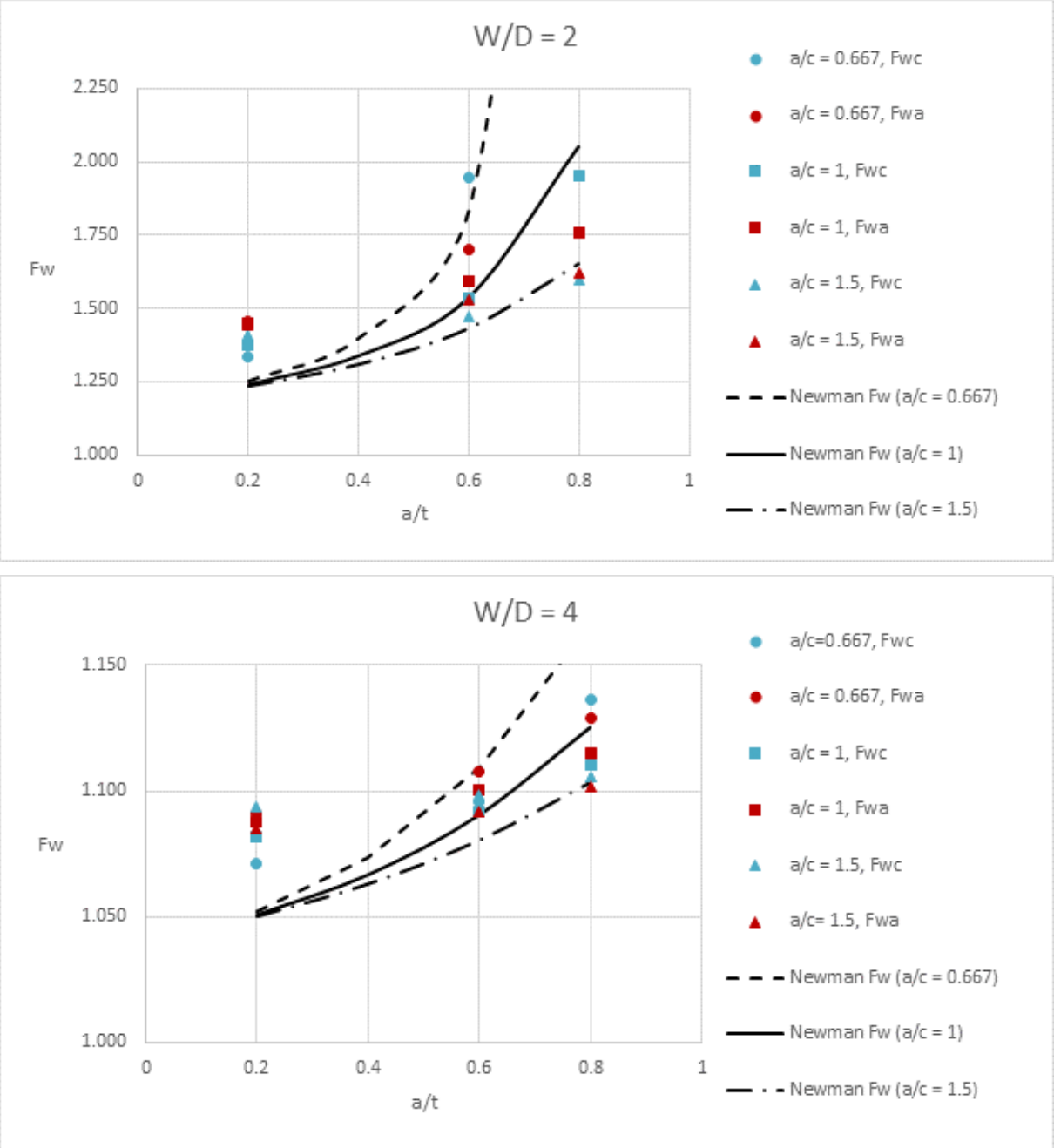

Figure 18: Required finite width corrections for several geometries (r/t = 1)

A few additional cases were analyzed using SimModeler for a different *r/t* and higher aspect ratio cracks to assess the sensitivity of the finite width correction to other geometric parameters. It appears that the width correction for narrow plates is a function of several parameters (i.e., *a/c*, *a/t*, and *r/t*). The additional cases included an extremely narrow plate (*W/D* = 1.5), an example for a narrow plate with *r/t* = 0.5, and two higher aspect ratio cracks (*a/c* = 4 & 6).

The results shown in Figure 19 indicate that *r/t* can have a significant effect on the required finite width correction. For a narrow plate with *W/D* =1.5, *a/c* = 1, *a/t* = 0.4, and *r/t* = 1, there is approximately 17% difference in the finite width corrections for the *a* and *c*-dimensions, with the Newman finite width correction 10 – 25% too low in this case. When *W/D* = 2.0, *a/c* = 1, *a/t* = 0.4, and *r/t* = 0.5, the difference in the finite width corrections is less than 1% while the Newman correction is approximately 7.5% too low.

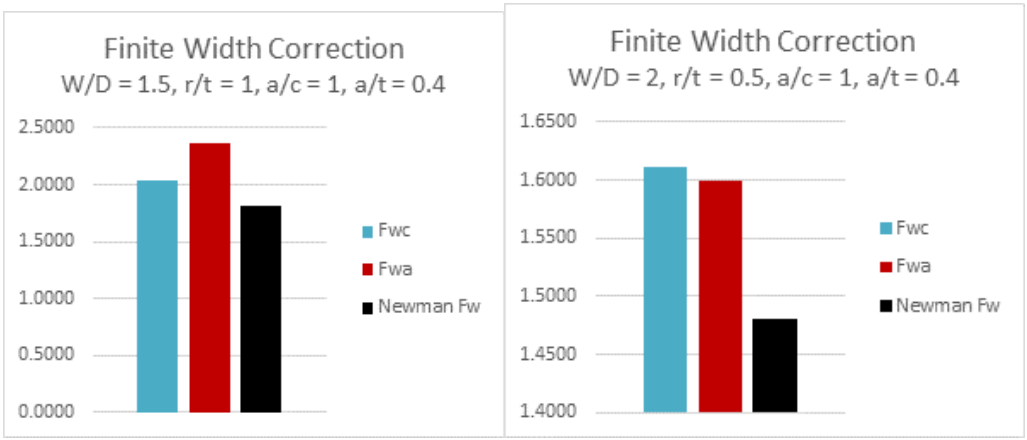

Figure 19: Finite width correction comparisons for narrow plates with a/c = 1, r/t = 0.5 and 1.0

The effect of crack aspect ratio is also very interesting. For the cases shown in Figure 20, the differences between the width correction in each growth direction is relatively minor (~3-5%). The Newman correction tends to be low in all cases, but the magnitude of the width correction switches from being higher in the a-direction for *a/c* = 1 and 2, to becoming lower in the a-direction for *a/c* = 6. This issue should be investigated thoroughly since major modifications are required to correct the closed-form finite width correction.

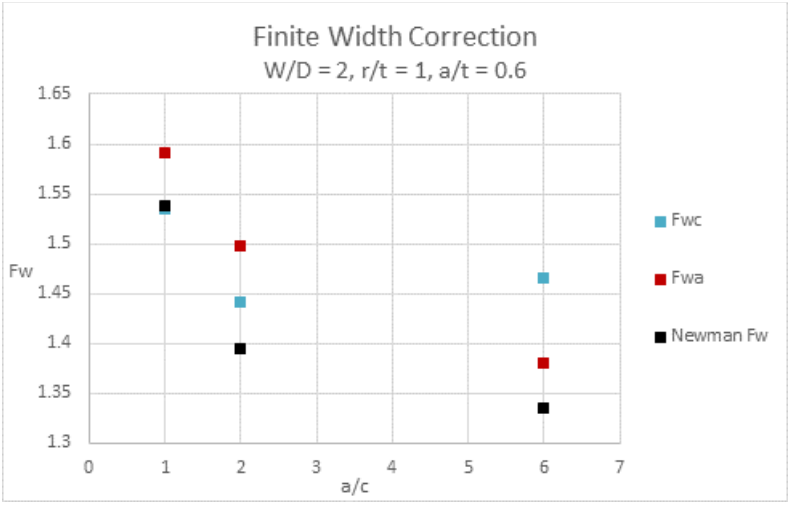

Figure 20: Finite width correction effect of crack aspect ratio

It is recognized that in 2013, Guo [9] developed revised finite width corrections for the a-tip and c-tip values, which could be used as a possible resource. As a follow-on to this round robin activity, Andersson created approximately 23,000 high-accuracy solutions covering the parameter range detailed in Table 11.

Table 11: Finite width analysis parameter range

Parameter	Range
r/t	0.2, 0.333, 0.5. 1.0, 2.0, 3.0 and 5.0
a/t	0.1, 0.2, 0.3, 0.4, 0.5, 0.6, 0.7, 0.8, 0.9 and 0.95
a/c	0.100, 0.111, 0.125, 0.1428, 0.1667, 0.200, 0.250, 0.333, 0.500, 0.667, 0.750, 0.800, 1.000, 1.250, 1.333, 1.500, 2.000, 3.000, 4.000, 5.000, 6.000, 7.000, 8.000, 9.000, and 10.000
W/D	1.6, 1.8, 2.0, 2.2, 2.4, 2.8, 3.2, 3.6, 4.0, 4.6, 5.2, 5.8, 6.4, 7.0, 8.0, 10.0, 12.0, and 15.0

Table 12, Table 13, and Table 14 detail a summary of the error in the finite width correction function (FW_{Newman}) from [6] for the three conditions of r/t= 0.5, 1.0 and 2.0. The relative error in the finite width correction factor near vertex 'a' is defined as:

$$Fw\_Err\_a\left(\frac{W}{D},\frac{r}{t},\frac{a}{t},\frac{a}{c}\right)=\left|\frac{K_{FEM}(\frac{W}{D})}{K_{FEM}(\frac{W}{t}=100)}-FW_{Newman}\right|/FW_{Newman} \quad \text{(EQ 5-1)}$$

and similarly for vertex 'c'. $K_{FEM}(W/D)$ denotes the peak value of K near the vertex 'a'. The blue dots in Figure 21 exemplify values of $K_{FEM}(W/D)$ for r/t=1.0, a/t=0.1, a/c=0.75 for 19 different W/D values. The red dots shown for comparison are the solution from 2017 for W/t=100 [14]. Table 12 shows the error distributions of Fw_Err_a and Fw_Err_c for r/t=1.0 (a total of 3656 conditions were analyzed) in the form of histogram data. It was observed that 55% of the 101 analyzed plates for W/D=1.6 have an error of 25%-40% at vertex 'a'. Table 12 also shows that the error at the 'a'-vertex is generally much larger than at the 'c'-vertex. Table 13 and Table 14 details similar results for conditions of r/t=0.5 and 2.0.

The blue line in Figure 13 (FA, Harter (2017)) shows errors of about 7 and 9% at vertices 'c' and 'a', respectively. The K-solution from 2017 [14] has an error in K of 0.03%. This indicates that the obtained errors of 7-9% are entirely due to the finite width correction factor. The line W/D=2 in Table 12 (Case 5 benchmark) shows that the error at vertex 'a' is between 7%-15% in 38% of the conditions analyzed. Similarly, the error at vertex 'c' is between 7%-15% for 40% of the 130 conditions analyzed.

Table 12: Error distribution of finite width correction factors at vertex 'a' and 'c' for r/t=1.0

	Error a-vertex						Error c-vertex						# of
W/D	0-1%	1-3%	3-7%	7-15%	15-25%	25-40%	0-1%	1-3%	3-7%	7-15%	15-25%	25-40%	Conditions Analyzed
1.6	2	6	8	13	17	55	5	7	11	20	32	26	101
1.8	4	7	12	17	55	8	6	11	16	35	34		117
2	7	8	10	38	39		10	12	24	40	15		130
2.2	8	8	17	62	7		10	17	35	40			143
2.4	9	12	26	53	2		12	25	38	27			156
2.8	14	19	46	22			21	36	39	5			170
3.2	18	24	55	5			25	46	30				184
3.6	21	35	40	4			36	46	19				191
4	27	47	23	3	1		44	51	6				197
4.6	36	56	7	2	1		57	42	2				200
5.2	44	49	6	1	1		69	30	1				204
5.8	54	40	5	1	1		79	21	1	1			210
6.4	65	28	5	2	1		85	14	2				217
7	80	12	6	2	1		93	6	2				221
8	84	8	5	4			92	6	2				228
10	84	7	5	4	1		91	6	4				240
12	83	8	5	4	1		91	6	3	1			247
15	86	7	4	3	1		93	5	3				250
100	100						100						250

Table 13: Error distribution of finite width correction factors at vertex 'a' and 'c' for r/t=0.5

	Error a-vertex						Error c-vertex						# of
W/D	0-1%	1-3%	3-7%	7-15%	15-25%	25-40%	0-1%	1-3%	3-7%	7-15%	15-25%	25-40%	Conditions Analyzed
1.6	5	7	7	11	20	54	2	1	7	14	40	41	77
1.8	6	7	11	24	37	19	3	1	12	34	50	4	89
2	7	12	14	26	44	1	3	10	10	58	23	1	98
2.2	8	12	21	52	9		1	13	19	62	7		104
2.4	9	16	21	54	2		7	13	34	46	3		113
2.8	12	19	43	26	1		8	20	51	23			123
3.2	13	28	55	3	3		13	36	37	15			139
3.6	20	39	37	4	2	1	17	51	19	14			154
4	22	52	23	5	1		22	61	5	13			162
4.6	31	58	9	3			34	54	13				170
5.2	38	50	9	4			52	37	12				181
5.8	49	38	9	5			67	22	11				188
6.4	59	30	8	4	1		80	10	11				194
7	76	14	8	2	1		87	3	11				197
8	81	12	6	2			88	2	11				198
10	84	10	5	1	1	1	87	3	10				208
12	84	9	5	2	1		85	4	1	10			217
15	84	8	5	3			85	5	2	9			228
200	100						100						250

Table 14: Error distribution of finite width correction factors at vertex 'a' and 'c' for r/t=2.0

	Error a-vertex						Error c-vertex						# of
W/D	0-1%	1-3%	3-7%	7-15%	15-25%	25-40%	0-1%	1-3%	3-7%	7-15%	15-25%	25-40%	Conditions Analyzed
1.6	1	5	11	15	23	47	4	8	13	28	25	24	143
1.8	3	8	11	27	45	8	8	12	22	28	30	2	164
2	4	14	15	39	30		12	16	27	33	14		173
2.2	6	14	22	55	5		12	20	31	38			188
2.4	9	16	27	47	1		16	22	34	29			195
2.8	14	24	42	20	1		21	31	37	12			200
3.2	18	32	50	1	1		27	39	34				205
3.6	25	39	35	1	1		33	44	23	1			214
4	32	44	21	3	1		39	50	12				221
4.6	39	52	6	4	0		49	47	5				229
5.2	48	42	6	4	1		60	35	6				237
5.8	58	32	6	4	2		69	26	5	1			243
6.4	70	20	5	4	2		81	15	4	1			247
7	82	9	5	3	2		87	8	4	1			249
8	85	7	5	3	1		90	7	3	1			250
10	88	7	4	1			94	5	1				250
12	91	7	3				96	4					250
15	94	6	1				99	1					250
50	100						100						250

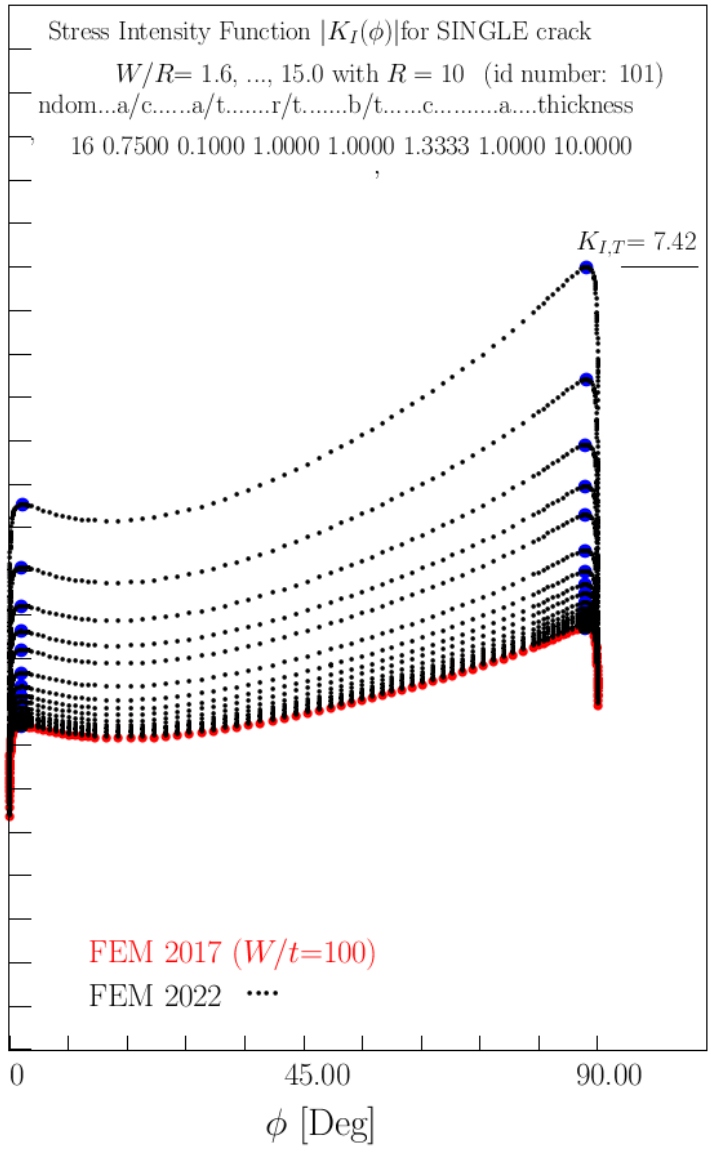

Figure 21: Andersson updated finite width solutions; 19 variations of W/t shown

5.3. Submission 8 (StressCheck FEA) Updated Meshing Routine and Associated Results

Nervi completed a follow-up submission to exemplify an approach used when an organization want to have handbook quality solutions for a wide range of cases, using a parametric model approach which can be used by the non-expert and are computationally efficient.

Since the original submission intended to represent the typical approach in engineering practice for more complex problems it used an automesh strategy. As noted in Section 3.8 a target estimated error of 2% on the computation of SIF factor was used, however, higher accuracy could be achieved by increasing the mesh refinement but at the cost of increased computational effort.

Alternatively, all use cases could be cast on a single parametric file with guided mesh (creation of a 'parent' coarse mesh followed by automatic h-discretization). The advantage of this approach is that

high accuracy can be achieved with minimal computational effort. For this study we targeted an estimated error of less than 0.5% on the SIF, taking less than a 1 minute to produce a sequence of solutions of increasing number of degrees of freedom by p-extension and to extract the SIFs along the crack front for each case.

In StressCheck the computation of the SIFs is performed using the Contour Integral Method described in [12]. Convergence in the estimated error in energy norm (global) and local convergence on SIF were obtained from a hierarchic sequence of solutions computed using uniform p-extension (from p-level 3 to 5 for automeshes, and 6 to 8 for guided meshes). Note that if the initial mesh refinement and p-extension does not converge within the target error, further refinement is added (h-extension) and a new sequence of solutions (p-extension) is computed. This process (hp-extension) is repeated until convergence with respect to the set tolerance is achieved.

For details on the recommended approach for computing SIF in StressCheck refer to [11].

The mesh for Case 1 is shown in Figure 22. Figure 23 and Figure 24 details an example of global and local convergence and error estimation study. The error estimation is performed using a conservative estimator based on the behavior of the solution projecting the degrees of freedom to infinity. This approach allows users to obtain accurate conservative error estimates without knowing the exact solution. Similar studies were performed for Cases 2 to 7 and are included in the Appendix.

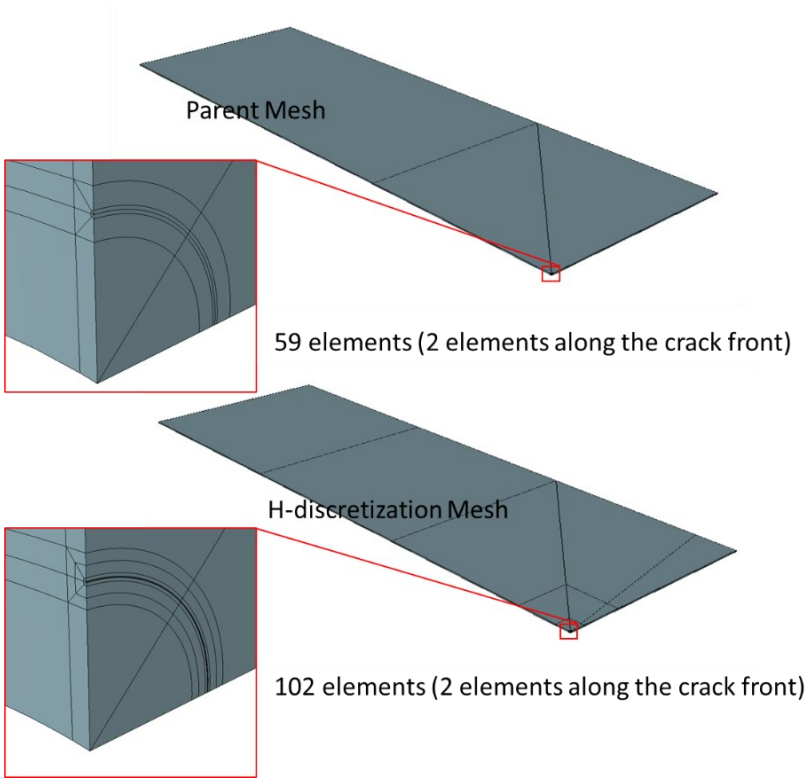

Figure 22: Guided mesh for Case 1. Symmetry boundary conditions used on both midplanes across the thickness. Note that only two element edges are used along the crack front.

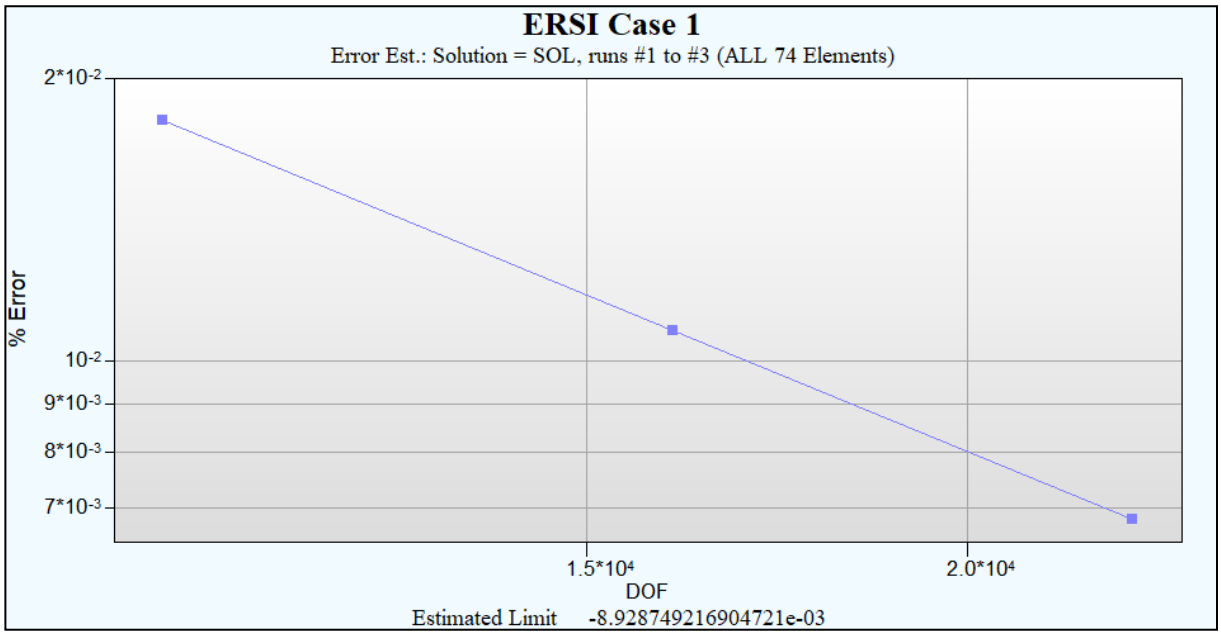

Figure 23: Convergence of the estimated relative error in energy norm.

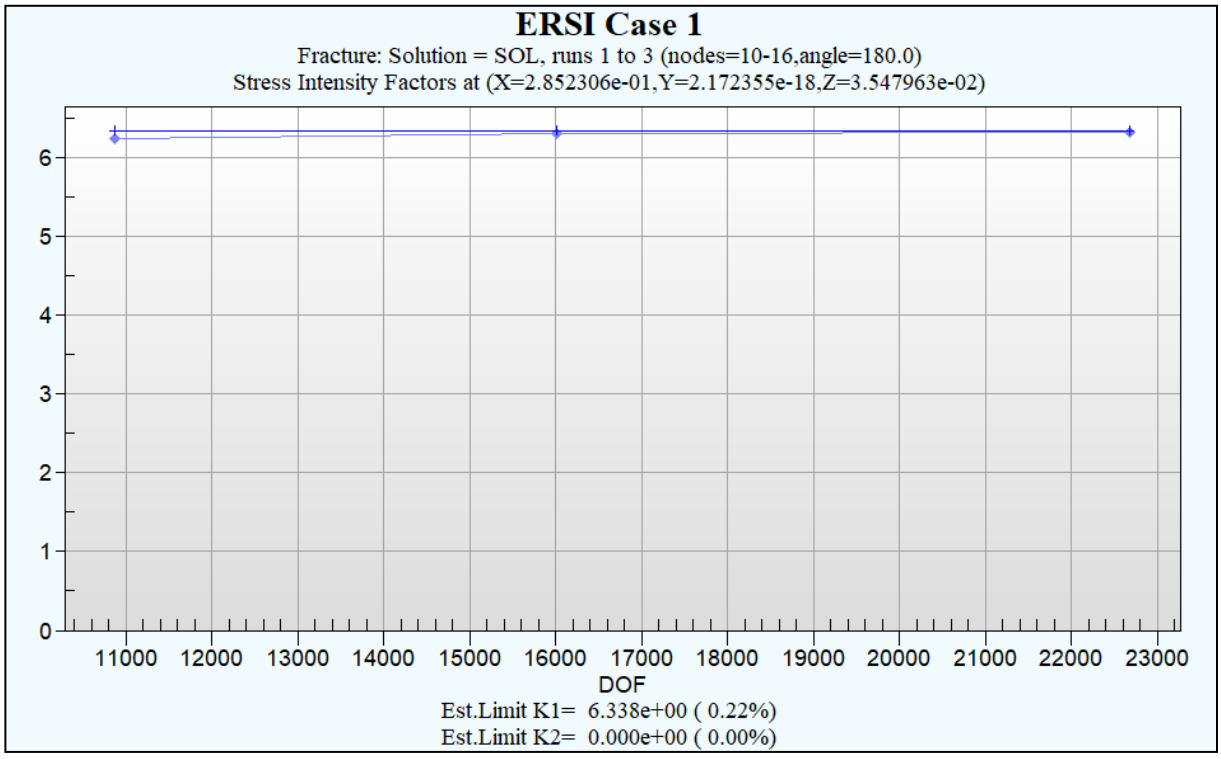

Figure 24: Convergence of KI for an arbitrary location, for a sequence of hierarchic solutions computed with uniform p-extension (p = 6 to 8).

Figure 25 and Figure 26 show the extraction for Mode I SIF along the crack front compared with the Andersson reference solution (also computed using hp-extension). Note that in StressCheck any number of points can be used for extraction, for this case 200 points were extracted along the crack front. Additional comparisons for Cases 2-7 are included in the Appendix.

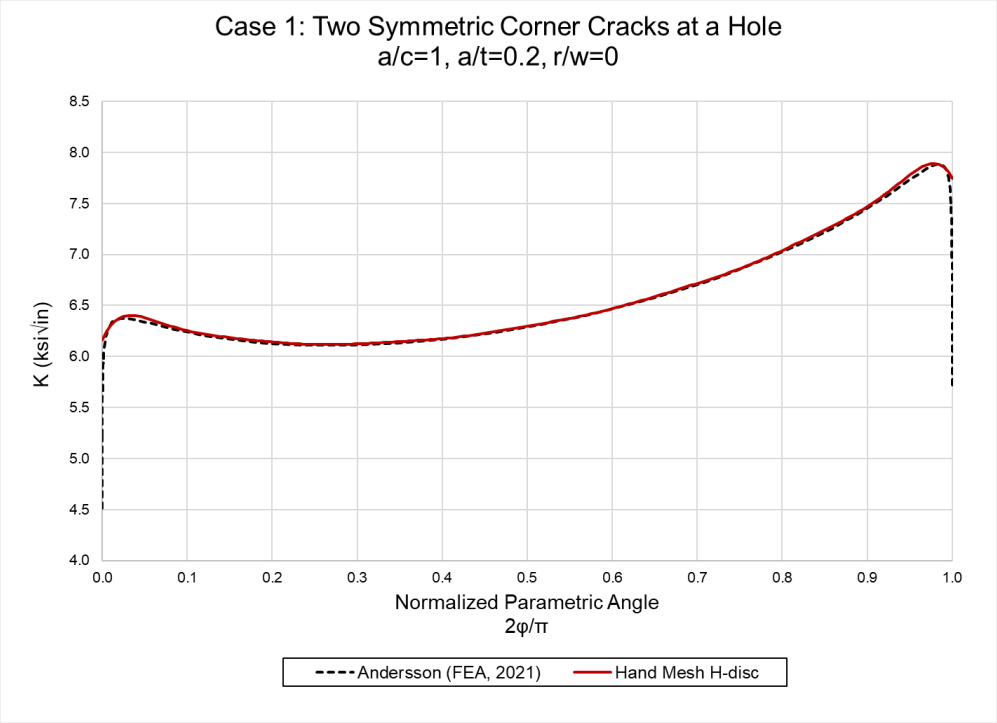

Figure 25: Comparison of SIF extraction along crack front with Andersson reference solution for Case 1

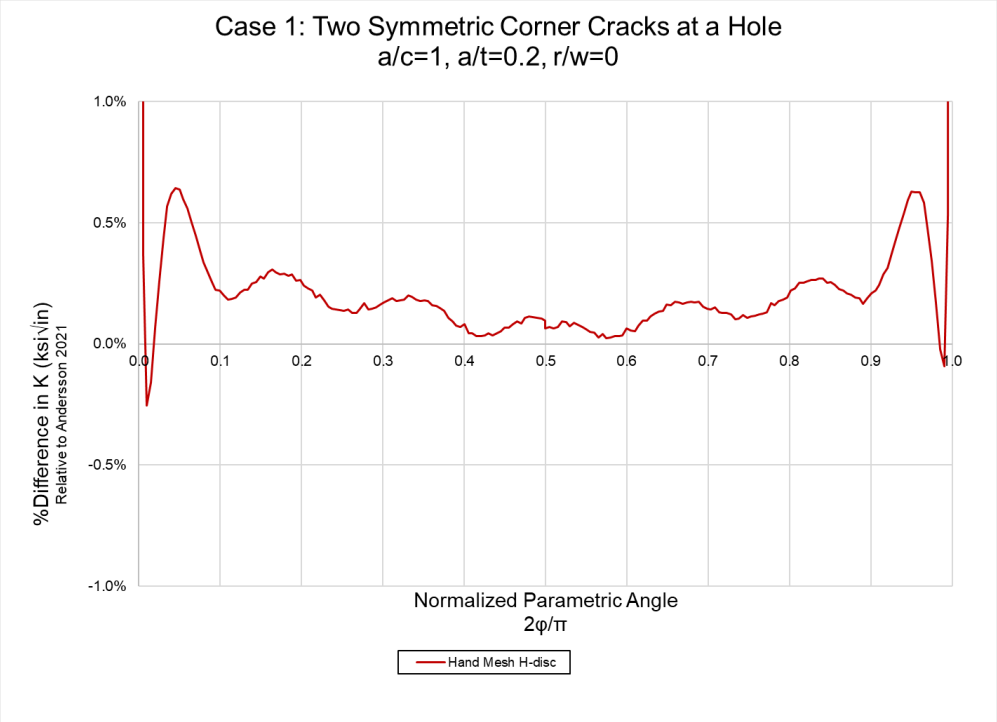

Figure 26: Percent difference comparison of SIF extraction along crack front with Andersson reference solution for Case 1

6. SUMMARY AND CONCLUSIONS

The following sections include a summary of each submission as well as an overall summary of the findings from the round robin.

6.1. Individual Submission Findings

6.1.1. Submission 1: Fawaz-Andersson Solutions, AFGROW

The Fawaz-Andersson solutions in AFGROW are interpolated directly from the digital data provided by BARE and are shown to be in excellent agreement with the most recent solutions provided by BARE for this study for the centered hole, infinite plate case. However, the Newman closed-form finite width correction [6] appears to be in error when W/D < 6. The errors become progressively more significant when W/D <= 4 and can been seen in the results shown for the narrow plate case (Case 5). These errors also impact the offset hole case (Case 4) since it is based on the solution for a centered hole with a width of twice the near edge distance and the application of an additional offset hole correction. Subsequent finite element analyses have shown that errors in the finite width solution are a complex function of W/D, a/c, a/t, and r/t. An improved finite width correction has been developed for AFGROW and will be included in the next major release.

6.1.2. Submission 2: Newman-Raju Fit to Fawaz-Andersson

The results are within 2% for all cases except case 4 (about 6% maximum error) and case 5 (about 8% maximum error). This is an improvement on the earlier Newman-Raju [6] solutions, and is due in part to the improved single crack correction. Solutions accurate to within 2% are considered acceptable for most analyses, but errors of 6-8% are larger than desired for a reliable analysis. The errors for Cases 4-5 are likely the result of limitations in the finite width correction. Improved finite width corrections are discussed in this report and if applied they would improve the accuracy for the Submission 2 results.

6.1.3. Submission 3: Newman-Raju (1986)

Submission 3 used the original stress-intensity factor (SIF) equations developed by Newman and Raju [6]. These equations were developed from finite-element analyses conducted by Raju and Newman [21] for two symmetric corner cracks at a hole. Case 1 had two-symmetric corner cracks, but all the others (Cases 2-7) had a single corner crack. Since the SIF equations were for two-symmetric corner cracks at a hole, a correction factor was needed to account for the single corner crack cases (2-7), the original correction developed by Shah [7] in 1976 was used.

The finite width (F_w) correction factor equation from Newman-Raju [7] was used where applicable (Cases 3, 4 and 5). Cases 1, 2, 6 and 7 are for an infinite width plate.

For all cases, the circular hole was in the center of the plate, except for Case 4 which has the offset hole. The single crack in the offset case was located on the short ligament side. That offset hole case (Case 4) was assessed in two separate ways as follows:

1. The offset distance from the hole center to the nearest edge is 0.6 inches. This first option was to assume the total width was 1.2 inches and the hole is in the center. This is a conservative option and is expected to produce stress intensity factors that are higher than the actual values.
2. The second option was to also assume a central hole in a finite width plate but modify the width such that the stress concentration at the edge of the hole at the location of interest (shortest ligament side) matches the correct stress concentration for the offset hole geometry. This was found to be a total width of 1.43 inches. The “true” total width is 4.0 inches, with the hole offset to one side such that the distance from the center of the 0.5-inch diameter hole to the closest edge is 0.6 inches. This is modelled as a 1.43-inch-wide plate with a 0.5-inch diameter central

hole, which will produce the same stress concentration at the location of interest. This option is expected to produce a more accurate solution than option 1.

In summary, for Cases 1, 2, 3, 6 and 7, the Shah [7] and finite-width [6] correction factors were not an issue (about 1 or 2% for Case 3, respectively); and the primary differences were attributed to the original Newman-Raju equations. In comparison to the very accurate Fawaz and Andersson [3] solutions, Cases 1 and 2 were within 2%, while Case 3 was within 3%. Case 2 was very much like the Cold-Worked-Hole Round Robin crack configuration (without residual stresses), which would indicate that the Newman-Raju equations were not the reason for the no-crack-growth issue. Case 4, corner crack at an offset hole, had large differences (-5 to -9%) from the Newman-Raju equations using the matching stress-concentration factor approach. Using the short edge distance as the half-width would have given an over estimation of the K-solutions. Only Case 5 with the large hole-diameter-to-width (D/W) ratio indicated that more work is needed on the finite width correction factor equation. The original finite width correction factor equation had a correction for both hole stress concentration and finite width. Case 5 had large differences (-7 to -12%) and Case 6 had +/- 4% differences with the Fawaz-Andersson [3] results. Also, Case 7 had large differences (-8%) with the more accurate results.

6.1.4. Submission 4: NASGRO (CC04 & CC02): Newman-Raju

For comparison purposes, the NASGRO (CC02) and (CC04) solutions were included in the round robin exercise, however, this solution has been superseded by CC16 and is not recommended for use. The comparisons shown for the a-tip provide evidence to no longer use the CC02 and CC04 solutions.

6.1.5. Submission 5: NASGRO (CC16): Fawaz-Andersson

Parametric angles for the a-tip and c-tip CC16 SIF values were provided that correspond approximately with the maximum SIF values from the Andersson (2021) solutions. This is the best way to make an apple-to-apples comparison with the Andersson (2021) solutions and is consistent with the CC16 development based on the earlier Fawaz-Andersson solutions. These parametric angles were generally from 1 to 3 degrees from the surface depending on the case considered. In NASGRO, for engineering purposes, the single (local maximum) values computed at the offset angles are assigned to 0 and 90 degrees.

6.1.6. Submission 6: Andersson: FEA (2021)

BARE has delivered several 100 million accurate K-solutions to the USAF Academy under contracts since 2003, which now are available in AFGROW and NASGRO. The method used for K-calculation was developed 30 years ago and is discussed in detail in the Appendix. A strongly graded mesh towards and along the crack fronts are used (hp-version FEA). All these meshes are designed to give relative errors of order ~0.03% along the entire crack front. These K-solutions follow the functional behavior $K=const*s^{0.04782}$, s being the distance to the vertex, and are very accurate in a large region near the vertex so '*const*' can easily be determined in each of these millions of solutions leading to analytical formulas for K(s) near vertices. Note that for countersunk hole geometries K often goes to infinity near vertices. In such cases it is practical to express the solution near the vertex as a constant, for example *const*=10 in $K=const*s^{(-0.10)}$.

For the seven benchmark cases discussed in this report, standard procedures were utilized for K-calculation. The relative error in K_I in all seven solutions $\leq$ 0.03%. In an extra effort, detailed convergence studies for Case 2 were performed and compared to the Loghin high accuracy solutions obtained with highly refined meshes (see the Appendix). For Case 2, the estimated error on the order of 0.01%, which was 30-200 times smaller than the error in all other participants FE-solutions obtained by direct comparison. As a result of these convergence studies, this submission was utilized as the reference solution for all submission comparisons completed in Section 4.

In an ongoing project BARE is presently deriving of order 10^5 accurate K-solutions for a single crack. The solutions cover a large (R/t, a/t, c/a, W/D)-space well for the three loading cases tension, bending and pin loading. The width/ratios considered are W/D=2.4, 2.8, 3.2, 3.6, 4.0, 4.6, 5.2, 5.8, 6.4, 7.0, 8.0,10.0, 12.0, 16.0, 20.0 and 30.0 (for a definition of W and D, see Figure 1). Hence, accurate K-data for single cracks will be available at the end of 2022.

6.1.7. Submission 7: SimModeler Crack: FEA (2021)

SimModeler Crack was employed to create 3D finite element models and compute Mode I SIF values for the benchmark problems considered in this study. SimModeler Crack follows an integrated CAD to FEA modeling procedure which allows users to easily adopt it in their design and life assessment process. Any SimModeler Crack user can duplicate the results provided in this submission. CAD representation of each benchmark model was used to define the crack, create the associated mesh, apply boundary conditions and loading using geometric entities. For all cases, ANSYS was used as a solver. SIF values (all three modes) along each crack front are computed by SimModeler. For each case, stress and displacement contours along with Mode I SIFs are provided for a detailed release of the results and a potential reference data for other studies.

In Case 2, six models containing different mesh refinement along the crack front were considered for a convergence study. The densest crack front mesh contains 8,200 element edges. It was shown that:

- With increased crack front mesh density. the Mode I SIF solution is convergent
- The converged solution is within 0.2% average relative difference from Andersson's semi-analytical solution (details in the Appendix)
- Even though different techniques and formulations were used to compute SIFs, solutions matched the results from Andersson within 0.2%. A comparison between the two solutions is provided in Figure 27, with results and comparisons for the other cases included in the Appendix.

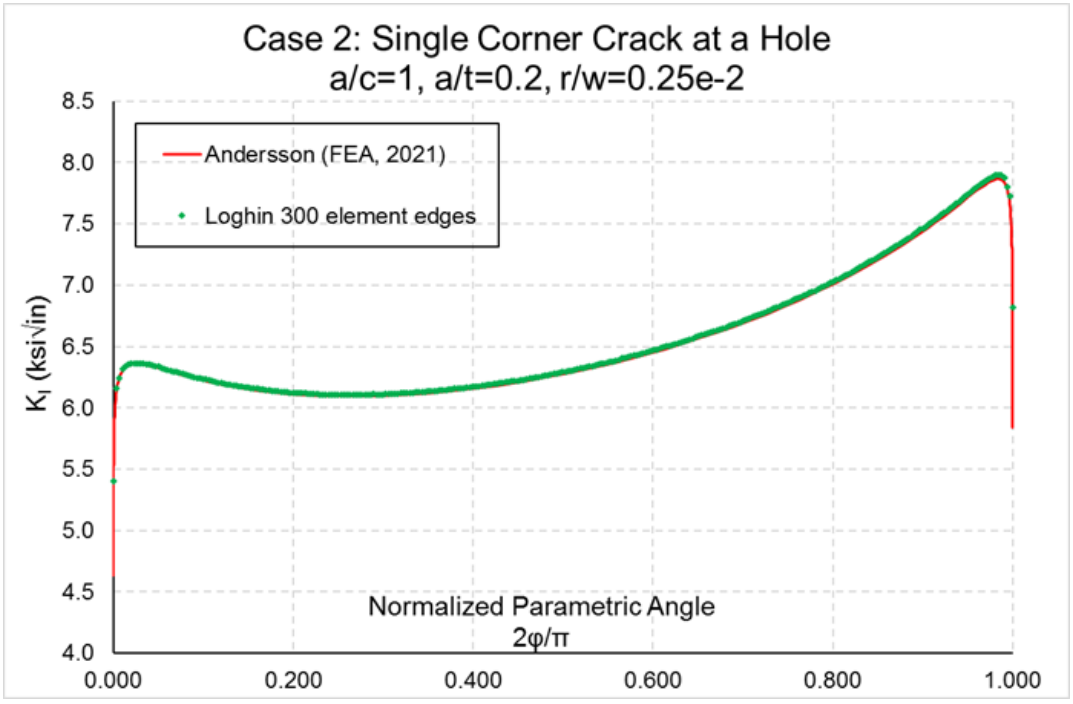

(a)

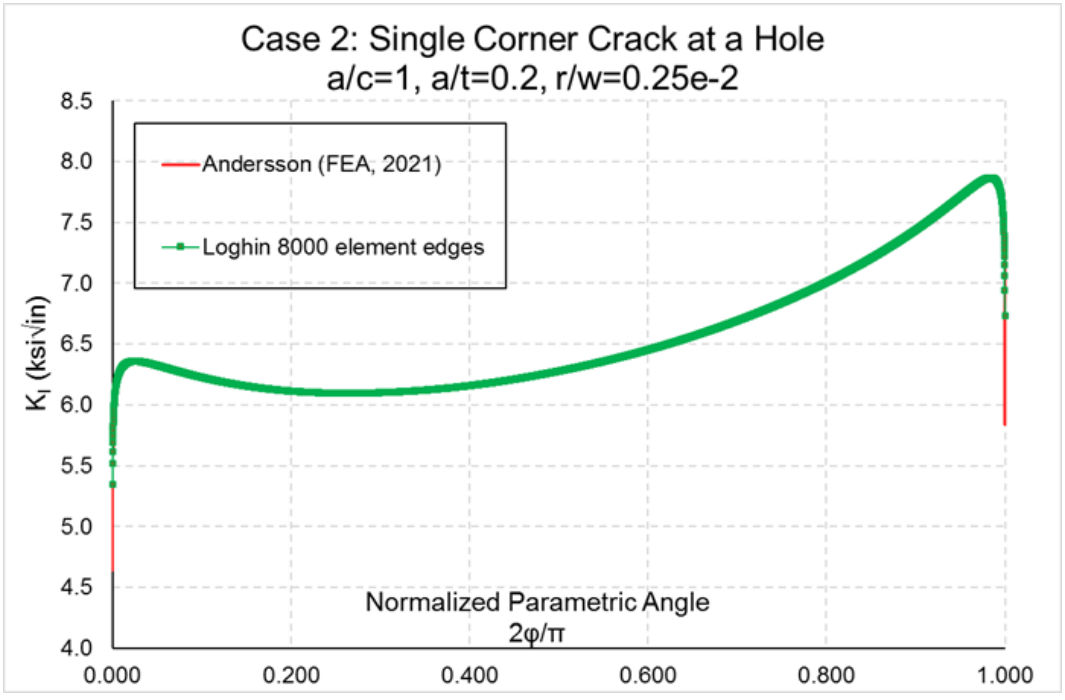

(b)

Figure 27: Case 2 comparison between Andersson semi-analytical formulation and two solutions provided in Submission 7; (a) 300 uniform size element edges along crack front were used, (b) a uniform mesh containing 8000 element edges was employed to compute Mode I SIFs

6.1.8. Submission 8: StressCheck: FEA (2021)

ESRD interpreted the objective of this round robin as establishing a reference and a framework for engineers when using these tools for computing SIFs in an industrial setting. Since the desired accuracy depends on the goal of the analysis, having the feedback information in the form of a reliable estimate of the relative error in the quantity of interest is an essential technical requirement. In addition, users must be provided means to reduce the relative error at the expense of a reasonable amount of additional computational effort, when necessary. The error of approximation was evaluated from a converging sequence of solutions obtained by p-extension on a fixed mesh. No prior knowledge of an exact solution or the reference results provided herein were used for error estimation, as such information is not available in industrial applications.

StressCheck is a detail oriented Finite Element software based on the p-version of the finite element. It is the first commercial finite element software product designed to support verification and validation in computational solid mechanics, allowing the user to access the quality of the computed solution with respect to predefined tolerances.

In this exercise, two sets of results were submitted. The first set was generated targeting a tolerance of 2% estimated error for the computation of mode I SIF. It was used to demonstrate the typical process followed in engineering practice for more complex problems where the exact solution or a reference solution is not previously known. In the second set, a specific tolerance of 0.5% was set. This tolerance is more typical to what within StressCheck is referred as a “handbook model”. “Handbook models” are models of simple geometry that are used as reference solutions and can be solved for a wide range of geometric values, materials, and load values and entered as typical handbook entries.

6.1.9. Submission 9: Marc: FEA (2021)

Marc is a general purpose commercial non-linear solver with special capabilities for crack initiation and crack growth using automatic remeshing, with a focus on ease-of-use for the user. Model setup was done using solid geometry, both for the plate and the crack location, and was accomplished in just minutes. The crack and refined mesh is automatically created inside the Marc solver. A special focused mesh with very regular mesh is used around the crack. VCCT was used for the SIF evaluation. Alternatively, the more accurate J-integral can be used (which typically is more accurate for the same mesh). However, the J-integral was not used in this study.

The cracks in the mesh are generated in an automated fashion starting from a mesh without cracks. A remeshing procedure is used for generating the mesh containing the cracks. No assumption was made about an exact solution. Standard lower order tetrahedral elements were used, and the analysis takes only a minute to run on a laptop. The mesh for the crack evaluation was generated automatically, using the recommended minimum number of evaluation point of 30 as the number of nodes along the crack front. Despite the relatively coarse mesh, results are within 2% thanks to the regular mesh. However, there is definitely a need to utilize a finer mesh to resolve the solution near the ends. One could easily bias the edge lengths towards the ends to accomplish this. Or if needed, the crack can also grow, and the refined region will follow the crack. No convergence study with increased mesh size was attempted.

6.2. Overall Round Robin Summary and Conclusions

This report details a comprehensive investigation into some common stress intensity solutions available in commercially available software such as AFGROW and NASGRO compared with explicit Finite Element Modelling (FEM). FEM can provide a highly accurate solution, but the closed form equations or tabular look up methods used in software such as AFGROW and NASGRO are very important because they allow users to conduct analyses for a range of geometry and crack scenarios. An explicit FE model for every case may not be practical. The investigation has quantified the difference/error for

the cases considered.

The overall summary and conclusions include:

- Successful SIF comparisons completed utilizing a wide array of available solutions and toolsets, with submissions provided by (8) different participants
- Overall, results were within 2% of the reference case, however, deviations were observed for narrow width and varying aspect ratio cases exceeding 10% in some cases
- Significant discrepancies were discovered with commonly utilized finite width corrections from [6], with differences/error up to 10%
- Follow-on actions are in work to resolve discrepancies uncovered by the round robin effort
- A robust dataset was developed that can be utilized as a reference set for follow-on studies
- Comparisons between varying FEA approaches have highlighted the opportunity to identify modeling best practices and provide guidance to the community

This report is accompanied by an Excel file containing all K_I datasets submitted in this round robin challenge.

7. RECOMMENDATIONS

- Accuracy of the crack propagation life assessment is dependent on the accuracy of the computed SIF values. Due to numerical error accumulation, a lack of accuracy in calculation of SIF values might lead to a large error in the predicted loading cycles. More effort must be allocated to determine implementation errors or, sources of numerical variability across different implementations.
- In fatigue crack growth round robin challenges, differences in Mode I SIFs might be a large contributor to the scatter associated with numerical predictions from all participants. This uncertainty source needs to be addressed along with other numerical uncertainties (for example the elliptical crack front assumption).
- More round robin challenges should be considered for advancing the knowledge of the entire damage tolerance design community. Simple geometries with more complex loading conditions as well as component level geometries should be considered in future challenges.
- Additional work should be initiated to resolve the issues discovered with the Newman finite width correction.
- Analysts wanting to use the closed form equation approach should strongly consider using the "Shah-Newman correction (2020)" to correct for a single crack from a double symmetric crack case, using the updated equations detailed in [5].

8. REFERENCES

1. R. Pilarczyk, et al, “Successful Round Robin Analyses Resulting from the Engineered Residual Stress Implementation Working Group”, Materials Performance and Characterization, ASTM, DOI: 10.1520/MPC20190210.
2. R. Pilarczyk, “Lifing Methods and Experimental Validation of Engineered Residual Stress, in Proceedings of the 2019 Aircraft Structural Integrity Program (ASIP) Conference (San Antonio, TX: Universal Technology Company, 2019).
3. S.A. Fawaz, B. Andersson, Accurate stress intensity factor solutions for corner cracks at a hole, Engineering Fracture Mechanics 71(9) (2004) 1235-1254.
4. Harter, James, A. “AFGROW User’s Guide and Technical Manual, Version 5.3”, Section 3.2.3.1.1.5. <https://afgrow.net/DocumentHandler.ashx?name=AFGROW_Technical_Manual_and_Users_Guide_5-3-5-24.pdf>
5. Newman, J.C., Jr., Evaluation of Structural Integrity Analysis Methodologies for Corrosion Prediction Models, Final Report S&K Technologies, Inc., July 2005 (Revision June 2012).
6. Newman, J. C., Jr. and Raju, I. S., “Stress-intensity Factor Equations for Cracks in Three-Dimensional Finite Bodies Subjected to Tension and Bending Loads,” Computational Methods in the Mechanics of Fracture, Vol. 2, S. N. Atluri (ed.), 1986, pp. 311-334.
7. R.C. Shah, Stress Intensity Factors for Through and Part-Through Cracks Originating at Fastener Holes, in: J.R. Rice, P.C. Paris (Eds.), ASTM International, West Conshohocken, PA, 1976, pp. 429-459.
8. Yeh, F., Mettu, S.R., and Forman, R.G., “Stress intensity factors for a through crack from an offset hole in a finite plate by boundary element method,” Johnson Space Center, Tech. Rep. JSC-29835, 2000.
9. Y. J. Guo, “Finite width correction and hole offset correction for one corner crack at an offset hole in a finite plate,” NASGRO, Houston, TX, USA, Tech. Rep. Internal, 2013.
10. M. Watkins. Pros and Cons of 3D Crack Growth Simulation using Finite Elements. ASIP Conference 2017, Jacksonville, FL.
11. https://www.esrd.com/product/computation-of-sifs-in-stresscheck/
12. Finite Element Analysis: Method, Verification and Validation, 2nd Edition. Barna Szabó and Ivo Babuška, John Wiley & Sons, Inc., United Kingdom, 2021. ISBN: 978-1-119-42642-4.
13. B. Andersson, U. Falk and I. Babuska, “Accurate and Reliable Calculation of Edge and Vertex Intensity Factors in Three-Dimensional Elastomechanics”, The 17th Congress of the International Council of the Aeronautical Sciences, Sept 9-14, 1990, Stockholm Sweden, Paper ICAS-90-4.9.2, pp 1730-1746.
14. B. Andersson and J. Greer, “Creation and Verification of World’s Largest K_I-Databases for Multiple Cracks at Countersunk and Straight-Shank Hole in a plate subject to Tension, Bending and Pin-Loading”, International Committee for Aeronautical Fatigue ICAF, 29th Symposium Nagoya, 7-9 June 2017, 10 pp.
15. A. Loghin, Life Prediction Modeling Capabilities for FE Applications, CAASE18, Cleveland, OH, USA, 2018. <https://www.researchgate.net/publication/325695699_life_prediction_modeling_capabilities_for_fe_applications>

16. A. Loghin, S. Ismonov, V&V 3D Fatigue Crack Growth Modeling: From Deterministic to Uncertainty Quantification (UQ) assessment, CAASE20. <https://www.researchgate.net/publication/342282698_VV_3D_Fatigue_Crack_Growth_Modeling_From_Deterministic_to_Uncertainty_Quantification_UQ_assessment>
17. A. Loghin, S. Ismonov, Application of Gaussian Process and Three-Dimensional FEA in Component Level Crack Propagation Life Assessment, NWC2019. <https://www.researchgate.net/publication/334044793_Application_of_Gaussian_Process_and_Three Dimensional_FEA_in_Component_Level_Crack_Propagation_Life_Assessment>
18. www.ansys.com
19. https://www.3ds.com/products-services/simulia/
20. http://www.dhondt.de/
21. Raju, I. S. and Newman, J. C., Jr., "Stress-Intensity Factors for Two Symmetric Corner Cracks," Fracture Mechanics, ASTM STP 677, 1979, pp. 411-430.

9. APPENDIX: FEA DETAILS

9.1. Submission 6: Andersson: FEA (2021)

9.1.1. Methods for K-calculation at edges and vertices

This section summarizes the numerical techniques used to derive the 7 accurate reference solutions. We do that in some detail as we believe that the solutions reviewed above are based on data generated with our methods.

The techniques we used were developed at the Aeronautical Research Institute of Sweden FFA by BARE personal for over 30 years ago. Reference [13] from 1990 gives a very detailed description of the methods for edge and vertex analysis that we used to analyze the 7 benchmark problems.

The basic principles for accurate and reliable extraction of vertex and edge stress intensity functions $K_\alpha(\varphi)$ where α denotes the Mode I, II or III stress intensity function are:

- Apply a *hp*-version of FEA
- Use advanced methods for extraction of edge and vertex stress intensity data

For edges the *K*-extraction method for 3D problems which we developed in [13] leads to a polynomial approximation $\widetilde{K}$ of $K_\alpha(\varphi)$ of the type given by (EQ 9-1),

$$\widetilde{K}(s) = \sum_{l=0}^{L} k_l \cdot P_l(s) \qquad \text{(EQ 9-1)}$$

In (EQ 9-1), *s* denotes a coordinate along the crack front, P_l are polynomials (for example s^0, s^1, s^2 etc) and k_l are coefficients which are determined from a *weighted average* of the finite element displacements inside a small volume Ω^e of extraction. The fact that we only use a *weighted average*, and *displacements* (not stresses) of the FE-solution leads to an *exponential* rate of convergence towards the exact *K*-solution for increasing polynomial order *p* of the finite elements. Figure 28 from [13] exemplify domains Ω^e which can be used for accurate calculation of *K* for a semi-elliptical crack. For extraction of data near vertices, that is vertex intensity factors (domains A and F) one can use similar techniques. Reference [13] gives most mathematical/numerical details of the methods we used in this benchmark for analysis of edges and vertices.

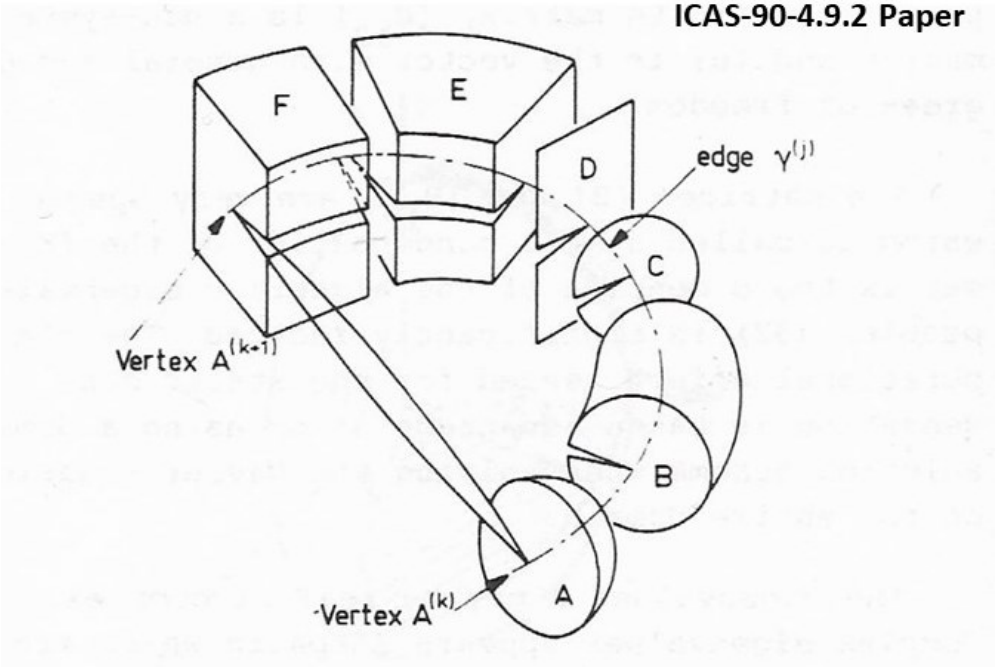

Figure 28: Domains Ω^e used for accurate calculation of K for a semi-elliptical crack [13]

Verification of the accuracy obtainable with a numerical method is always difficult in a 3-dimensional case due to the lack of analytic solutions. Figure 29 from [11] exemplify one rare exception. An analytic solution for the case of an elliptical crack in an infinite domain is available and was used in [13] to exemplify the accuracy obtainable. The computational domain is shown in Figure 28, i.e. a finite domain with traction loads on the outer surface which were calculated from the analytic solution (and applied via a user-supplied subroutine). Hence, we know the exact K-solution for this three-dimensional problem and can therefore calculate the exact error in the numerical solution. The loading is such that the Mode I, II and III intensity factors are all non-zero.

The finite element mesh used is extremely simple in this case. Figure 30 from [13] shows the mesh. Note that each single finite element inside the torus-shaped domain has element surfaces on the planes x=0 and y=0, that is, each single finite element covers the angle-range $0 \le \varphi \le \pi/2$. The only meshing parameter is the number m of radial element layers inside the torus.

Figure 31 from [13] shows the maximum relative errors in Mode I, II and III SIFs K along the entire crack front as function of (m, p). We see that despite the very coarse mesh it is possible to bring down the maximum relative pointwise error to about 0.010% for the Mode I, II and III intensity functions using p=10 finite elements.

BARE has used the methods sketched above, which is detailed in [13], during generation of K-data bases consisting of several 100 million K-functions [14]. In all the analyses we used m=6 and torus-shaped domains (compare domain of type 'B' in Figure 5 from [13]). For open crack fronts, i.e. cracks having two vertices, we used strongly graded meshes towards the vertices as detailed below.

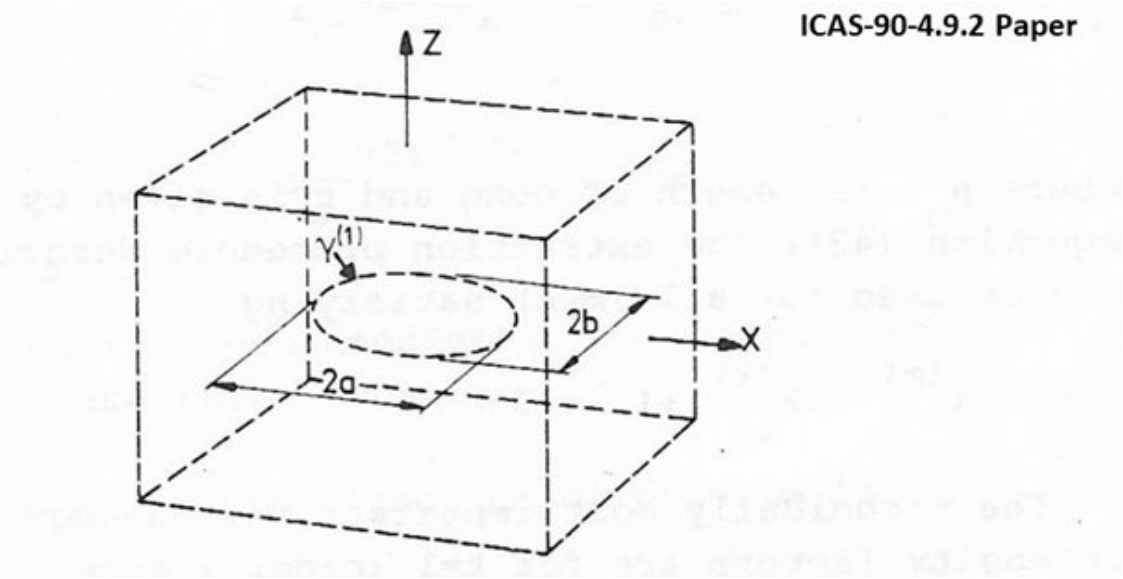

Figure 29: Embedded elliptical crack in infinite space subject to remote uniform stresses σ_z=1 and τ_{xz}=1. Dimension of crack is a/b=2 [13]

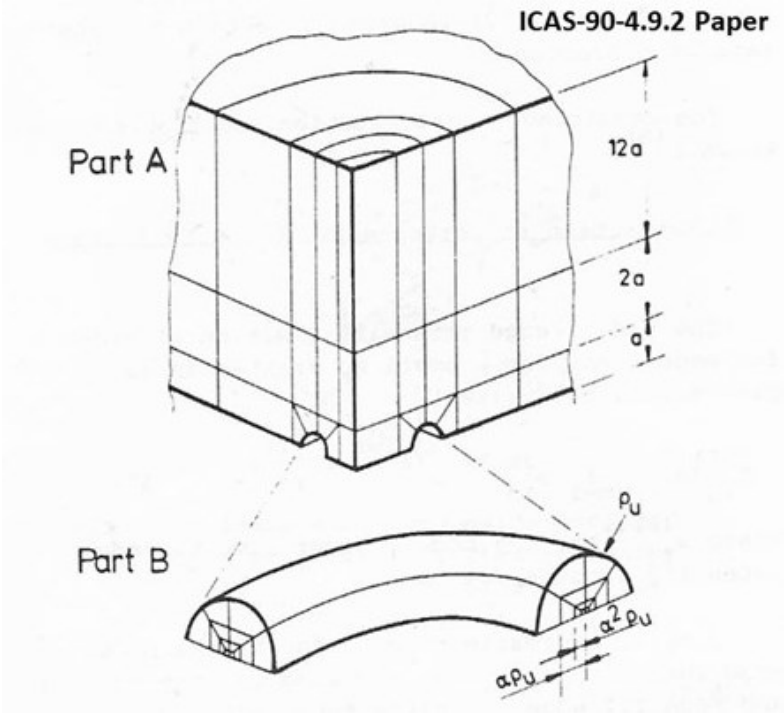

Figure 30: Principal mesh used for analysis of elliptical crack [13]

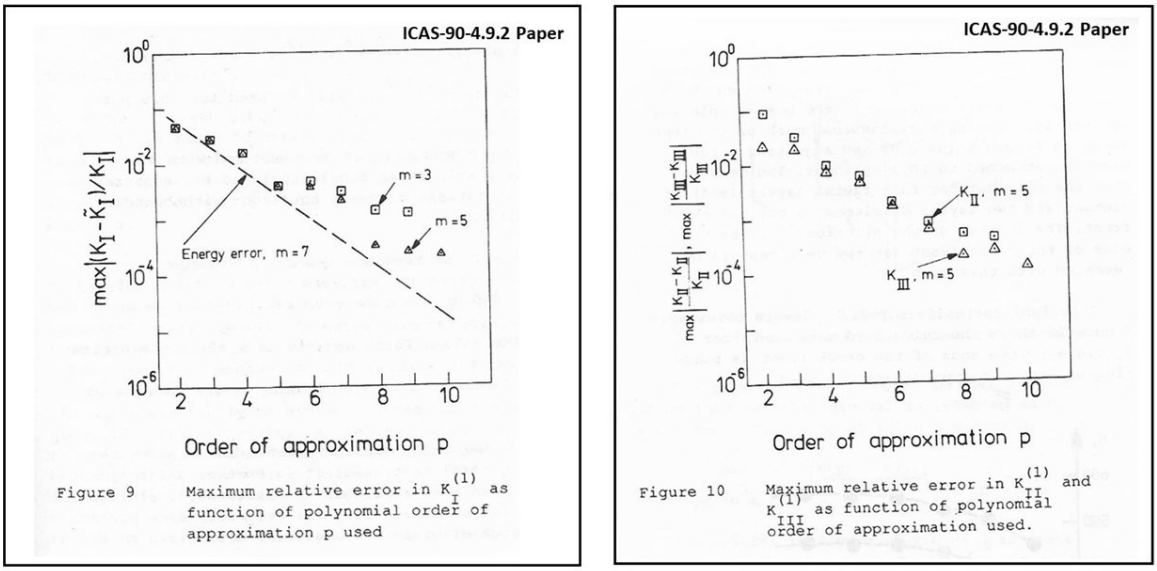

Figure 31: Maximum relative errors in Mode I, II, and III SIFs along the entire crack front as a function of (m, p) [13]

9.1.2. Detailed Analysis of Case 2

Figure 32 shows the principles behind the mesh designed used to construct the 7 meshes. Note that the figure shows a countersunk hole but the principle is the same for the straight-shank holes analyzed.

In the seven benchmark analyses BARE used standard parameters m=6 and a hp-type of FE-mesh and polynomial order p=5, the same as used during data base generation of K-functions [3,14]. Errors in the seven solutions are calculated below in order to make sure that the BARE data used in Robert Pilarczyk's report of 30 March 2021 are sufficient accurate.

Sixteen elements along the crack front are utilized which are strongly graded towards the vertices. The two smallest elements near the two vertices occupies only 0.005 degrees of the 90-degree crack front. This mesh design is, based on long experience, used as it well captures the strong K-gradients near the two vertices.

The finite elements used in the analysis have, where appropriate, exact cylindrical, elliptical and torus-shaped forms (Figure 32), i.e. there are no geometrical approximations of the computational domain. The total volume of all the finite elements is checked against the analytical expression for the specimen volume and was found to agree with sixteen digits accuracy. The plates with large width/thickness ratio are prone to round-off errors. For the seven cases studied here, and tensile loading, the round of errors did not influence K-data for accuracies of interest.

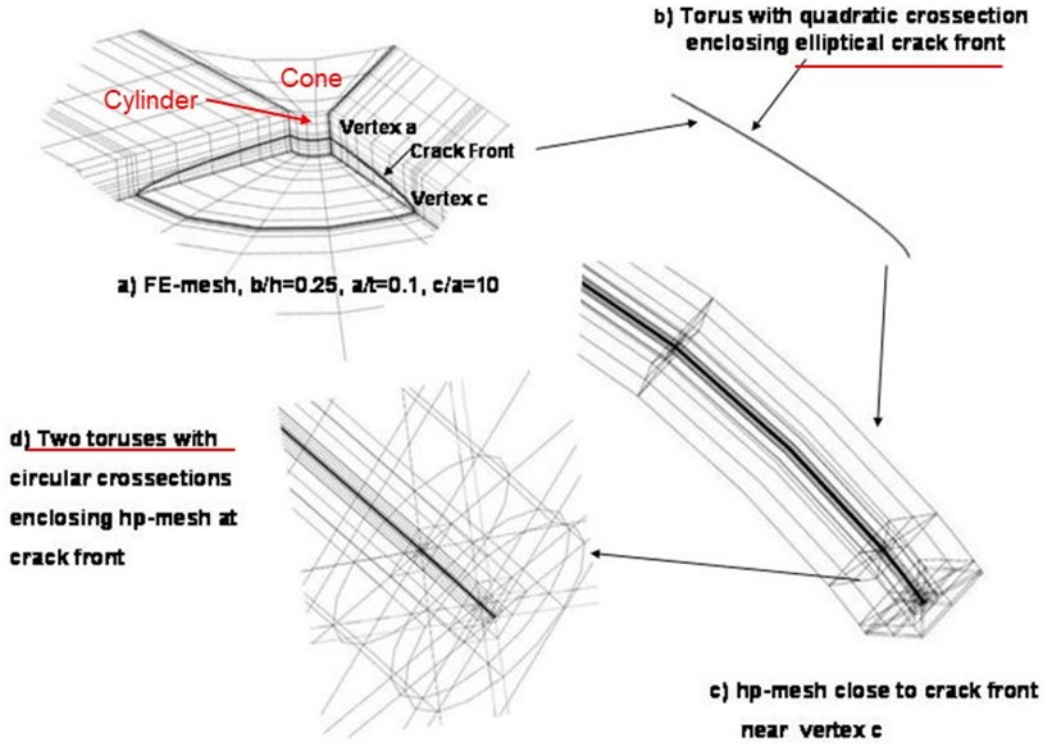

Figure 32: Principles behind mesh design for a mesh typical for the hp-version of FEM for fracture mechanics analysis.

Demonstrated below is the process to calculate the stress intensity functions with a maximum error of order 0.01% along the entire crack front, i.e. including vertex regions for all seven test cases in the benchmark. We will use this solution to check the accuracy of the BARE-solutions (m=6, p=5) sent to Robert Pilarczyk in early February 2021.

The first step is to check the accuracy by increasing the polynomial order p of the solution. Table 15 shows the estimated relative error Err in the stress intensity function K where Err, in %, is defined as:

$$Err(p,\varphi)=100 \cdot (K\_I\ (p=8,\varphi)-K\_I\ (p=5,\varphi))\backslash K\_I\ (p=8,\varphi) \qquad \text{(EQ 9-2)}$$

Polynomial (EQ 9-1) is utilized, with L=p, to calculate K_I in eleven points in each of the sixteen finite elements along the crack front. K_I can be calculated at any point φ on the crack front. At interfaces between two of the sixteen elements we calculated the average value of the two adjacent polynomials.

Table 15: Estimated error in $K_I(\varphi, p)$ assuming that the p=8 solution is the exact solution. In sections between two finite elements, the average $K_I(\varphi, p)$ value is used.

No	$2 \cdot \varphi/\pi$	*Err* in % in $K_I(\varphi)$			
		p=5	*p*=6	*p*=7	*p*=8
2	0.000006	0.34	0.04	0.02	0.00
3	0.000012	0.08	0.06	0.08	0.00
4	0.000017	0.10	0.17	0.06	0.00
5	0.000023	0.11	0.04	0.05	0.00
6	0.000029	0.01	0.09	0.05	0.00
7	0.000035	0.04	0.03	0.08	0.00
8	0.000041	0.01	0.15	0.13	0.00
9	0.000046	0.00	0.16	0.05	0.00
10	0.000052	0.16	0.10	0.14	0.00
----	0.000058	0.76	0.14	0.65	0.00
13	0.000081	0.03	0.03	0.01	0.00
14	0.000104	0.01	0.02	0.01	0.00
15	0.000128	0.01	0.02	0.01	0.00
16	0.000151	0.00	0.02	0.01	0.00
17	0.000174	0.01	0.01	0.01	0.00
18	0.000197	0.03	0.01	0.01	0.00
19	0.000220	0.04	0.01	0.01	0.00
20	0.000244	0.05	0.01	0.01	0.00
21	0.000267	0.01	0.01	0.00	0.00
----	0.000290	0.21	0.08	0.04	0.00
24	0.000406	0.06	0.02	0.01	0.00
25	0.000522	0.03	0.00	0.00	0.00
26	0.000638	0.04	0.00	0.01	0.00
27	0.000754	0.04	0.00	0.01	0.00
28	0.000870	0.04	0.00	0.00	0.00
29	0.000986	0.05	0.00	0.00	0.00
30	0.001102	0.06	0.00	0.00	0.00
31	0.001218	0.04	0.00	0.00	0.00
32	0.001334	0.00	0.01	0.00	0.00
---	0.001450	0.06	0.03	0.03	0.00
35	0.002030	0.03	0.00	0.00	0.00
36	0.002609	0.03	0.00	0.00	0.00
37	0.003189	0.03	0.00	0.00	0.00
38	0.003769	0.03	0.00	0.00	0.00
39	0.004349	0.03	0.00	0.00	0.00
40	0.004929	0.04	0.01	0.00	0.00
41	0.005509	0.04	0.01	0.00	0.00
42	0.006089	0.05	0.00	0.00	0.00
43	0.006668	0.04	0.01	0.00	0.00
---	0.007248	0.02	0.01	0.01	0.00
46	0.009568	0.02	0.00	0.00	0.00

47	0.011887	0.02	0.00	0.00	0.00
48	0.014207	0.03	0.00	0.00	0.00
49	0.016527	0.03	0.01	0.00	0.00
50	0.018846	0.04	0.01	0.00	0.00
51	0.021166	0.03	0.00	0.00	0.00
52	0.023485	0.02	0.00	0.00	0.00
53	0.025805	0.02	0.00	0.00	0.00
54	0.028125	0.02	0.00	0.00	0.00
---	0.030444	0.02	0.00	0.00	0.00
57	0.039730	0.03	0.00	0.00	0.00
58	0.049017	0.03	0.00	0.00	0.00
59	0.058303	0.03	0.00	0.00	0.00
60	0.067589	0.04	0.00	0.00	0.00
61	0.076875	0.04	0.00	0.00	0.00
62	0.086161	0.03	0.00	0.00	0.00
63	0.095448	0.03	0.00	0.00	0.00
64	0.104734	0.03	0.00	0.00	0.00
65	0.114020	0.03	0.00	0.00	0.00
---	0.123306	0.03	0.00	0.00	0.00
68	0.142141	0.04	0.00	0.00	0.00
69	0.160976	0.04	0.00	0.00	0.00
70	0.179810	0.03	0.00	0.00	0.00
71	0.198645	0.02	0.00	0.00	0.00
72	0.217480	0.02	0.00	0.00	0.00
73	0.236314	0.02	0.00	0.00	0.00
74	0.255149	0.03	0.00	0.00	0.00
75	0.273984	0.03	0.00	0.00	0.00
76	0.292818	0.03	0.00	0.00	0.00
---	0.311653	0.02	0.00	0.00	0.00
79	0.330488	0.03	0.00	0.00	0.00
80	0.349323	0.03	0.00	0.00	0.00
81	0.368157	0.03	0.00	0.00	0.00
82	0.386992	0.02	0.00	0.00	0.00
83	0.405827	0.02	0.00	0.00	0.00
84	0.424661	0.02	0.00	0.00	0.00
85	0.443496	0.02	0.00	0.00	0.00
86	0.462331	0.03	0.00	0.00	0.00
87	0.481165	0.03	0.00	0.00	0.00
---	0.500000	0.02	0.00	0.00	0.00
90	0.518835	0.03	0.00	0.00	0.00
91	0.537669	0.03	0.00	0.00	0.00
92	0.556504	0.02	0.00	0.00	0.00
93	0.575339	0.02	0.00	0.00	0.00
94	0.594173	0.02	0.00	0.00	0.00
95	0.613008	0.02	0.00	0.00	0.00
96	0.631843	0.02	0.00	0.00	0.00
97	0.650677	0.03	0.00	0.00	0.00

98	0.669512	0.03	0.00	0.00	0.00
---	0.688347	0.02	0.00	0.00	0.00
101	0.707182	0.03	0.00	0.00	0.00
102	0.726016	0.03	0.00	0.00	0.00
103	0.744851	0.02	0.00	0.00	0.00
104	0.763686	0.02	0.00	0.00	0.00
105	0.782520	0.01	0.00	0.00	0.00
106	0.801355	0.01	0.00	0.00	0.00
107	0.820190	0.02	0.00	0.00	0.00
108	0.839024	0.02	0.00	0.00	0.00
109	0.857859	0.02	0.00	0.00	0.00
---	0.876694	0.01	0.00	0.00	0.00
112	0.885980	0.01	0.00	0.00	0.00
113	0.895266	0.01	0.00	0.00	0.00
114	0.904552	0.01	0.00	0.00	0.00
115	0.913839	0.01	0.00	0.00	0.00
116	0.923125	0.02	0.00	0.00	0.00
117	0.932411	0.02	0.00	0.00	0.00
118	0.941697	0.02	0.00	0.00	0.00
119	0.950983	0.01	0.00	0.00	0.00
120	0.960270	0.01	0.00	0.00	0.00
---	0.969556	0.01	0.01	0.00	0.00
123	0.971875	0.00	0.00	0.00	0.00
124	0.974195	0.00	0.00	0.00	0.00
125	0.976515	0.00	0.00	0.00	0.00
126	0.978834	0.01	0.00	0.00	0.00
127	0.981154	0.01	0.00	0.00	0.00
128	0.983473	0.01	0.00	0.00	0.00
129	0.985793	0.01	0.00	0.00	0.00
130	0.988113	0.00	0.01	0.00	0.00
131	0.990432	0.00	0.00	0.00	0.00
---	0.992752	0.03	0.01	0.01	0.00
134	0.993332	0.01	0.01	0.00	0.00
135	0.993911	0.02	0.01	0.00	0.00
136	0.994491	0.02	0.00	0.00	0.00
137	0.995071	0.02	0.00	0.00	0.00
138	0.995651	0.01	0.00	0.00	0.00
139	0.996231	0.00	0.01	0.00	0.00
140	0.996811	0.00	0.01	0.00	0.00
141	0.997391	0.00	0.01	0.00	0.00
142	0.997970	0.01	0.01	0.00	0.00
---	0.998550	0.08	0.03	0.03	0.00
145	0.998666	0.03	0.00	0.01	0.00
146	0.998782	0.02	0.00	0.00	0.00
147	0.998898	0.03	0.01	0.00	0.00
148	0.999014	0.02	0.01	0.00	0.00
149	0.999130	0.02	0.01	0.00	0.00

150	0.999246	0.01	0.01	0.01	0.00
151	0.999362	0.01	0.01	0.01	0.00
152	0.999478	0.00	0.00	0.00	0.00
153	0.999594	0.08	0.03	0.01	0.00
---	0.999710	0.24	0.09	0.04	0.00
156	0.999733	0.02	0.01	0.01	0.00
157	0.999756	0.02	0.02	0.01	0.00
158	0.999780	0.02	0.02	0.01	0.00
159	0.999803	0.00	0.02	0.01	0.00
160	0.999826	0.02	0.02	0.01	0.00
161	0.999849	0.03	0.03	0.01	0.00
162	0.999872	0.02	0.03	0.02	0.00
163	0.999896	0.02	0.02	0.01	0.00
164	0.999919	0.06	0.03	0.01	0.00
---	0.999942	0.79	0.14	0.65	0.00
167	0.999948	0.19	0.10	0.14	0.00
168	0.999954	0.03	0.17	0.05	0.00
169	0.999959	0.01	0.15	0.13	0.00
170	0.999965	0.01	0.02	0.08	0.00
171	0.999971	0.03	0.09	0.05	0.00
172	0.999977	0.14	0.05	0.05	0.00
173	0.999983	0.13	0.18	0.07	0.00
174	0.999988	0.05	0.06	0.08	0.00
175	0.999994	0.37	0.05	0.02	0.00

As shown, convergence with increasing p is very fast, except for the two smallest elements located at the vertices where there is no convergence by increasing p. The reason is that K_I goes to zero so quickly near the vertex. It is simply not possible to approximate this K_I behavior which has the following functional form $s^{0.04782}$, with one single polynomial (see below).

Note that by using this type of strongly graded mesh towards the crack front and towards the vertices the overall FE-solution converges exponentially fast in the pre-asymptotic range to the exact solution. Approximating $K_I(\varphi)$ with a polynomial of order p=8, equation (EQ 9-1), in the small range $0 \leq \varphi \leq 0.000058$ is perhaps not optimal. We will however below show that the errors obtained even in these smallest elements are still small. Away from the vertices, say for $0.002 \leq \varphi \leq 0.998$ we see that the p=5 solution sent to Robert Pilarczyk in February seems to underestimate the exact $K_I(\varphi)$-solution with 0.00 to 0.04%.

Next, the error in the p=5 solution is calculated, which is also arbitrary close to the vertex. This is of course of more academic interest, but it still has some interest to see how accurate the p=5 solution is in the vertex regions, despite the lack of convergence mentioned above.

9.1.3. Near vertex behavior of K

The asymptotic behavior of *K* near a vertex can be written in the following form (EQ 9-3) where *s* is the distance to the vertex, see [13].

$$K_I(s) = S_1 \cdot s^{\Lambda_1 - \frac{1}{2}} + S_2 \cdot s^{\Lambda_2 - \frac{1}{2}} + S_3 \cdot s^{\Lambda_1 + 1 - \frac{1}{2}} + \text{higher terms}$$

$\Lambda_1 = 0.54782$
$\Lambda_2 = 1.21826$

(EQ 9-3)

The coefficients Λ_1 and Λ_2 are constants which depends on the angle at which the crack front intersects with the surface and the Poisson's ratio [14]. The data given in (EQ 9-3) is valid for an angle 90 degrees and a Poisson's ratio 0.30.

9.1.4. A Semi-Analytical Expression for $K_I(\varphi)$ having an error < 0.01% for benchmark Case 2

Next, the three unknown coefficients S_1, S_2, S_3 are determined by doing a least square fit of equation (EQ 9-3) to data in Table 15. In doing that, data points most close to the vertex are not utilized (due to the oscillations), nor, too far away from the vertex as a three terms approximation is not valid far away from the vertex. One least square fit equation is created for each of the two vertices. In the least square fit, points 122-165 are used for vertex 'a' and points 12-55 for vertex 'c' in Table 15.

For vertex 'a' the S_1, S_2, S_3 factors in equation (EQ 9-4) and for vertex 'c' equation (EQ 9-5) are calculated.

$$\begin{aligned} S_1 &= \ \ 8.1656200 \\ S_2 &= -0.4529495 \\ S_3 &= 0.080899910 \end{aligned} \qquad \text{(EQ 9-4)}$$

$$\begin{aligned} S_1 &= \ \ 6.4817140 \\ S_2 &= -0.29692940 \\ S_3 &= 0.055438272 \end{aligned} \qquad \text{(EQ 9-5)}$$

In Table 16 and Table 17 the difference *Diff* between the FE-solutions for *p*=8 and the analytical expressions given by equations (EQ 9-3-EQ 9-5) are compared. The comparisons are only made in the φ-intervals used when making the least square fits (i.e. over four finite elements along the crack front). The difference *Diff* is defined, in %, as,

$$Diff = 100 \cdot (K_I(Analytic) - K_I(p = 8))/K_I(Analytic) \qquad \text{(EQ 9-6)}$$

Table 16: Relative difference in the analytic expression (EQ 9-3, EQ 9-4) for $K_I(\varphi, p)$ near vertex 'a' and the p=8 K_I-solution.

No	φ	$K_I(p=8)$	$K_I(Analytic)$	*Diff* (%)
165	0.999942	6.51284	6.50757	-0.08
164	0.999919	6.61296	6.60928	-0.06
163	0.999896	6.68833	6.68590	-0.04
162	0.999872	6.74868	6.74711	-0.02
161	0.999849	6.79920	6.79816	-0.02
160	0.999826	6.84259	6.84204	-0.01
159	0.999803	6.88047	6.88032	-0.00
158	0.999780	6.91410	6.91433	0.00
157	0.999756	6.94450	6.94499	0.01
156	0.999733	6.97222	6.97274	0.01
155	0.999710	6.99687	6.99816	0.02
154	0.999710	6.99802	6.99816	0.00
153	0.999594	7.09893	7.10031	0.02
152	0.999478	7.17436	7.17583	0.02
151	0.999362	7.23379	7.23539	0.02
150	0.999246	7.28274	7.28440	0.02
149	0.999130	7.32427	7.32584	0.02
148	0.999014	7.36014	7.36161	0.02
147	0.998898	7.39158	7.39300	0.02
146	0.998782	7.41958	7.42087	0.02
145	0.998666	7.44480	7.44586	0.01
144	0.998550	7.46702	7.46848	0.02
143	0.998550	7.46828	7.46848	0.00
142	0.997970	7.55566	7.55636	0.01
141	0.997391	7.61765	7.61776	0.00
140	0.996811	7.66365	7.66364	-0.00
139	0.996231	7.69943	7.69936	-0.00
138	0.995651	7.72818	7.72794	-0.00
137	0.995071	7.75165	7.75128	-0.00
136	0.994491	7.77097	7.77060	-0.00
135	0.993911	7.78712	7.78676	-0.00
134	0.993332	7.80087	7.80039	-0.01
133	0.992752	7.81209	7.81193	-0.00
132	0.992752	7.81257	7.81193	-0.01
131	0.990432	7.84390	7.84332	-0.01
130	0.988113	7.86010	7.85946	-0.01
129	0.985793	7.86722	7.86655	-0.01
128	0.983473	7.86849	7.86785	-0.01
127	0.981154	7.86575	7.86522	-0.01

126	0.978834	7.86017	7.85984	-0.00
125	0.976515	7.85257	7.85250	-0.00
124	0.974195	7.84350	7.84372	0.00
123	0.971875	7.83322	7.83389	0.01
122	0.969556	7.82232	7.82328	0.01

Table 17: Relative difference in the analytic expression (EQ 9-3, EQ 9-5) for $K_I(\varphi, p)$ near vertex 'c' and the p=8 K_I-solution.

No	φ	$K_I(p=8)$	$K_I(Analytic)$	*Diff* (%)
12	0.000058	5.17197	5.16767	-0.08
13	0.000081	5.25201	5.24896	-0.06
14	0.000104	5.31236	5.31029	-0.04
15	0.000128	5.36074	5.35936	-0.03
16	0.000151	5.40129	5.40033	-0.02
17	0.000174	5.43617	5.43560	-0.01
18	0.000197	5.46665	5.46640	-0.00
19	0.000220	5.49375	5.49379	0.00
20	0.000244	5.51826	5.51852	0.00
21	0.000267	5.54064	5.54093	0.01
22	0.000290	5.56058	5.56147	0.02
23	0.000290	5.56148	5.56147	-0.00
24	0.000406	5.64327	5.64427	0.02
25	0.000522	5.70468	5.70578	0.02
26	0.000638	5.75327	5.75452	0.02
27	0.000754	5.79346	5.79480	0.02
28	0.000870	5.82769	5.82901	0.02
29	0.000986	5.85737	5.85866	0.02
30	0.001102	5.88349	5.88478	0.02
31	0.001218	5.90685	5.90808	0.02
32	0.001334	5.92796	5.92905	0.02
33	0.001450	5.94666	5.94810	0.02
34	0.001450	5.94767	5.94810	0.01
35	0.002030	6.02205	6.02299	0.02
36	0.002609	6.07589	6.07638	0.01
37	0.003189	6.11678	6.11710	0.01
38	0.003769	6.14931	6.14950	0.00
39	0.004349	6.17607	6.17603	-0.00
40	0.004929	6.19846	6.19820	-0.00
41	0.005509	6.21738	6.21704	-0.01
42	0.006089	6.23365	6.23325	-0.01
43	0.006668	6.24789	6.24732	-0.01
44	0.007248	6.25999	6.25964	-0.01

45	0.007248	6.26038	6.25964	-0.01
46	0.009568	6.29711	6.29632	-0.01
47	0.011887	6.32065	6.31985	-0.01
48	0.014207	6.33613	6.33541	-0.01
49	0.016527	6.34634	6.34573	-0.01
50	0.018846	6.35285	6.35241	-0.01
51	0.021166	6.35667	6.35648	-0.00
52	0.023485	6.35854	6.35860	0.00
53	0.025805	6.35894	6.35925	0.00
54	0.028125	6.35813	6.35876	0.01
55	0.030444	6.35662	6.35739	0.01

Table 16 and Table 17 shows that the analytic expression (EQ 9-3) differs very little from the p=8 solution, i.e. typically 0.01%.

Now, very accurate solution in the entire range $0 \leq \varphi \leq \pi/2$ are achievable by using the analytic solutions for points with number less than 53 and higher than 128 (the K-peaks) and the p=8 solution for all other points.

Table 18 shows the highly accurate solution obtained in this way. The p=5 solution is shown for comparison. Note that by using the analytic expression K_I can be calculated at a distance of $s = 10^{-100}$ (as a silly example) with an accuracy of about 0.01%. Of special interest is to see how large the error is in the finite elements most close to a vertex, elements where convergent results could not be achieved (see Table 15).

Table 18: Relative difference in the analytic expression (EQ 9-3, EQ 9-5) for $K_I(\varphi, p)$ near vertex 'c' and the p=8 K_I-solution.

No	φ	$K_I(p=5)$	$K_I(Analytic)$	*Diff* (%)
2	0.000006	4.67169	4.63546	-0.78
3	0.000012	4.80188	4.79053	-0.24
4	0.000017	4.89680	4.88334	-0.28
5	0.000023	4.96487	4.95010	-0.30
6	0.000029	5.01406	5.00239	-0.23
7	0.000035	5.05180	5.04585	-0.12
8	0.000041	5.08484	5.08239	-0.05
9	0.000046	5.11907	5.11420	-0.10
10	0.000052	5.15943	5.14237	-0.33
11	0.000058	5.20974	5.16767	-0.81
12	0.000058	5.18453	5.16767	-0.33
13	0.000081	5.25353	5.24896	-0.09
14	0.000104	5.31169	5.31029	-0.03
15	0.000128	5.36044	5.35936	-0.02
16	0.000151	5.40125	5.40033	-0.02
17	0.000174	5.43565	5.43560	-0.00
18	0.000197	5.46516	5.46640	0.02

19	0.000220	5.49134	5.49379	0.04
20	0.000244	5.51575	5.51852	0.05
21	0.000267	5.53993	5.54093	0.02
22	0.000290	5.56541	5.56147	-0.07
23	0.000290	5.57999	5.56147	-0.33
24	0.000406	5.64639	5.64427	-0.04
25	0.000522	5.70302	5.70578	0.05
26	0.000638	5.75088	5.75452	0.06
27	0.000754	5.79117	5.79480	0.06
28	0.000870	5.82518	5.82901	0.07
29	0.000986	5.85435	5.85866	0.07
30	0.001102	5.88018	5.88478	0.08
31	0.001218	5.90424	5.90808	0.06
32	0.001334	5.92813	5.92905	0.02
33	0.001450	5.95343	5.94810	-0.09
34	0.001450	5.94724	5.94810	0.01
35	0.002030	6.02020	6.02299	0.05
36	0.002609	6.07407	6.07638	0.04
37	0.003189	6.11513	6.11710	0.03
38	0.003769	6.14758	6.14950	0.03
39	0.004349	6.17406	6.17603	0.03
40	0.004929	6.19612	6.19820	0.03
41	0.005509	6.21474	6.21704	0.04
42	0.006089	6.23082	6.23325	0.04
43	0.006668	6.24568	6.24732	0.03
44	0.007248	6.26153	6.25964	-0.03
45	0.007248	6.25991	6.25964	-0.00
46	0.009568	6.29573	6.29632	0.01
47	0.011887	6.31922	6.31985	0.01
48	0.014207	6.33441	6.33541	0.02
49	0.016527	6.34422	6.34573	0.02
50	0.018846	6.35056	6.35241	0.03
51	0.021166	6.35461	6.35648	0.03
52	0.023485	6.35696	6.35860	0.03
53	0.025805	6.35779	6.35894	0.02
54	0.028125	6.35711	6.35813	0.02
55	0.030444	6.35493	6.35662	0.03
56	0.030444	6.35568	6.35655	0.01
57	0.039730	6.34229	6.34397	0.03
58	0.049017	6.32483	6.32672	0.03
59	0.058303	6.30562	6.30771	0.03
60	0.067589	6.28614	6.28839	0.04
61	0.076875	6.26722	6.26946	0.04

62	0.086161	6.24922	6.25130	0.03
63	0.095448	6.23220	6.23409	0.03
64	0.104734	6.21612	6.21792	0.03
65	0.114020	6.20102	6.20285	0.03
66	0.123306	6.18719	6.18889	0.03
67	0.123306	6.18726	6.18889	0.03
68	0.142141	6.16140	6.16368	0.04
69	0.160976	6.14066	6.14284	0.04
70	0.179810	6.12431	6.12612	0.03
71	0.198645	6.11180	6.11329	0.02
72	0.217480	6.10271	6.10409	0.02
73	0.236314	6.09676	6.09828	0.02
74	0.255149	6.09378	6.09558	0.03
75	0.273984	6.09367	6.09571	0.03
76	0.292818	6.09643	6.09845	0.03
77	0.311653	6.10208	6.10360	0.02
78	0.311653	6.10208	6.10360	0.02
79	0.330488	6.10898	6.11083	0.03
80	0.349323	6.11857	6.12036	0.03
81	0.368157	6.13063	6.13219	0.03
82	0.386992	6.14500	6.14633	0.02
83	0.405827	6.16153	6.16275	0.02
84	0.424661	6.18014	6.18143	0.02
85	0.443496	6.20078	6.20230	0.02
86	0.462331	6.22349	6.22524	0.03
87	0.481165	6.24838	6.25019	0.03
88	0.500000	6.27564	6.27706	0.02
89	0.500000	6.27562	6.27706	0.02
90	0.518835	6.30381	6.30559	0.03
91	0.537669	6.33436	6.33609	0.03
92	0.556504	6.36714	6.36863	0.02
93	0.575339	6.40206	6.40332	0.02
94	0.594173	6.43909	6.44027	0.02
95	0.613008	6.47824	6.47956	0.02
96	0.631843	6.51962	6.52121	0.02
97	0.650677	6.56339	6.56526	0.03
98	0.669512	6.60981	6.61175	0.03
99	0.688347	6.65921	6.66074	0.02
100	0.688347	6.65921	6.66074	0.02
101	0.707182	6.71011	6.71210	0.03
102	0.726016	6.76423	6.76618	0.03
103	0.744851	6.82151	6.82316	0.02
104	0.763686	6.88193	6.88322	0.02

105	0.782520	6.94556	6.94657	0.01
106	0.801355	7.01258	7.01352	0.01
107	0.820190	7.08330	7.08440	0.02
108	0.839024	7.15824	7.15960	0.02
109	0.857859	7.23813	7.23957	0.02
110	0.876694	7.32397	7.32490	0.01
111	0.876694	7.32400	7.32490	0.01
112	0.885980	7.36813	7.36902	0.01
113	0.895266	7.41406	7.41462	0.01
114	0.904552	7.46126	7.46180	0.01
115	0.913839	7.50971	7.51057	0.01
116	0.923125	7.55963	7.56090	0.02
117	0.932411	7.61123	7.61270	0.02
118	0.941697	7.66443	7.66575	0.02
119	0.950983	7.71855	7.71948	0.01
120	0.960270	7.77208	7.77260	0.01
121	0.969556	7.82239	7.82224	-0.00
122	0.969556	7.82159	7.82232	0.01
123	0.971875	7.83323	7.83322	-0.00
124	0.974195	7.84350	7.84350	-0.00
125	0.976515	7.85224	7.85257	0.00
126	0.978834	7.85936	7.86017	0.01
127	0.981154	7.86465	7.86575	0.01
128	0.983473	7.86747	7.86849	0.01
129	0.985793	7.86655	7.86655	-0.00
130	0.988113	7.85973	7.85946	-0.00
131	0.990432	7.84368	7.84332	-0.00
132	0.992752	7.81371	7.81193	-0.02
133	0.992752	7.81568	7.81193	-0.05
134	0.993332	7.79980	7.80039	0.01
135	0.993911	7.78525	7.78676	0.02
136	0.994491	7.76934	7.77060	0.02
137	0.995071	7.75044	7.75128	0.01
138	0.995651	7.72743	7.72794	0.01
139	0.996231	7.69909	7.69936	0.00
140	0.996811	7.66346	7.66364	0.00
141	0.997391	7.61727	7.61776	0.01
142	0.997970	7.55528	7.55636	0.01
143	0.998550	7.46975	7.46848	-0.02
144	0.998550	7.47749	7.46848	-0.12
145	0.998666	7.44702	7.44586	-0.02
146	0.998782	7.41834	7.42087	0.03
147	0.998898	7.38944	7.39300	0.05

148	0.999014	7.35835	7.36161	0.04
149	0.999130	7.32312	7.32584	0.04
150	0.999246	7.28185	7.28440	0.03
151	0.999362	7.23279	7.23539	0.04
152	0.999478	7.17431	7.17583	0.02
153	0.999594	7.10494	7.10031	-0.07
154	0.999710	7.02344	6.99816	-0.36
---	---	---	---	---
155	0.999710	7.00497	6.99816	-0.10
156	0.999733	6.97333	6.97274	-0.01
157	0.999756	6.94333	6.94499	0.02
158	0.999780	6.91305	6.91433	0.02
159	0.999803	6.88055	6.88032	-0.00
160	0.999826	6.84388	6.84204	-0.03
161	0.999849	6.80109	6.79816	-0.04
162	0.999872	6.75023	6.74711	-0.05
163	0.999896	6.68941	6.68590	-0.05
164	0.999919	6.61678	6.60928	-0.11
165	0.999942	6.53054	6.50757	-0.35
---	---	---	---	---
166	0.999942	6.56230	6.50757	-0.84
167	0.999948	6.49908	6.47590	-0.36
168	0.999954	6.44843	6.44060	-0.12
169	0.999959	6.40551	6.40073	-0.07
170	0.999965	6.36409	6.35491	-0.14
171	0.999971	6.31673	6.30037	-0.26
172	0.999977	6.25498	6.23474	-0.32
173	0.999983	6.16946	6.15089	-0.30
174	0.999988	6.05014	6.03424	-0.26
175	0.999994	5.88640	5.83921	-0.81

Consider now the error in the $K_I(p=5)$-solution in elements most close to the vertices (points 2-11 for example). The largest errors appear at the ends of the interval which is typical when approximation very non-smooth functions like $K_I = s^{0.04782}$, for s small, equation (EQ 9-3) with a high order polynomial. Note that with crack dimension a=c=0.05 for benchmark Case 2, point 11 is located at a distance $0.000058 \cdot 0.05$ from the vertex, that is very-very close. The exact error in this point (number 11) is 0.8% that is acceptably small.

So a general conclusion is that away from the vertex, say for $0.002 \leq \varphi \leq 0.998$, the p=5 solution sent to Robert Pilarczyk in February 2021 seems to underestimate the exact solution with 0.00% to 0.04%. Closer to the vertices the p=5 solution is still very-very accurate, save for a few points in Table 18 where the relative error reaches 0.8%.

9.1.5. Crack Errors in $K_I(\varphi)$-functions of order p=5 for benchmark Case 1 to 7

The analysis for benchmark Case 1 and Cases 3-7 were repeated, respectively. The results were found to be close to identical to those obtained for Case 2, i.e., the right column in Table 18, so all the data was not shown in the report. If anyone is interested in the more exact solutions, they are available on demand.

9.1.6. Summary

BARE benchmark results sent to Robert Pilarczyk in February 2021 and used as reference solutions in this report are, say for $0.002 \leq \varphi \leq 0.998$ underestimating the exact solutions with 0.00 to 0.04%. Since solutions reviewed in subsections 3.2, 3.3 and 3.7, respectively are based on data generated with methods briefly described in this subsection these solutions are of the similar accuracy. More accurate solutions, i.e., semi-analytic solutions with maximum errors of order 0.01% are through the recent work now available, but these solutions, if utilized, do not change any conclusions of the present benchmark work.

9.2. Submission 7: SimModeler Crack: FEA (2021)

9.2.1. About SimModeler Crack

SimModeler Crack is a pre- and post-processor designed for component level finite element-based 3D fatigue crack growth simulations. Meshes with no underlying geometry as well as component level geometries can be used as input to the automatic fatigue crack propagation modeling process: crack insertion, meshing of the model containing the crack, finite element model definition, solution, post processing, crack advancement. A relationship between geometric definition and the mesh is maintained during the automatic crack propagation process which provides a robust and automatic procedure to update the finite element model definition for each crack front increment. In SimModeler Crack, SIFs are computed via displacement correlation technique based on a model solution performed in ANSYS [18], ABAQUS [19] or CalculiX [20]. A different solver can be added via a Plugin capability. Since the solution is performed in ANSYS, ABAQUS or CalculiX, all pre-processing and post-processing capabilities are accessible to the user in the definition of the finite element model and visualization of the results respectively.

More information about SimModeler Crack development is available in [15]. Different experimental results available in literature were considered for validation purposes in the development of SimModeler Crack [16], [17].

9.2.2. 3D Models and Results for Each Benchmark Case

The same modeling process was followed for each 3D model generated in this study. For all models, a similar overall mesh refinement and a uniform mesh size that provides about 300 element edges along the crack front were used for all benchmark cases.

Case 1

A Parasolid based geometric model is used to insert the two symmetric cracks, mesh the model, assign boundary conditions and far field loading and, prepare input files for Ansys. The SIF values are computed by SimModeler from the ANSYS solution. Model geometry and two contour plots from ANSYS are provided in Figure 33. Mode I SIFs (K_I) values are provided in Figure 34.

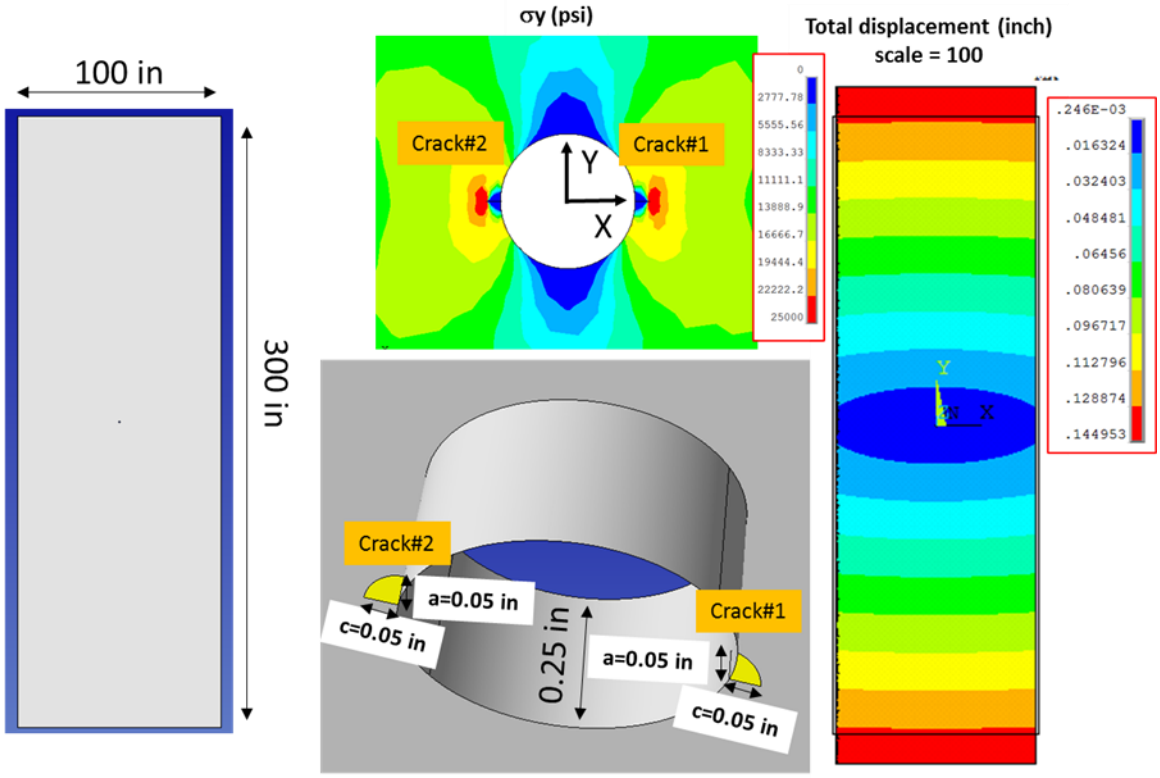

Figure 33: Case 1 3D geometry along with contour plots for σ_y normal stress component and total displacement.

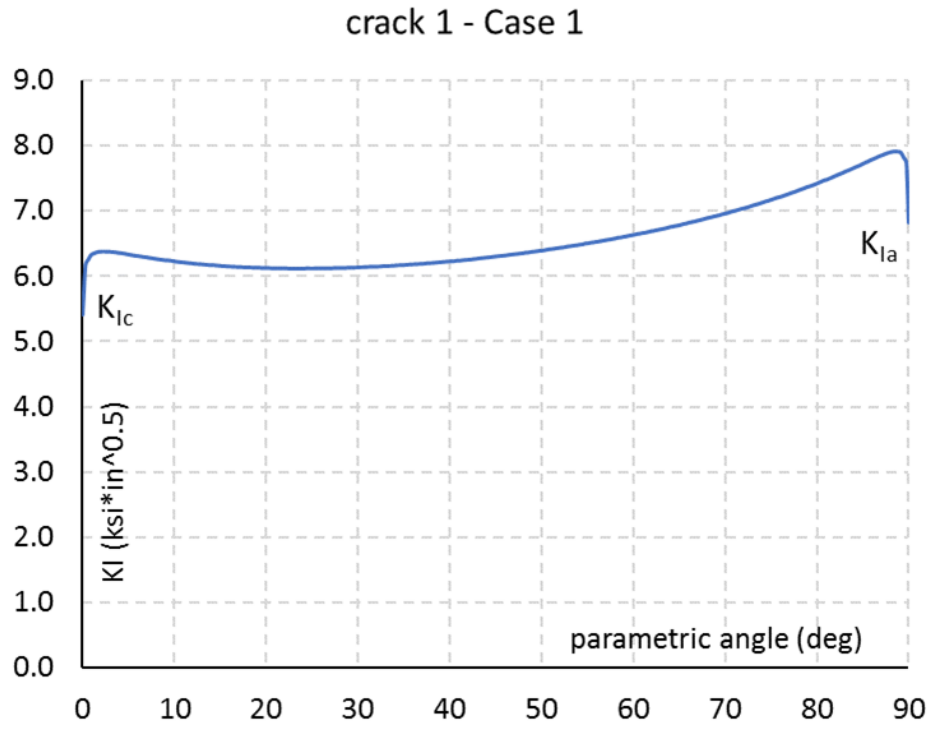

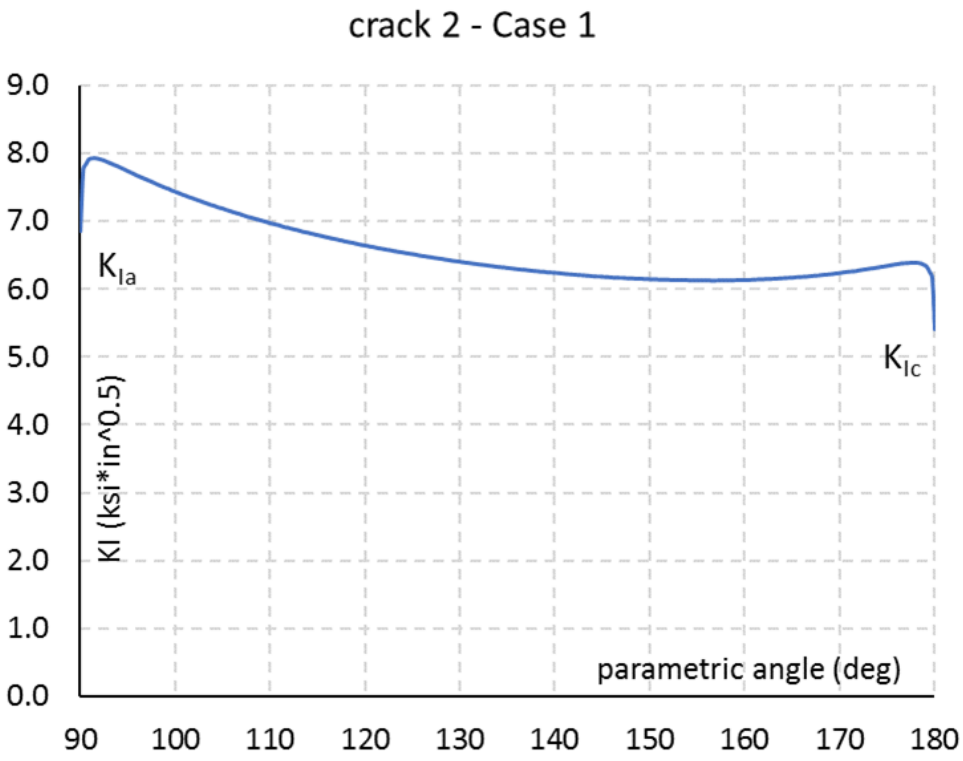

Figure 34: Model I SIF along the two crack fronts, crack #1 and crack #2.

Case 2

This model is a duplicate of Case 1 model definition except number of cracks: only one crack defined instead of two. Mode I SIFs are provided in Figure 35.

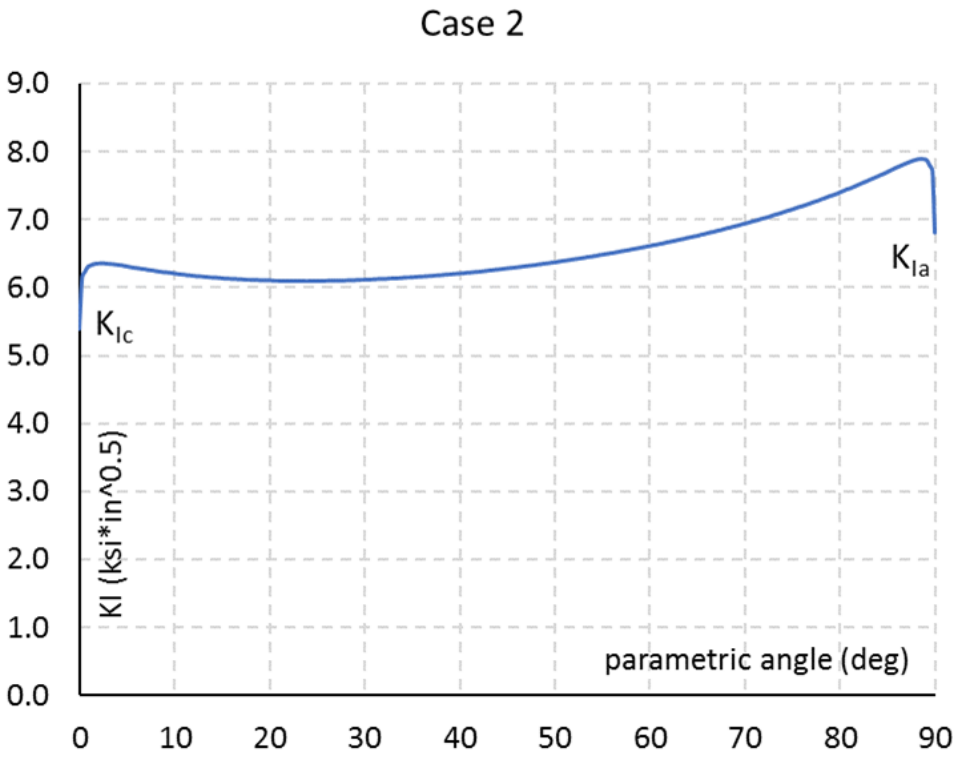

Figure 35: Model I SIFs along the crack front, Case 2.

For Case 2 example, a convergence study was conducted along with a comparison against the semi-analytical solution provided by Andersson (see Submission 6).

Seven meshes were used to perform the convergence study: {100, 200, 300, 1000, 2000, 3070, 8200} uniformly spaced element size along the crack front. A typical crack front mesh is provided in Figure 36. The metric used for assessing the difference between the reference solution and all solutions generated for this benchmark case is the average of relative difference (absolute values) between K_I values at the same normalized parametric angle. The first and last K_I values (crack front intersections with model boundary or vertex locations) are omitted. Two normalized parametric angle intervals are considered for computing the differences between the two solutions: $0.01 < 2*\phi/\pi < 0.99$ and, $0.001 < 2*\phi/\pi < 0.999$. Parametric angle definition ϕ is provided in Figure 2. As it can be observed in

Table 19 and Figure 37 all meshes provide very good K_I solutions when compared to Andersson semi-analytic reference (all solutions are below 0.5%) and for 200 element edges or higher density, solution is within 0.25% average relative difference from the reference. It can be concluded that 300 element edges along the crack front is a good choice for providing an accurate solution for all cases considered in this benchmark.

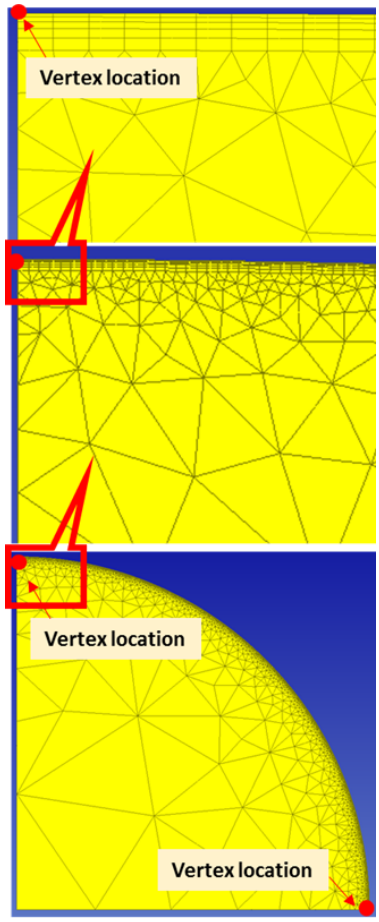

Figure 36: Mesh pattern for the 2000 element edges along crack front. The two crack front ends are the vertex locations.

Table 19: Average of relative differences (absolute values) between K_I values from different crack front mesh refinements and semi-analytic solution provided by Andersson (submission 6).

No. element edges along crack front	Average of relative differences (absolute values) using Andersson' semi-analytic solution as reference	
	0.01 < 2*phi/pi < 0.99	0.001 < 2*phi/pi < 0.999
100	0.42%	
200	0.15%	
300	0.23%	
1000	0.13%	0.13%
2000	0.14%	0.14%
3070	0.19%	0.19%
8200	0.18%	0.18%

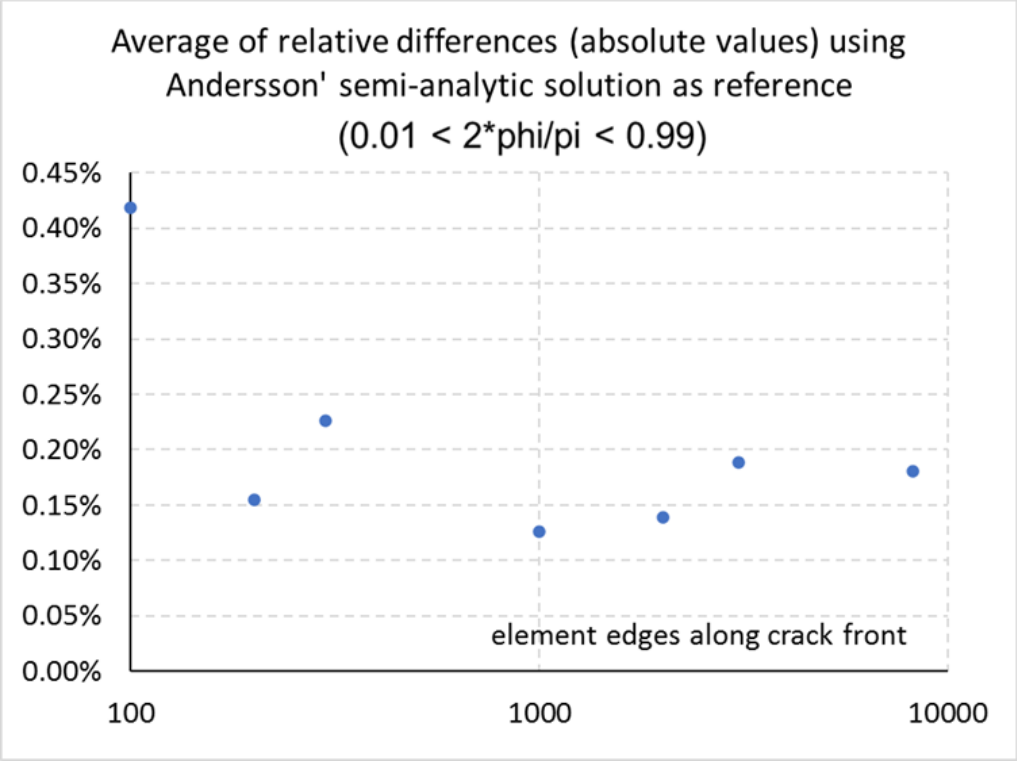

Figure 37: Graphical semi-log representation of data in Table 19.

Since the largest error occurs in the vicinity of two crack front vertices (Figure 36), a comparison between K_I values from four meshes and the reference solution is provided in Figure 38 and Figure 39 to demonstrate solution convergence. It can be easily observed that, with increased mesh density along the crack front, the solution provided by SimModeler Crack converges and, is consistent with Andersson's solution using a highly graded mesh and an hp-FE formulation.

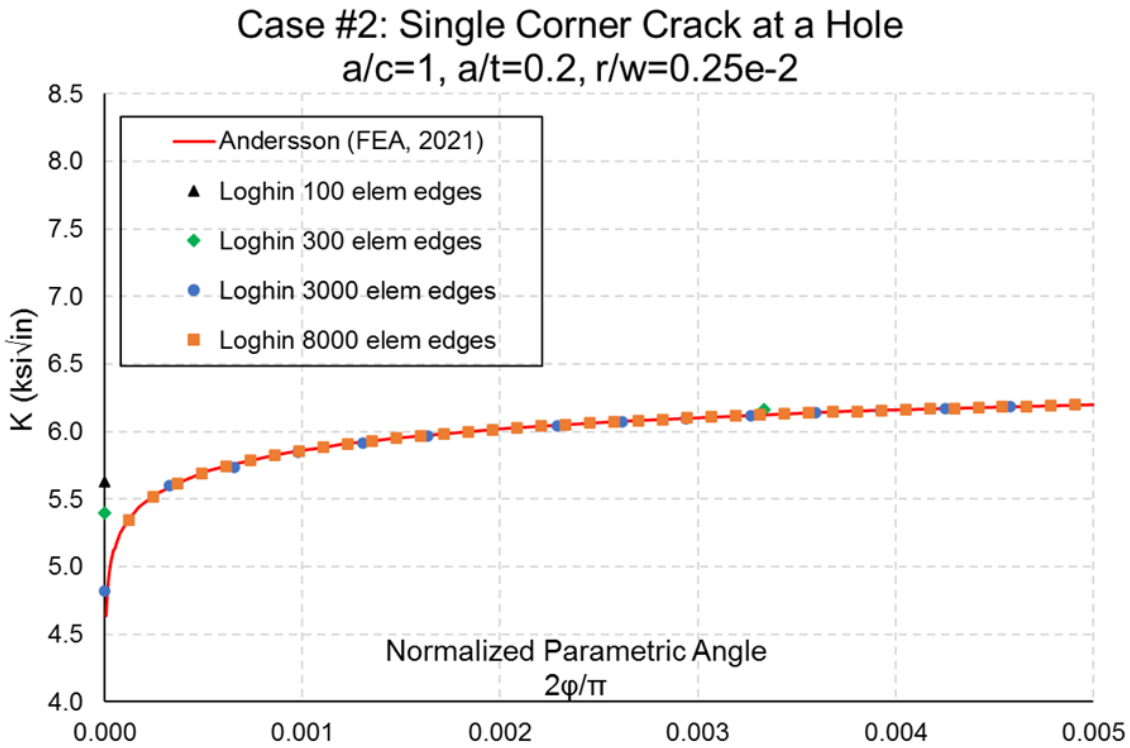

Figure 38: Comparison between K_I values at the "c" vertex location for four meshes and Andersson' solution

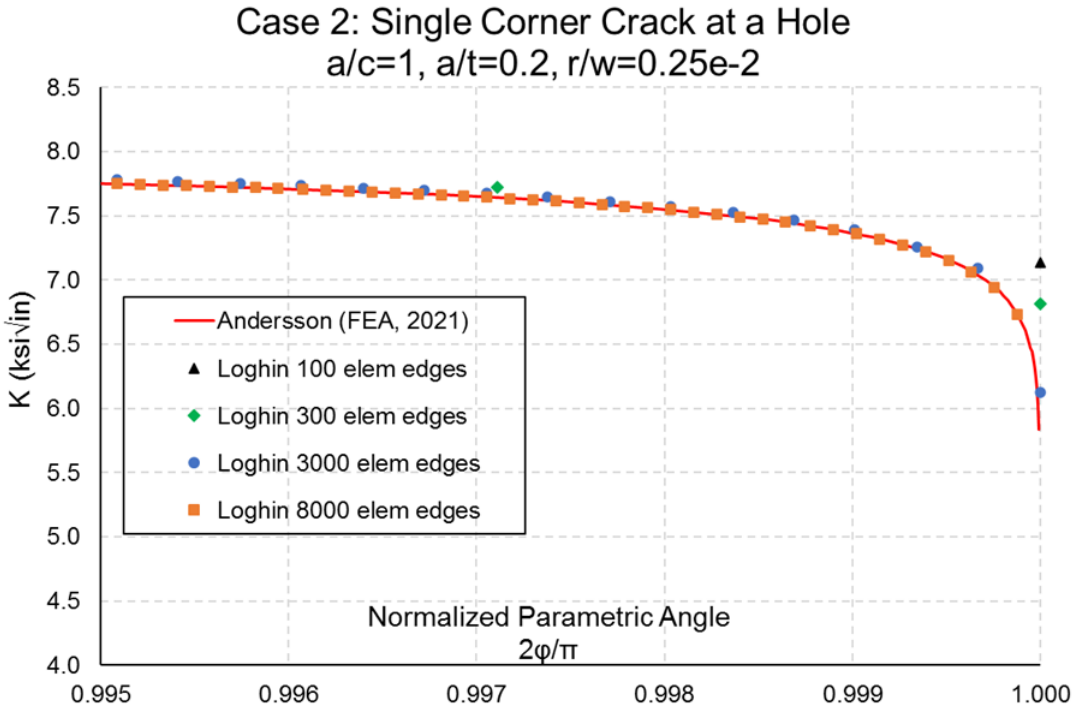

Figure 39: Comparison between K_I values at the "a" vertex location for four meshes and Andersson' solution

Case 3

3D geometry for this case is simply created from the model associated with Case 1 by ofsetting the model faces to reach the required dimensions. This allows the the entire model setup (meshing parameters, boundary conditions and loading assignment) to be preserved in SimModeler Crack. The overall dimensions, crack location, crack size, contour plot of normal stress along loading direction and contour plot of the total displacement field is provided in Figure 40. Mode I SIFs along the crack front are provided in Figure 41.

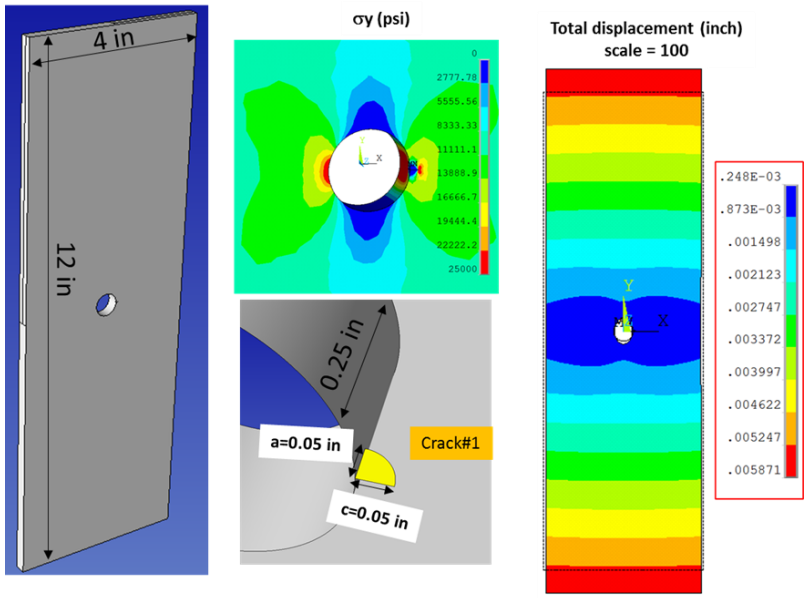

Figure 40: Case 3 3D geometry along with contour plots for σ_y normal stress component and total displacement

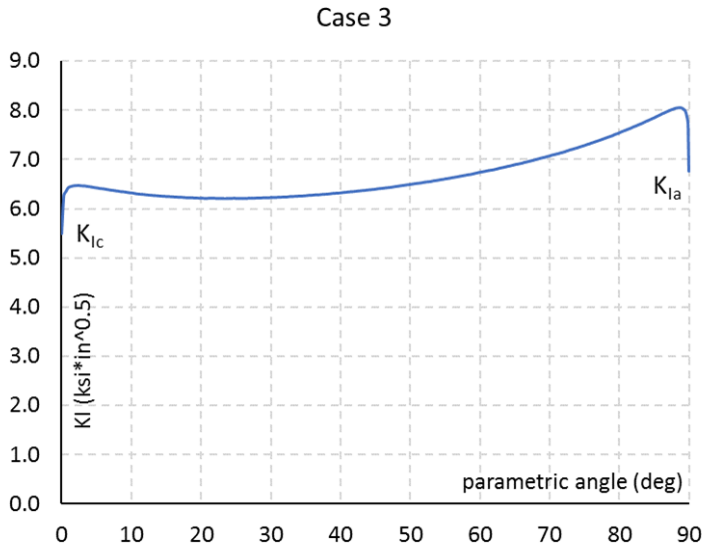

Figure 41: Model I SIFs along the crack front Case 3

Case 4

The same geometric manipulation capability is used to shift the position of the central hole in Case 3 model to create an ofset hole model required in this benchmark Case 4. Similar to the other cases, model dimensions, crack location and size, post-processing contour plots are provided in Figure 42 while Figure 43 provides K_I values along the crack front.

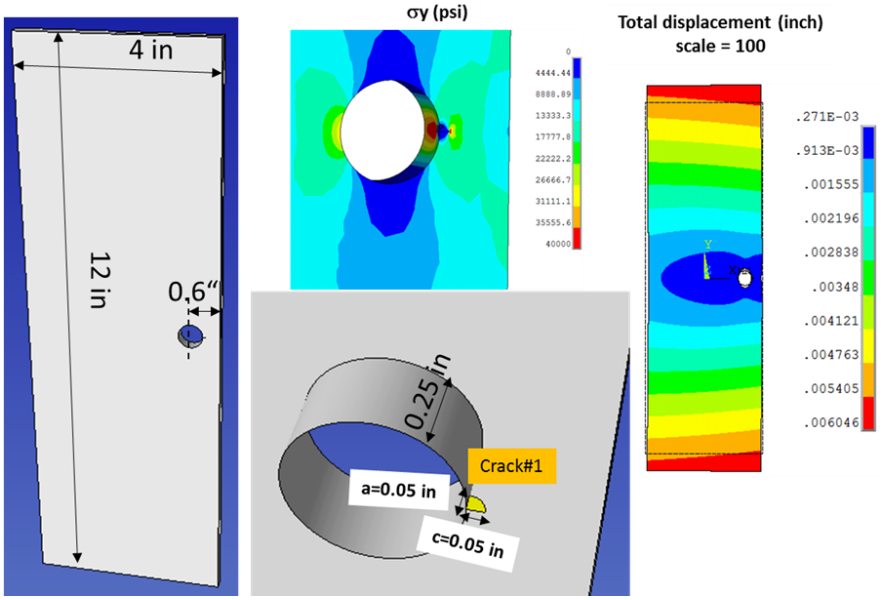

Figure 42: Case 4 3D geometry along with contour plots for σ_y normal stress component and total displacement

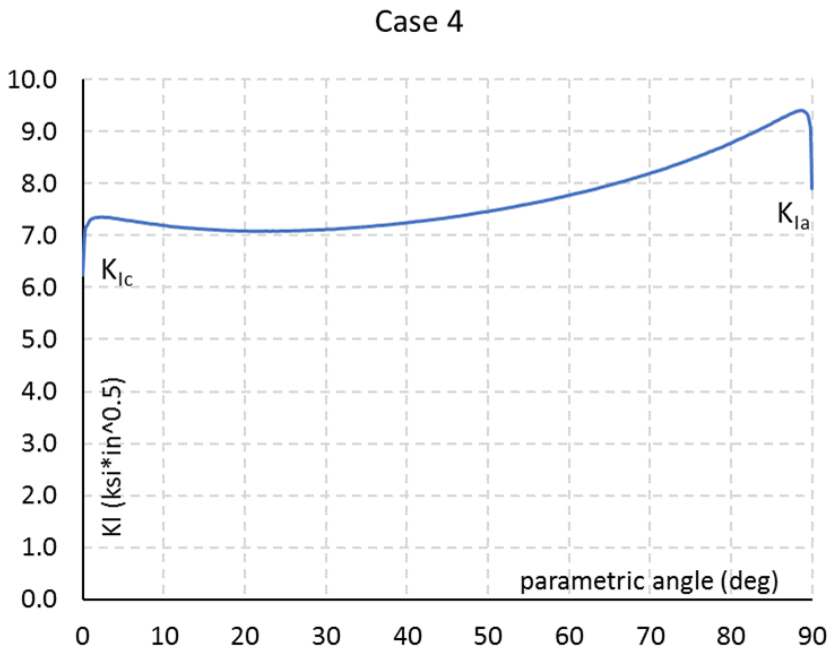

Figure 43: Model I SIFs along the crack front, Case 4

Case 5

Similar to the other benchmark cases, SimModeler Crack is used to create the required geometry for Case 5 by adjusting position of side faces. Figure 44 and Figure 45 provide pre- and post-processing information about the model and, K_I values along the crack front respectively.

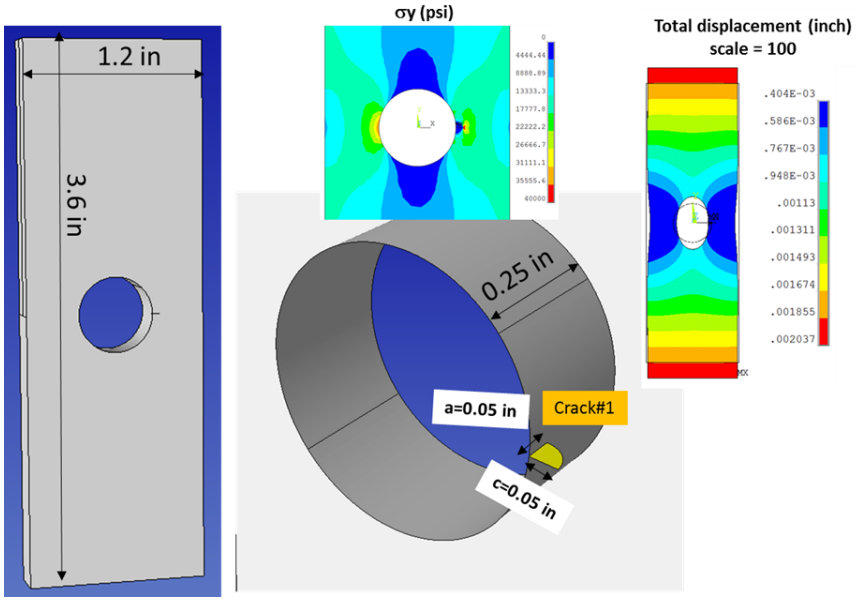

Figure 44: Case 5 3D geometry along with contour plots for σ_y normal stress component and total displacement

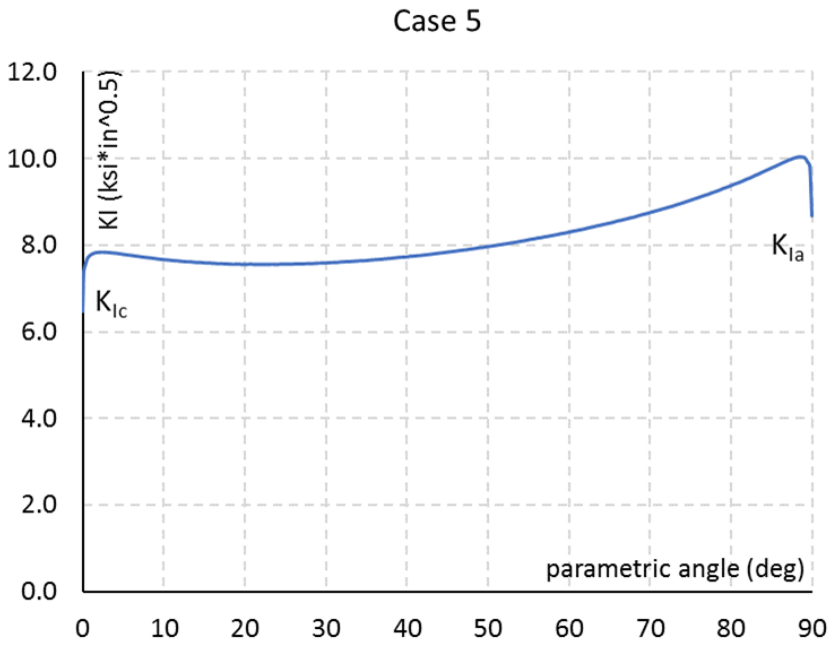

Figure 45: Model I SIFs along the crack front, Case 5

Case 6

Overall geometry used for this case is identical to Case 1. The difference between this benchmark case and Case 1 consists in a different crack size and shape. Overall geometry and results are provided in Figure 46 and Figure 47.

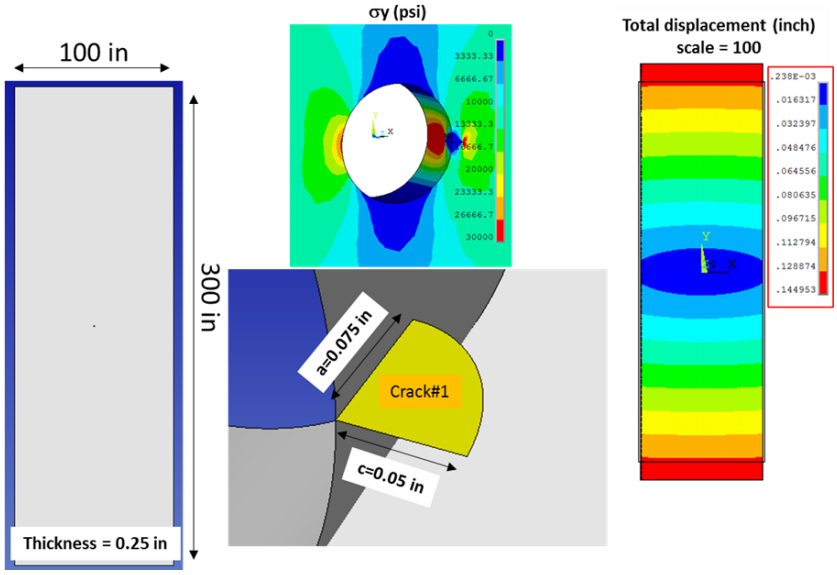

Figure 46: Case 6 3D geometry along with contour plots for σ_y normal stress component and total displacement

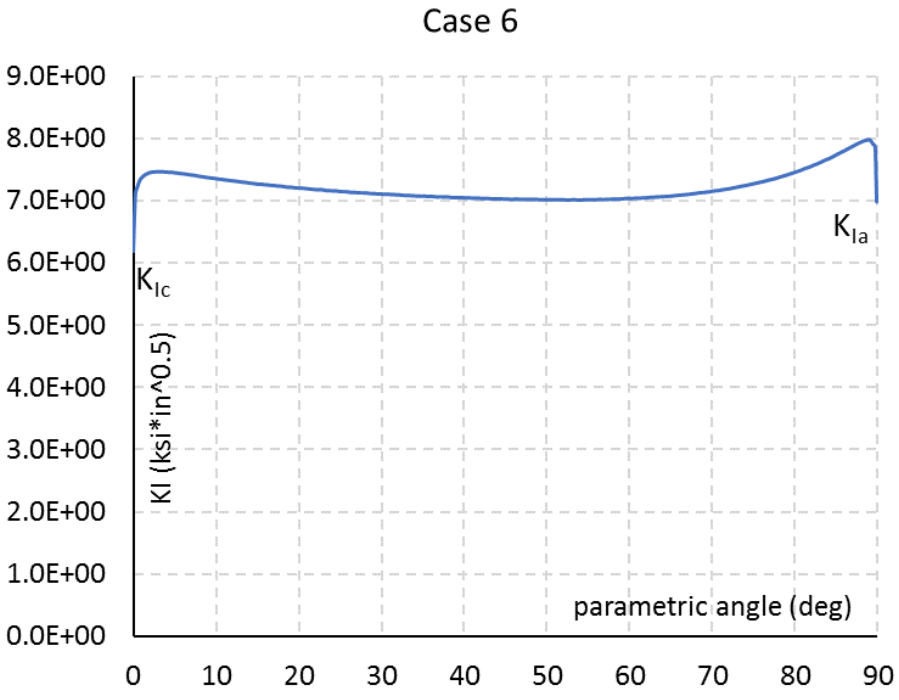

Figure 47: Model I SIFs along the crack front, Case 6

Case 7

This model is another variation of Case 1 (see Figure 48 and Figure 49).

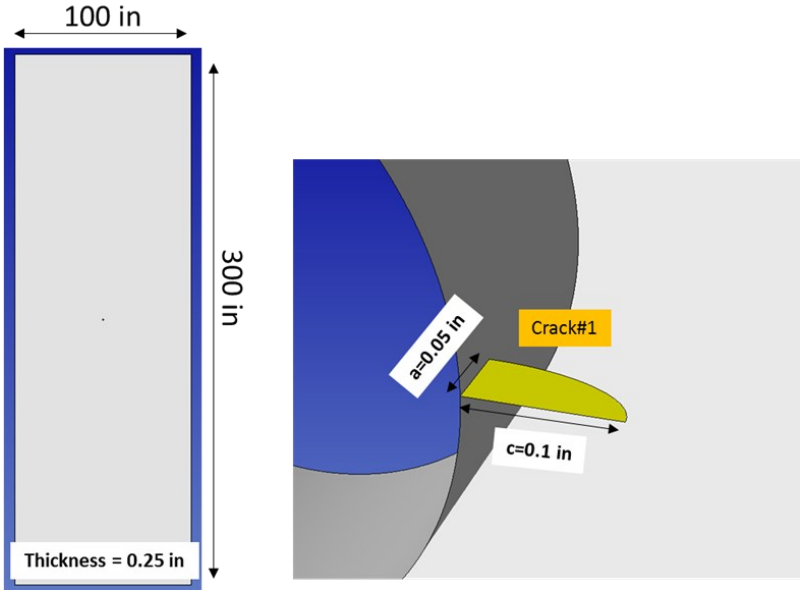

Figure 48: Case 7 3D geometry (same as Case 6 except crack size)

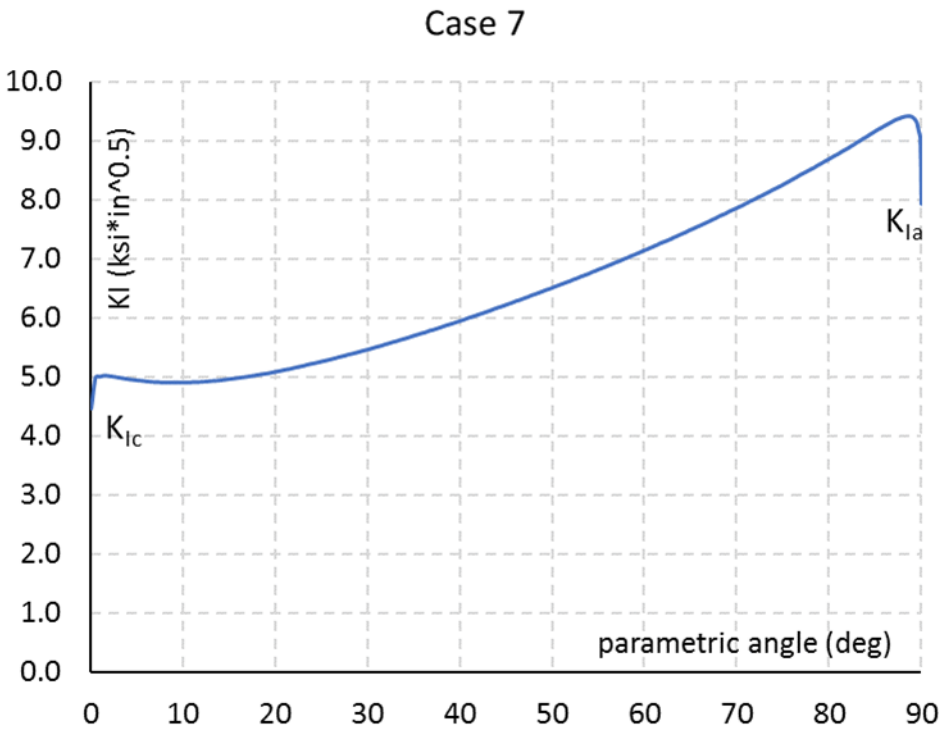

Figure 49: Model I SIFs along the crack front, Case 7

9.3. Submission 8: StressCheck: FEA (2021)

Updated Meshing Routine and Associated Results

9.3.1. Case 2: Single Corner Crack (Infinite Plate)

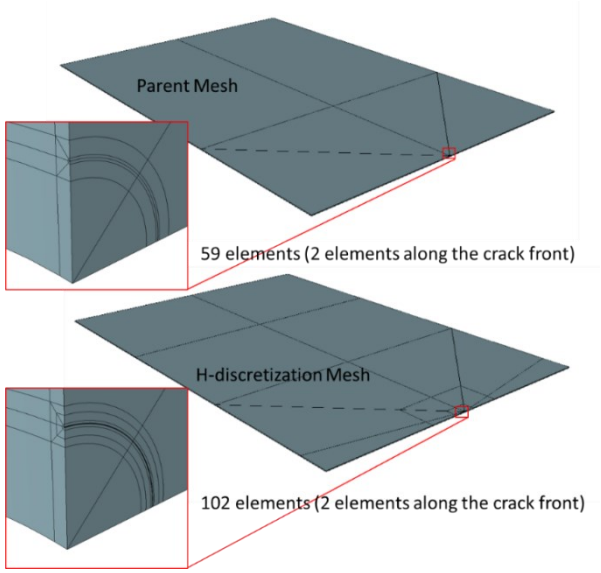

Figure 50: Guided mesh for Case 2. Symmetry boundary condition used on the short midplane across the thickness. Note that only two element edges are used along the crack front.

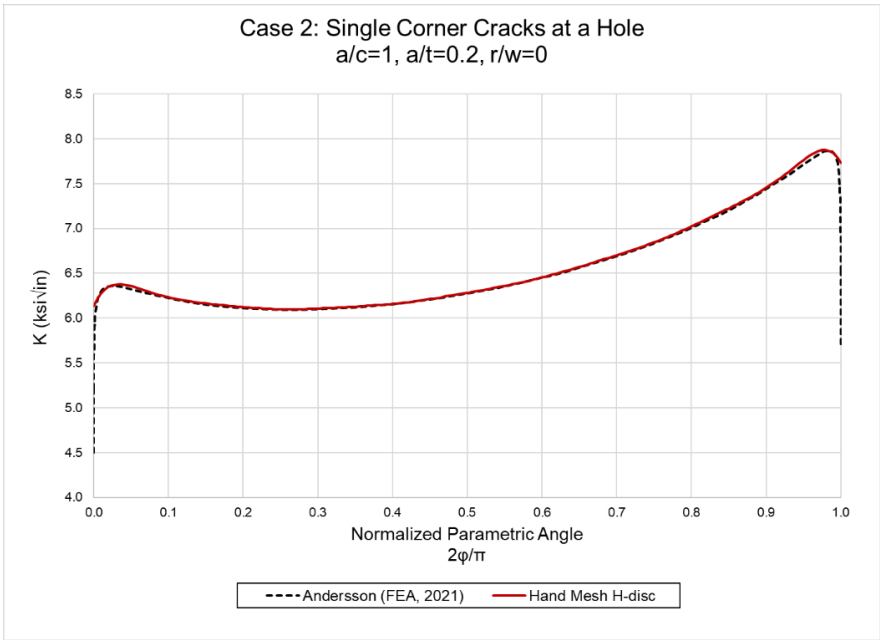

Figure 51: Comparison of SIF extraction along the crack front with Andersson's reference solution for Case 2

9.3.2. Case 3: Single Corner Crack (Finite Plate)

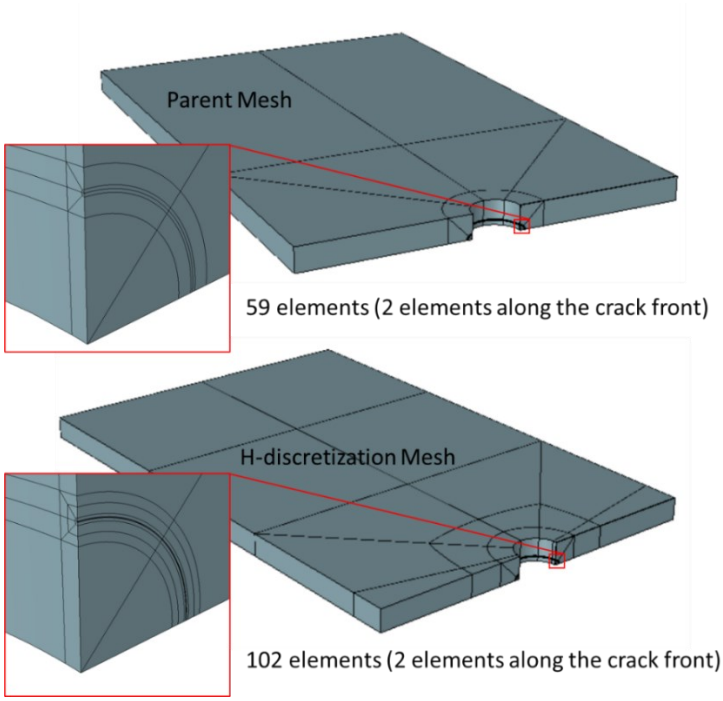

Figure 52: Guided mesh for Case 3. Symmetry boundary condition used on the short midplane across the thickness. Note that only two element edges are used along the crack front.

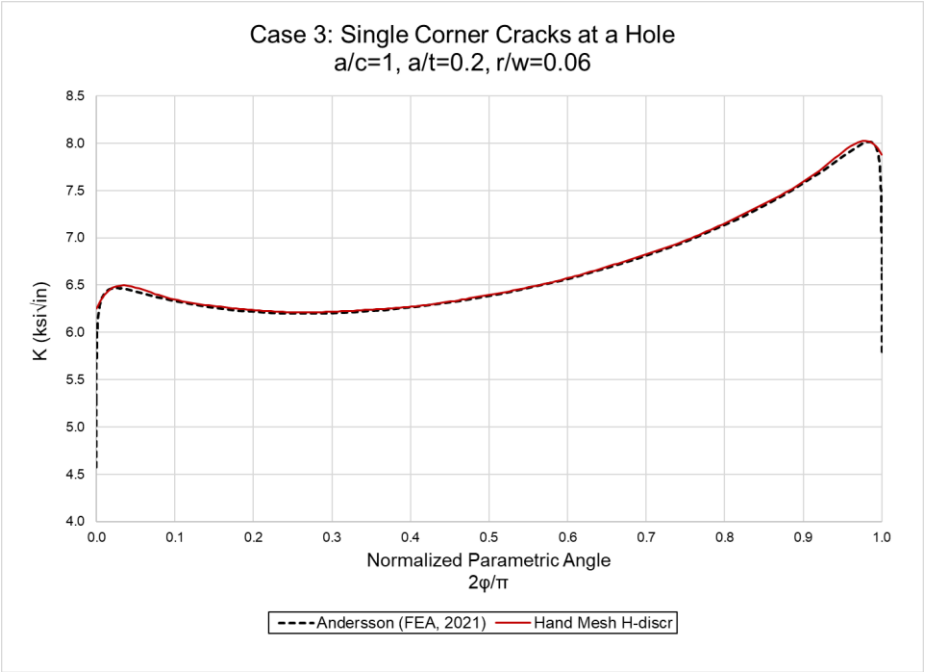

Figure 53: Comparison of SIF extraction along the crack front with Andersson's reference solution for Case 3.

9.3.3. Case 4: Single Corner Crack (Finite Plate, Offset Hole)

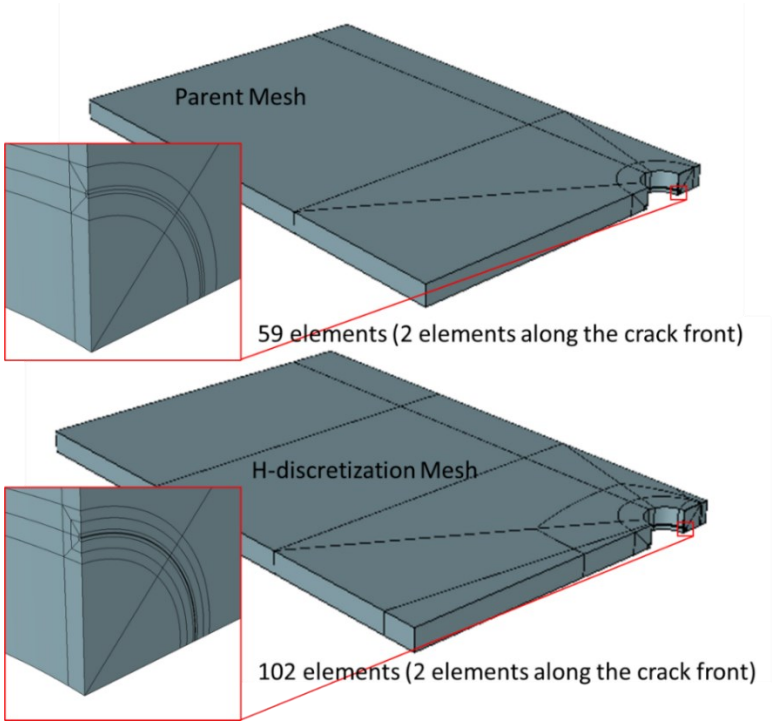

Figure 54: Guided mesh for Case 4. Symmetry boundary condition used on the short midplane across the thickness. Note that only two element edges are used along the crack front.

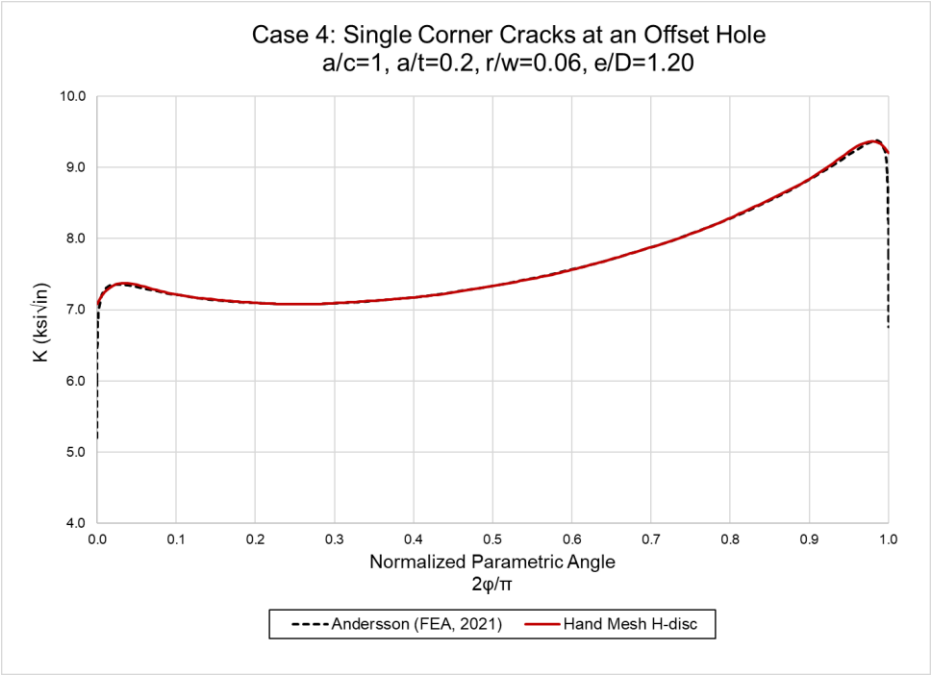

Figure 55: Comparison of SIF extraction along the crack front with Andersson's reference solution for Case 4.

9.3.4. Case 5: Single Corner Crack (Narrow Plate)

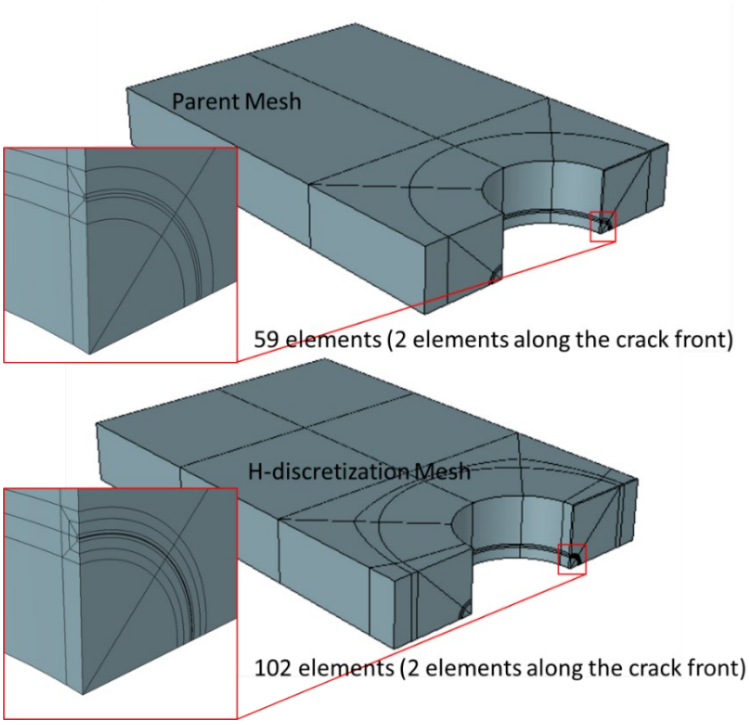

Figure 56: Guided mesh for Case 5. Symmetry boundary condition used on the short midplane across the thickness. Note that only two element edges are used along the crack front.

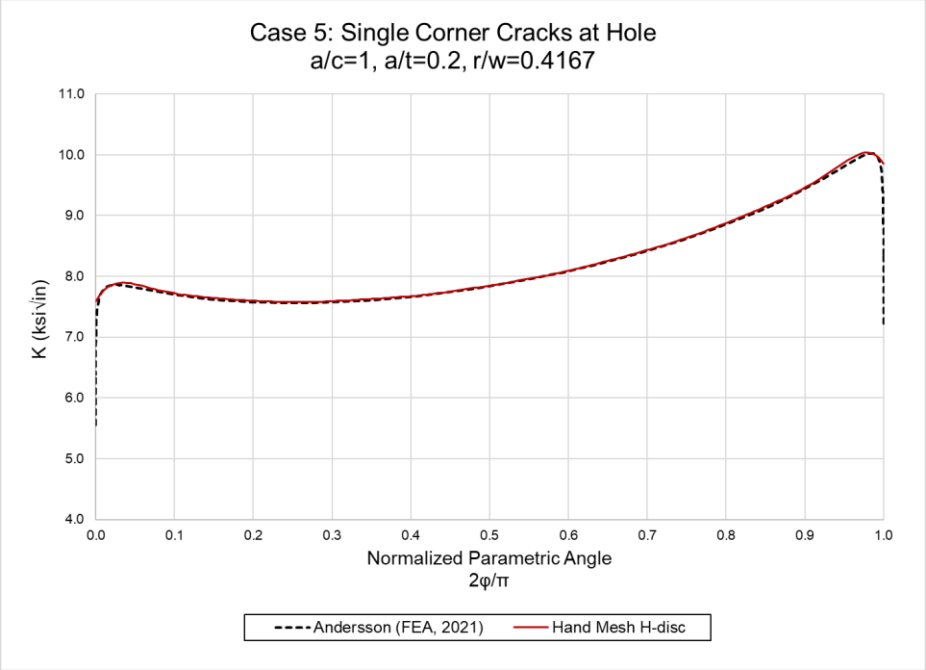

Figure 57: Comparison of SIF extraction along the crack front with Andersson's reference solution for Case 5.

9.3.5. Case 6: Single Corner Crack (Infinite Plate, elliptical crack a/c = 1.5)

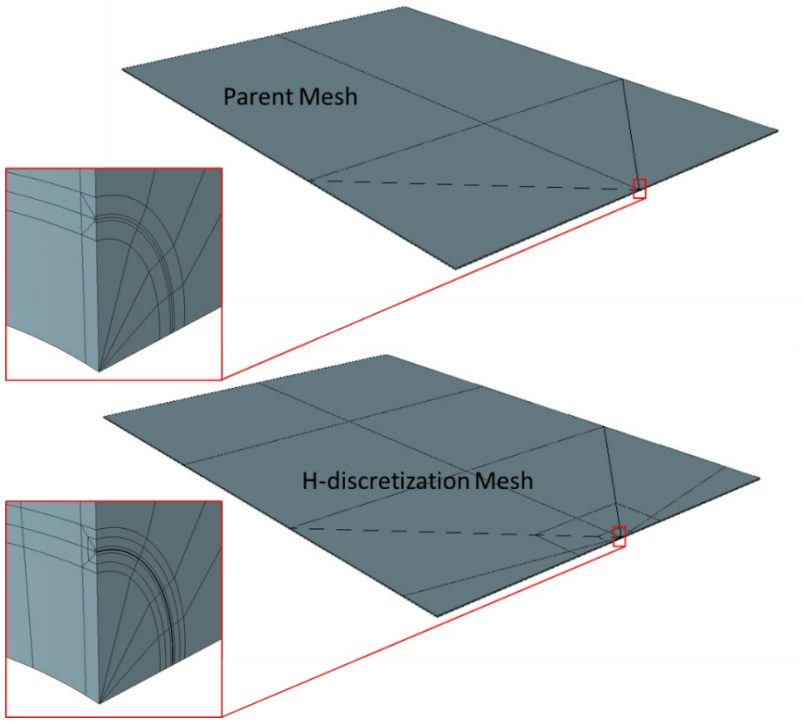

Figure 58: Guided mesh for Case 6. Symmetry boundary condition used on the short midplane across the thickness. Note that only four element edges are used along the crack front.

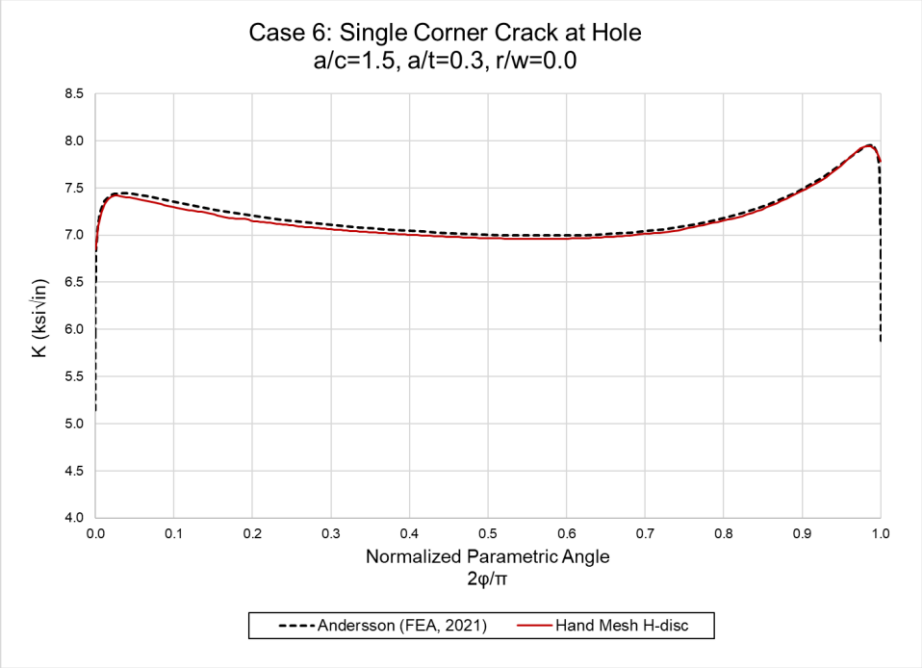

Figure 59: Comparison of SIF extraction along the crack front with Andersson's reference solution for Case 6.

9.3.6. Case 7: Single Corner Crack (Infinite Plate, elliptical crack a/c = 0.5)

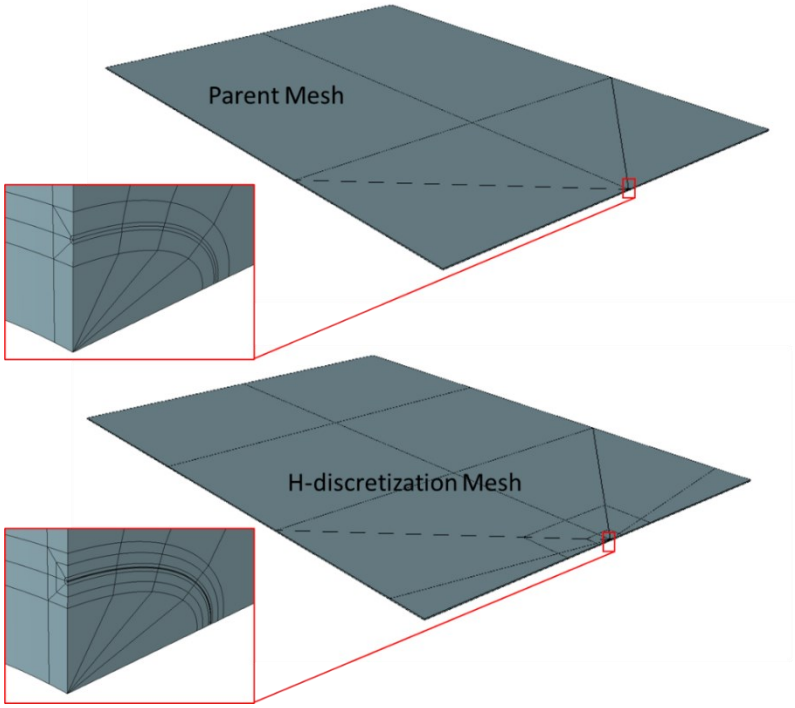

Figure 60: Guided mesh for Case 7. Symmetry boundary condition used on the short midplane across the thickness. Note that only four element edges are used along the crack front.

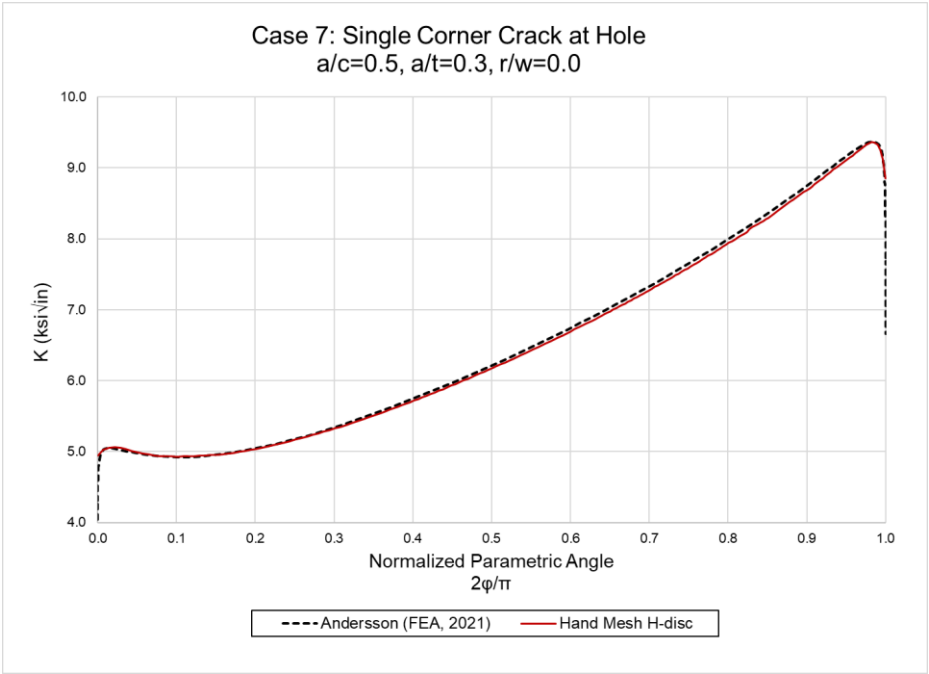

Figure 61: Comparison of SIF extraction along the crack front with Andersson's reference solution for Case 7.

9.4. Submission 9: Marc: FEA (2021)

The modelling of the various cases is done using Marc's pre-processor Mentat. The geometry is described using Parasolid geometry, as shown below. Here using a smaller and thicker plate for easier illustration. To simplify the creation of the various cases, the hole in the plate is generated in the Marc analysis itself. The blue cylinder models the hole, and the yellow disks are used for generating the cracks in the model. Hence, we start with a mesh without a hole.

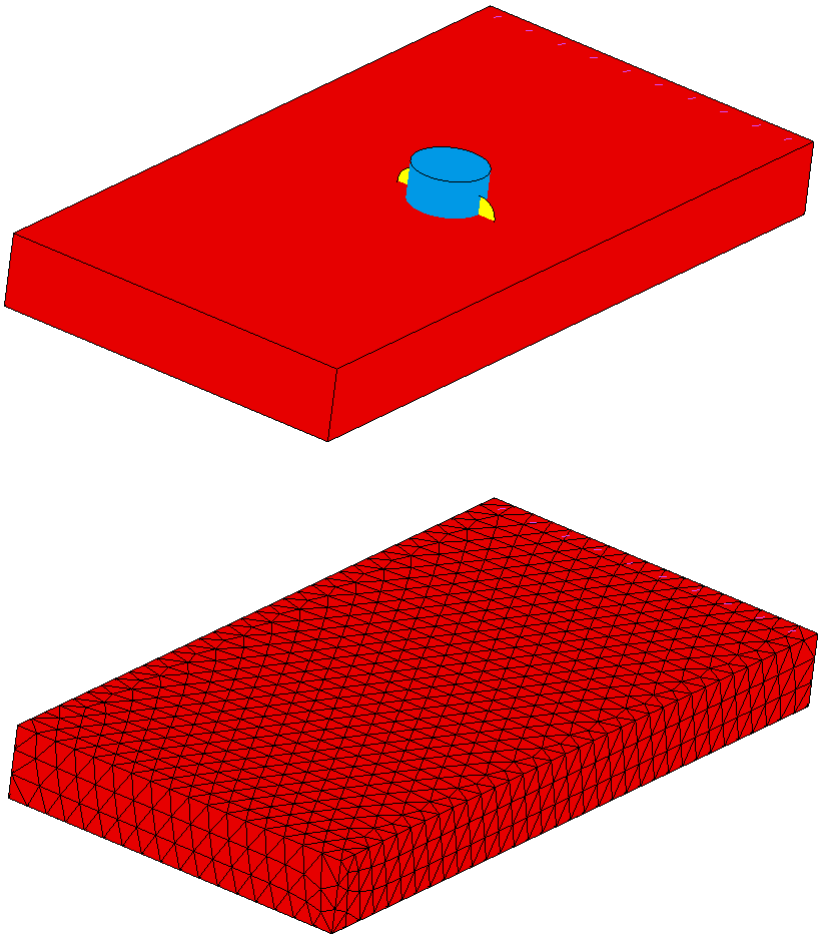

Figure 62: Parasolid geometry and meshing details for Marc's pre-processor Mentat

The analysis in Marc is then performed in two steps. The first step to generate the hole, and the second to initiate the cracks and generate a refined mesh around them. The cracks are obtained as the intersection between the yellow disks and the base material.

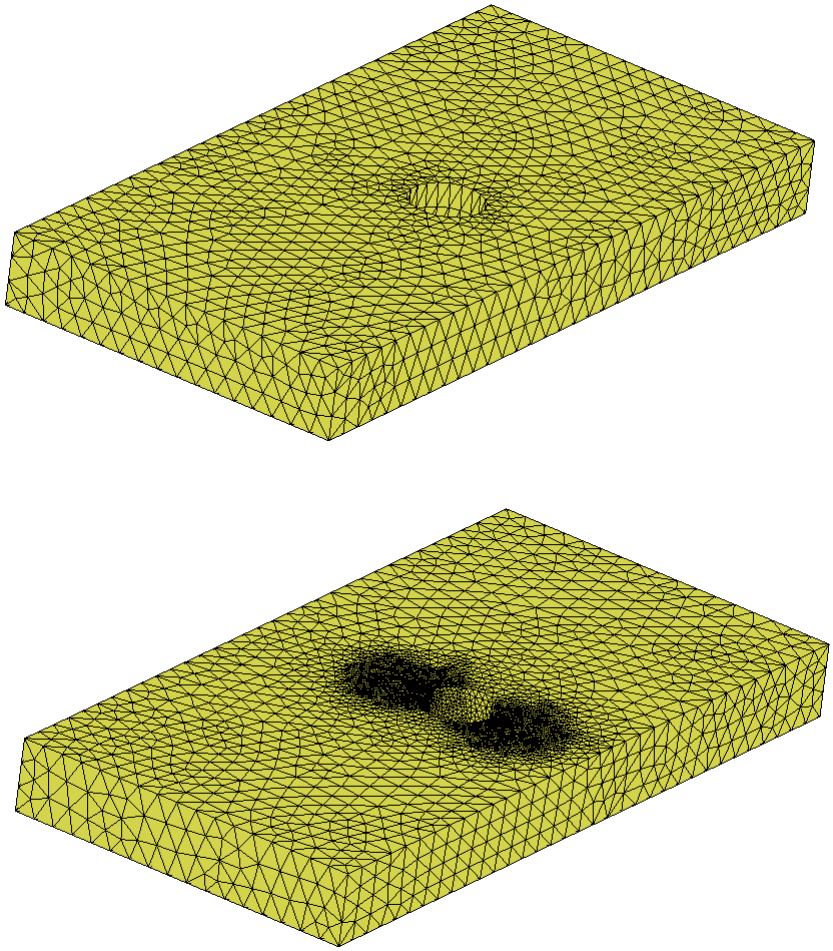

Figure 63: Hole and crack insertion in Marc model

Zooming in on the crack region we see a fine regular mesh around the cracks. The part of the mesh region with the crack front highlighted is shown on the right hand side. The mesh consists entirely of tetrahedral element, and is fully connected. This regular mesh around the crack fronts is generated automatically in the remeshing process. Experience has shown that when using this type of elements, it is critical with a fine and regular mesh near the crack front, and with a smooth mesh transition to the rest of the structure.

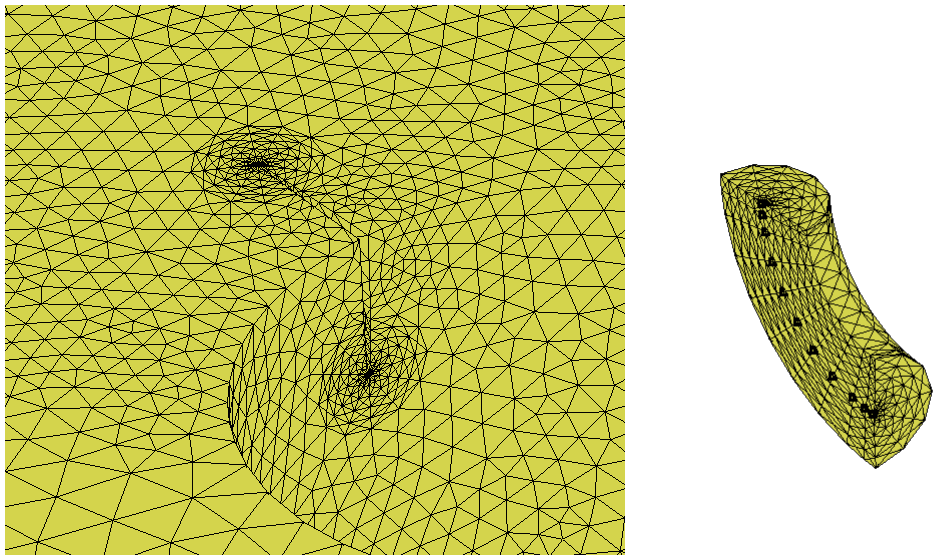

Figure 64: Crack front meshing in Marc model

Looking at Case 5 as an example, we see that the Marc results are quite close to the reference by Andersson. The solution time on a regular laptop is about one minute. The Marc solution does not accurately capture the sharp gradient at the ends, but this is not possible with the use of only 30 equally spaced nodes along the front. A quick study with finer meshes (still uniformly spaced along the front) show that we can capture the end effects better with a finer mesh. To really capture this one would use a non-uniform distribution along the front with a fine mesh at the ends.

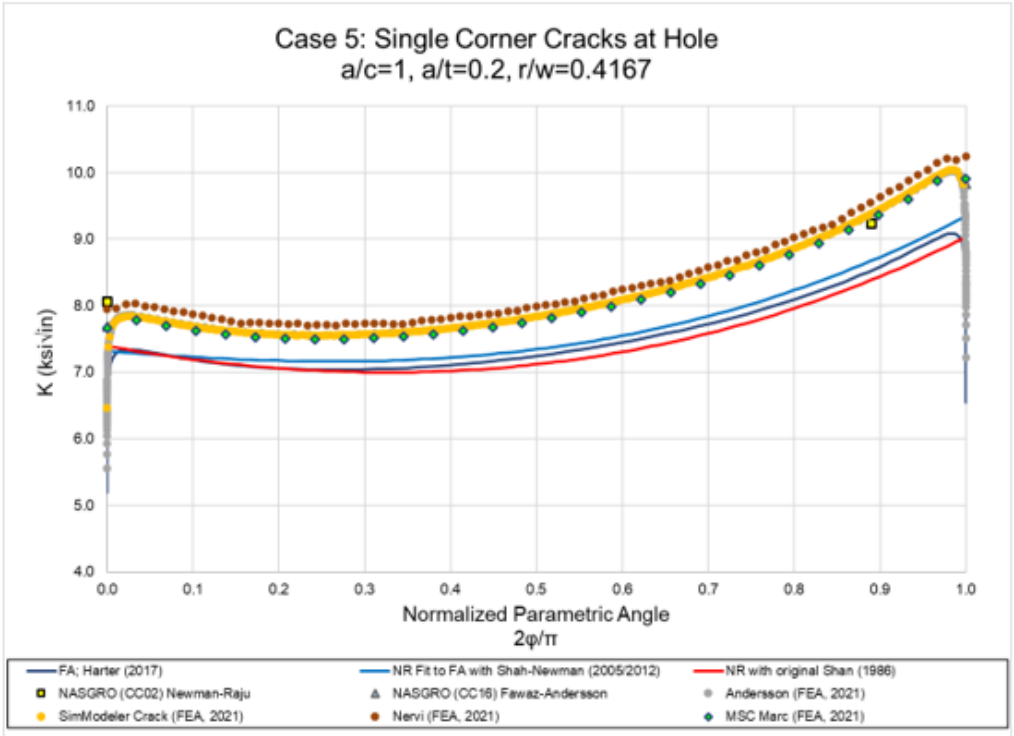

Figure 65: Case 5 results demonstrating Marc comparisons to Andersson reference solution

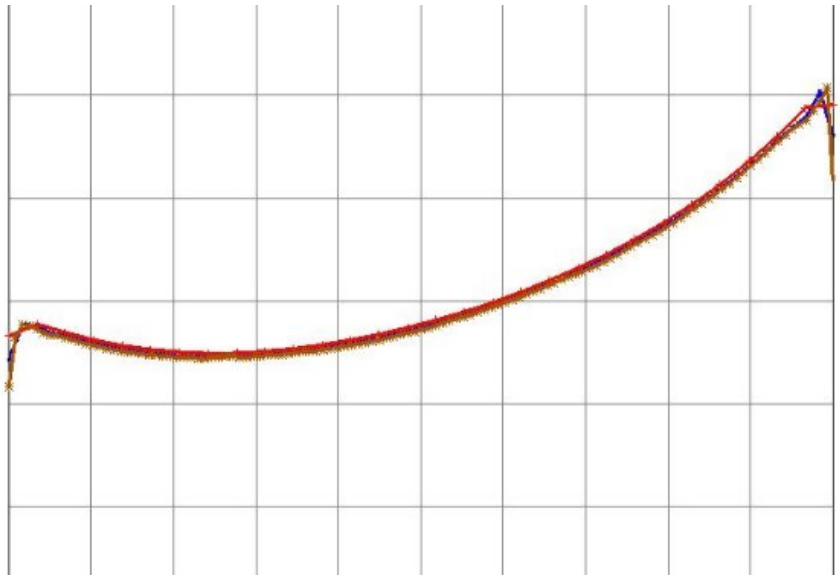

Figure 66: Refined meshing results for near surface SIF factor behavior